Submitted in accordance with the requirements for the degree of
Doctor of Philosophy

UNIVERSITY OF LEEDS

SCHOOL OF PHYSICS & ASTRONOMY

Relativistic entanglement of single and two particle systems

Veiko Palge

May 2013

The candidate confirms that the work submitted is his/her own, except where work which has formed part of jointly-authored publications has been included. The contribution of the candidate and the other authors to this work has been explicitly indicated below. The candidate confirms that appropriate credit has been given within the thesis where reference has been made to the work of others.

Chapter 3 is based on a jointly authored paper. I am responsible for calculations, text and figures, the coauthors provided valuable consultation, feedback and comment.
Paper: Palge, V. & Dunningham, J. Generation of maximally entangled states with subluminal Lorentz boosts. *Physical Review A* **85,** 042322 (2012).

Chapter 3 also contains some material from the following jointly authored paper. I am responsible for some calculations, the coauthors provided text, figures and the rest of the calculations.
Paper: Dunningham, J., Palge, V. & Vedral, V. Entanglement and nonlocality of a single relativistic particle. *Physical Review A* **80,** 044302 (2009).

Some material in chapter 4 is implicit in the following jointly authored paper. I am responsible for calculations and parts of text. The coauthor provided other parts of text, some calculations and figures.
Paper: Palge, V., Vedral, V. & Dunningham, J. A. Behavior of entanglement and Cooper pairs under relativistic boosts. *Physical Review A* **84,** 044303 (2011).

The material in chapter 4 that has not appeared in print is currently being prepared for publication. This paper will contain work carried out by me under supervision of Jacob Dunningham.

Chapter 5 is currently under preparation for publication. This paper will contain work carried out by me under supervision of Jacob Dunningham.

Acknowledgements

I would like to thank many people for their support during the time I have been working on this thesis. Firstly, I would like to thank Jacob Dunningham who has advised and supported me in many ways, in both matters academic and non-academic, and provided encouragement throughout the project. He created a relaxed and friendly atmosphere to work in and was always generous. I could not have wished for a better supervisor.

I would also like to thank Eric Curiel and Kaupo Palo for helpful conversations that confirmed my intuitions on the role of geometry. Madis Kõiv is my first teacher in philosophy. He continues to be the source of inspiration and the reason to pursue my studies. I thank Viv Kendon for advice on computing and Jiannis Pachos for useful feedback on parts of earlier work. I have benefitted greatly from interactions with my fellow students. Thanks to Katie Barr, Rob Wagner, Katherine Brown, Paul Knott, Tony Blake, Andreas Kurcz, Ville Lahtinen, Martin Aulbach, Suvabrata De, James De Lisle, Abbas Al Shimary, Shane Dooley, Tom Barlow and Luis Gutiérrez, and anyone I have missed off this list for fun times and useful discussions. And of course to Adam Stokes for listening to my rants on physics and philosophy and providing his own insights on the matters. Particular thanks to Tim Proctor for help with proofreading. Kerry McKenzie and Vijay Teeluck deserve special mention for being good friends and sharing the experiences of being a PhD student. I also want to thank Vijay and Tom Bethell for great times in Leeds.

I am very grateful to my parents who have supported me through the years I have spent educating myself. I express my deep gratitude to my partner, Katrin, for keeping me sane and happy, and putting up with long hours of work, especially in the last stages of writing up. Finally, special thanks to our little daughter Säde who has inspired me greatly; her achievements in the last year vastly surpass mine.

Abstract

Veiko Palge "Relativistic entanglement of single and two particle systems", Ph.D. thesis, University of Leeds, May 2013.

One of the defining features of quantum theory is entanglement, the notion that quantum systems can display correlations that are impossible from the classical point of view. In quantum information theory entanglement has come to be recognised as a physical resource that enables new technologies that perform information processing tasks which are beyond the limits of the classical realm. It has been realised only recently that entanglement is dependent on the frame of reference in both inertial and accelerated systems. In this thesis, we investigate the relativistic entanglement of massive spin-$1/2$ particles in inertial frames by focussing on the dependence of entanglement on the geometry of the underlying boost scenario. We first explore the 'qubit' of the relativistic setting: a single particle with spin and momentum, with momentum given by a Gaussian distribution. We study the system in a variety of different boost scenarios, analysing the behaviour of entanglement from a geometric point of view. The spin-spin entanglement of two particle systems is then surveyed for many different discrete product and entangled momenta, with the spins in the Werner state. We also extend the analysis to continuous momentum states and study them in a variety of geometries. The results obtained from the analysis of discrete states are applied to continuous states, leading to a better understanding of the behaviour of entanglement. We lastly discuss the common view according to which Lorentz boosts leave the total entanglement of the state invariant.

Contents

List of Figures

List of Tables

Publications

1. Palge, V. & Dunningham, J. Generation of maximally entangled states with subluminal Lorentz boosts. *Physical Review A* **85,** 042322 (2012).

2. Palge, V., Vedral, V. & Dunningham, J. A. Behavior of entanglement and Cooper pairs under relativistic boosts. *Physical Review A* **84,** 044303 (2011).

3. Dunningham, J., Rico Gutiérrez, L. & Palge, V. Observing superpositions of different number states. *Optics and Spectroscopy* **111,** 528–534 (2011).

4. Gutiérrez, L. M. R., Palge, V. & Dunningham, J. Observing the Superposition of a Single Particle with the Vacuum. *Mathematical Structures in Computer Science* **20,** 1051–1065 (2010).

5. Dunningham, J., Palge, V. & Vedral, V. Entanglement and nonlocality of a single relativistic particle. *Physical Review A* **80,** 044302 (2009).

Chapter 1

Introduction

Quantum mechanics and relativity were born around the same time at the beginning of 20th century. They changed the perception of the world around us in different but equally disturbing ways. Relativity teaches us that the Newtonian preconceptions so deeply ingrained in our everyday views of time and space are at odds with the deeper structure of spacetime. Quantum theory tells a story that seems even more peculiar: the behaviour of objects at very small scales does not fit the framework of any classical theory, exhibiting the peculiar phenomena of superposition and entanglement [1–4, 12]. The quantum world seems to tell us that the description of nature at microscopic scales implies an overhaul of our classical notions of logic and probability theory is needed [5, 6, 13]. The rise of quantum information theory made physicists realise that in addition to fundamental significance, the quantum weirdness also has practical utility. Entangled systems are at the heart of a whole range of classically impossible communication protocols and they give quantum computer its speed.

1.1 Relativistic quantum information

Although questions about the relationship between quantum theory and relativity had been raised early on, it is since the end of 1990s that one can discern an increasing number of works focussing on topics concerning relativistic quantum information. We can divide them into two groups according to whether one deals with inertial or accelerated frames.

That inertial frames in relativity pose challenges for quantum information that are not present in Galilean space-time was recognised in [14], which considered the relativistic version of the famous Einstein-Podolsky-Rosen-Bohm experiment

with massive spin-$1/2$ particles. It argued that the degree of violation of the Bell inequality is dependent on the velocity of the particles, leading to implications for quantum cryptography. Soon afterwards, the authors of [15, 16] reach the conclusion that the entanglement of a Bell state depends on velocity of an observer, while in [17] it is stated that it remains invariant if momenta are given by plane wave states. Almost simultaneously it is demonstrated in [18] that the entropy of a single massive spin-$1/2$ particle changes non-trivially under Lorentz boosts. Massless particles were considered in [16, 19] and shown to undergo qualitatively similar non-trivial transformations, while in [20] a single massless particle was claimed to retain its linear polarisation for a moving observer.

These works, along with others, belong to the literature that established the field and paved way for a great many papers that have raised a number of different issues. Questions range from clock synchronisation [21] and distillability [22] to whether or not one can define a Lorentz-covariant reduced spin density matrix for single particles [23–25]. The EPR situation has been revisited a number of times [26–28]. The maps that Lorentz transformations induce on spins have also been studied from the point of view of open quantum systems [29], as well as in the context of entanglement generation [30]. Links have been explored to the phenomena of decoherence and sudden death of entanglement [31–33]. As a natural extension of bipartite entanglement, there are now also studies into tripartite entanglement [34–36]. Discussion of massless particles in the context of quantum information can be found in [37–43]. It is intriguing that one can find similarities between relativistic phenomena and Berry's phase [37].

Systems in accelerated frames introduce an even higher level of complexity, while also showing non-trivial changes of entanglement [44–47]. Various quantum communication tasks, including key distribution and teleportation have been studied in noninertial frames and in the vicinity of black holes [48–51]. Recent studies have focussed on localised systems and investigated entanglement generation, and even the prospect of creating quantum gates through non-uniform motion [52–57]. Tripartite entanglement has been found to exhibit somewhat different properties from bipartite entanglement [58, 59].

The overarching conclusion emerging from the literature on both inertial and accelerated systems is that relativistic entanglement is *observer dependent* [60]. This is in stark contrast to the non-relativistic situation where spacetime plays the role of a passive background canvas on which the quantum events are painted. The more active character of the relativistic spacetime means it can have two faces:

that of a friend, or a foe. It appears as a friend to the quantum information theorist when the transformations induced by spacetime can be used, for example, to generate entangled states [54] or either realise, or enhance quantum communication or computation [61]. Alternatively, relativity may appear as a hindrance when it causes unwanted disturbances, e.g. in the context of quantum communication, which need to be taken into account and compensated for, if possible, by clever engineering [62].

1.2 Thesis aim and motivation

Understanding entanglement in the relativistic context is a key issue in relativistic quantum information. In this thesis, we confine attention to inertial frames. The main aim of this thesis is to investigate the relativistic entanglement of massive spin-$1/2$ particles in single and two particle systems. Whereas previous work has been somewhat restricted with regards to the boost scenarios and momentum states involved, in this thesis we wish to extend the treatment. Firstly, although the literature on Thomas-Wigner rotation is quite clear that the phenomenon is highly dependent on the underlying geometry, there is almost no work in quantum information taking this into account. We attempt to fill this lacuna by studying the dependence of entanglement on the geometry of the underlying boost scenario. Secondly, in quantum information theory superposition and entanglement are regarded as various kinds of resources that can be harnessed to create new quantum technology, leading to extensive research of such states. This provides a motivation to study how different sorts of momentum states affect the changes of entanglement under Lorentz boosts in single and two particle systems. Finally, we extend the analysis to continuous momentum states and study them in a variety of geometries.

1.3 Thesis overview

The thesis is structured as follows. Chapter 2 provides an overview of the topics that form the background of the discussion in the rest of the thesis. We begin by outlining the Lorentz group and see how the Thomas-Wigner rotation arises from the structure of the Lorentz group. Thomas-Wigner rotation is central to the thesis, hence we need to know how it is represented in quantum mechanics. This is discussed in the next section, where we give a useful representation of the rotation for massive spin-$1/2$ particles, the systems on which the thesis focusses. Thereafter we

detail the properties of Thomas-Wigner rotation, which will play an important role in explaining the behaviour of entanglement in both single and two particle systems. We lastly focus on the notion of entanglement and discuss how to quantify it for pure and mixed bipartite states.

Chapter 3 explores the 'qubit' of our relativistic quantum system: a single massive spin-$1/2$ particle. It is the simplest non-trivial system and hence the studying of which is a prerequisite to the understanding the behaviour of multiparticle systems. The work on single particle entanglement was initiated in [18], where the authors establish an intriguing phenomenon: the reduced density matrix of a massive free spin-$1/2$ particle is not covariant under Lorentz transformations, implying that spin entropy has no invariant meaning in relativity. Our treatment begins by revisiting two idealised models discussed in the literature. This is followed by the study of a model consisting of a spin-momentum product state with momentum given by a Gaussian distribution. This system will be then studied in a variety of different boost scenarios. To analyse the behaviour of entanglement, we adopt a geometric point of view. We conclude with an analysis of the features observed.

Chapter 4 turns to two particle systems with spin and momenta. The focus now shifts importantly. Whereas in the single particle chapter we were concerned with how boosts entangle spin and momenta of a single particle, in this chapter we will look at how boosts affect the entanglement of the spin degree of freedom of a two particle system. A key aspect one notices is that the (sometimes seemingly contradictory) results in the literature rely on different boost scenarios, that is, the momentum states and geometries assumed. This confirms what we discovered in our investigation of single particle systems, namely, that entanglement under Lorentz boosts is highly dependent on the boost scenario in question. The central question we pose in this chapter is: How do different momentum states and boost geometries affect the entanglement of a bipartite spin state under Lorentz boosts? In order to tackle the issue, we focus on an idealised model involving discrete momentum states. This enables a systematic survey of the structure of the maps that momenta induce on the spin degree of freedom under Lorentz boosts. Spins in the Bell and Werner states will be investigated.

Although idealised systems provide valuable insight into the behaviour of entanglement, realistic situations involve wave packets. In chapter 5 we complete the study of two particle systems by focussing on states with continuous momenta. We proceed in parallel with the previous chapter in discussing a variety of momentum states in different boost geometries. Due to the complexity of calculations, our

treatment is numerical throughout and attention is restricted to the states where the spin subsystem is given by a Bell state.

In chapter 6 we raise the question of how to explain the behaviour of entanglement in relativistic systems. We have learned that it changes non-trivially under Lorentz boosts. But do we witness a genuine change of the amount of entanglement or is it just that entanglement is shuffled around between subsystems of the total system while its total amount remains invariant? With a few exceptions, the latter verdict seems almost unanimous in the literature. We think there are grounds to believe that the issue needs further analysis. To make progress in clarifying the issue, we concentrate on the discrete models studied in chapter 4 and examine the entanglement of different partitions of the systems.

The final chapter 7 contains the summary and discussion of our main results.

Chapter 2

Preliminaries

This chapter reviews the topics that form the background of the discussion in the rest of the thesis. We begin by giving a brief overview of the Lorentz group and see how the Thomas-Wigner rotation arises. In the next section we will discuss how the Thomas-Wigner rotation is represented in quantum mechanics. Some of the properties of Thomas-Wigner rotation will be then highlighted, which will play an important role in explaining the behaviour of entanglement in both single and two particle systems. Lastly, we focus on the notion of entanglement and discuss how to quantify it for pure and mixed bipartite states.

2.1 Special relativity

In the transition from non-relativistic to relativistic quantum mechanics the group of spacetime symmetries changes from the Galilei group to the Poincare group. The Poincare group consists of spacetime translations, rotations and Lorentz boosts. The relativistic effects of interest to quantum information theory that are the focus of this thesis arise from the properties of the Lorentz group, a subgroup of the Poincare group, which consists of boosts and rotations [63]. In the following we will thus restrict attention to the Lorentz group.

The centrepiece of the Lorentz group are the so-called *Lorentz boosts* which relate two observers in inertial frames that move with constant velocity v relative to each other. Suppose the motion is along the common x-axis, then the transformations are

$$x' = \gamma\left(x - vt\right) \ , \quad y' = y \ , \quad z' = z \ , \quad t' = \gamma\left(t - vx/c^2\right) \ , \tag{2.1}$$

where $\gamma = (1 - v^2/c^2)^{-1/2}$. For convenience, let us denote $\beta = v/c$ and define a four vector $x^\mu = (x^0, x^1, x^2, x^3) = (t, x, y, z) = (t, \mathbf{x})$. Let us also assume that we work in natural units where $\hbar = c = 1$, then the Equations (2.1) become

$$\begin{pmatrix} t' \\ x' \\ y' \\ z' \end{pmatrix} = \begin{pmatrix} \gamma & -\gamma\beta & 0 & 0 \\ -\gamma\beta & \gamma & 0 & 0 \\ 0 & 0 & 1 & 0 \\ 0 & 0 & 0 & 1 \end{pmatrix} \begin{pmatrix} t \\ x \\ y \\ z \end{pmatrix} , \tag{2.2}$$

or in a more compact notation

$$x' = \Lambda(v)x \ , \tag{2.3}$$

where $\Lambda \equiv \Lambda(v)$ is a boost in the x-direction. We will oftentimes parameterise boosts using *rapidity*, defined as $\xi = \operatorname{arctanh} v$, so

$$\beta = \tanh\xi \ , \quad \gamma = \cosh\xi \ , \quad \gamma\beta = \sinh\xi \ , \tag{2.4}$$

and the matrix of a Lorentz boost in Equation (2.2) can be expressed as

$$\Lambda(\xi) = \begin{pmatrix} \cosh\xi & -\sinh\xi & 0 & 0 \\ -\sinh\xi & \cosh\xi & 0 & 0 \\ 0 & 0 & 1 & 0 \\ 0 & 0 & 0 & 1 \end{pmatrix} . \tag{2.5}$$

For a particle with mass m we write its four momentum $p^\mu = (p^0, p^1, p^2, p^3) = (E, p_x, p_y, p_z) = (E(\mathbf{p}), \mathbf{p})$, with $E(\mathbf{p}) = \sqrt{\mathbf{p}^2 + m^2}$, where the relation to rapidity is

$$\cosh\xi = \frac{\sqrt{\mathbf{p}^2 + m^2}}{m} \ , \quad \sinh\xi = \frac{|\mathbf{p}|}{m} \ . \tag{2.6}$$

The matrix elements of a generic Lorentz boost in the direction of a unit vector $\mathbf{e} = (e_x, e_y, e_z) = \mathbf{p}/|\mathbf{p}|$ are given by [64],

$$\begin{aligned} \Lambda_{ij}(\xi) &= \delta_{ij} + (\cosh\xi - 1)\, e_i e_j \ , \\ \Lambda_{i0}(\xi) &= \Lambda_{0i}(\xi) = \sinh\xi\, e_i \\ \Lambda_{00}(\xi) &= \cosh\xi \ . \end{aligned} \tag{2.7}$$

The Lorentz group also contains pure spatial rotations which are of the form

$$R = \begin{pmatrix} 1 & 0 & 0 & 0 \\ 0 & & & \\ 0 & & R(\phi) & \\ 0 & & & \end{pmatrix} , \tag{2.8}$$

where $R(\phi) \in \mathrm{SO}(3)$ is a three dimensional rotation matrix. The collection of all three rotations forms a subgroup of the Lorentz group.

Now it is an important fact that the same does not hold in general for Lorentz boosts: they do not form a subgroup of the Lorentz group. This can be verified by combining two boosts [65], which for simplicity, we choose in the x-direction and z-direction with rapidities ξ_x and ξ_z, respectively,

$$\Lambda_z = \begin{pmatrix} \cosh\xi_z & 0 & 0 & -\sinh\xi_z \\ 0 & 1 & 0 & 0 \\ 0 & 0 & 1 & 0 \\ -\sinh\xi_z & 0 & 0 & \cosh\xi_z \end{pmatrix} , \quad \Lambda_x = \begin{pmatrix} \cosh\xi_x & -\sinh\xi_x & 0 & 0 \\ -\sinh\xi_x & \cosh\xi_x & 0 & 0 \\ 0 & 0 & 1 & 0 \\ 0 & 0 & 0 & 1 \end{pmatrix} . \tag{2.9}$$

Their product is given by

$$\Lambda_z\Lambda_x = \begin{pmatrix} \cosh\xi_z\cosh\xi_x & -\cosh\xi_z\sinh\xi_x & 0 & -\sinh\xi_z \\ -\sinh\xi_x & \cosh\xi_x & 0 & 0 \\ 0 & 0 & 1 & 0 \\ -\sinh\xi_z\cosh\xi_x & \sinh\xi_z\sinh\xi_x & 0 & \cosh\xi_z \end{pmatrix} , \tag{2.10}$$

which cannot be written in the symmetric form (2.7). Instead, it can be shown that the result is a boost and a rotation [66, 67],

$$\Lambda_z\Lambda_x = R(\omega)\Lambda \, . \tag{2.11}$$

where $R(\omega)$ is a three rotation. This is the origin of the celebrated *Wigner* rotation or *Thomas-Wigner* rotation (occasionally abbreviated as TWR), where the latter form is used in the literature to honour Thomas' contribution by discovering the Thomas precession [68, 69]. We will discuss its properties in detail shortly in section 2.3 below, for now we we would like to stress that Thomas-Wigner rotation is a consequence of the structure of the Lorentz group, which characterises relativistic

spacetime. The relations above show that it occurs when one is dealing with a situation that involves non-collinear boosts. Incidentally, note that the commutation relations imply that *collinear* boosts *do form* a subgroup. Collinear boosts by v_1 and v_2 are subject to the familiar formula of relativistic velocity addition[1]

$$v = \frac{v_1 + v_2}{1 + v_1 v_2} \, . \tag{2.12}$$

It is noteworthy that by itself, the Thomas-Wigner rotation is a purely kinematic effect which is independent of the dynamics of the system [71]. It has to be taken into account both in classical and quantum relativistic situations. In the context of quantum theory, Thomas-Wigner rotation gives rise to unexpected effects like the Thomas precession [68].[2] More importantly, it also gives rise to intricate entanglement relations when a quantum system is observed from different inertial frames of reference, the investigation of which is the subject of this thesis.

2.2 Wigner's little group

To discuss relativistic effects in quantum theory, we need to know how the Lorentz group is represented on the space of quantum states. This was derived in the seminal work of Wigner [74]. In the following, we give only a brief outline and summarise the results needed for the subsequent discussion; for detailed accounts see [67, 75–77] .

In the language of group theory, we are seeking to represent an element of the Lorentz group Λ by a unitary operator $U(\Lambda)$ on the Hilbert space of quantum states. Let us label basis states $|p, \sigma\rangle$ in terms of their momentum p and spin σ. Considerations based on the structure of the Lorentz group imply that the action of $U(\Lambda)$ on a basis state,

$$U(\Lambda)\,|p, \sigma\rangle = \sum_{\lambda} Q_{\lambda\sigma}(\Lambda, p)\,|\Lambda p, \lambda\rangle \ , \tag{2.13}$$

is a linear combination of states with label Λp.[3] The action of the unitary operator $U(\Lambda)$ leaves p^2, and if $p^2 > 0$, then also the sign of E, unchanged. Thus it turns out that for each p^2 a different set of operators $U(\Lambda)$ can be constructed. Since our inter-

[1] The literature on Thomas-Wigner rotation is large, see e. g. [70] for a very readable overview.

[2] By way of historical note, it is interesting that '[E]ven the cognoscenti of relativity theory (including Einstein himself!) were quite surprised' that one needed to take into account a relativistic effect to correctly characterise the hydrogen atom [72, 73].

[3] See e.g. [67] for a detailed account.

est lies in massive particles, in the following we focus on the case $p^2 = m^2 > 0$. We will denote the vectors of the representation by $|\mathbf{p}, \sigma\rangle$, where the intended meaning is that p^2 is fixed and the zeroth component E can be calculated if necessary. The notation $\Lambda\mathbf{p}$ signifies that one can supply the zeroth component, calculate the transformation and remove the zeroth component [75].

Equation (2.13) describes a group homomorphism. One can ensure that it holds by choosing Q in such a way that it leaves invariant a chosen standard momentum. For massive particles one can fix the standard momentum k to be the particle's momentum in the rest frame,

$$k = \begin{pmatrix} m \\ 0 \end{pmatrix} \ . \tag{2.14}$$

Arbitrary momenta p can be then expressed in terms of the standard momentum,

$$p = L(p)k \ , \tag{2.15}$$

where $L(p)$ is a transformation which depends on p and takes $k \mapsto p$. This implies state vectors $|\mathbf{p}, \sigma\rangle$ can be defined in terms of standard momentum states $|\mathbf{k}, \sigma\rangle$,

$$|\mathbf{p}, \sigma\rangle = U[L(p)] \, |\mathbf{k}, \sigma\rangle \ . \tag{2.16}$$

Now the Thomas-Wigner rotation is commonly explained to arise from transforming $|\mathbf{p}, \sigma\rangle$ with an arbitrary $U(\Lambda)$,

$$\begin{aligned} U(\Lambda) \, |\mathbf{p}, \sigma\rangle &= U(\Lambda) U[L(p)] \, |\mathbf{k}, \sigma\rangle \\ &= U\left[L(\Lambda p) L^{-1}(\Lambda p)\right] U(\Lambda) U[L(p)] \, |\mathbf{k}, \sigma\rangle \\ &= U[L(\Lambda p)] \, U\left[L^{-1}(\Lambda p) \Lambda L(p)\right] \, |\mathbf{k}, \sigma\rangle \ , \end{aligned} \tag{2.17}$$

where in the second line we have inserted the identity transformation of the form $L(\Lambda p)L^{-1}(\Lambda p)$ in the argument of U and in the third we used the fact we are dealing with a group homomorphism. The transformation,

$$W(\Lambda, \mathbf{p}) \equiv L^{-1}(\Lambda p) \Lambda L(p) \ , \tag{2.18}$$

is the Thomas-Wigner rotation. It leaves the standard momentum invariant, i.e. reading from right to left, Equation (2.18) describes the sequence of maps

$$W : k \mapsto p \mapsto \Lambda p \mapsto k \ , \tag{2.19}$$

The collection of all W forms a subgroup of proper ortochronous Lorentz group $L_+^\uparrow$ known as *Wigner's little group*. Now since $U(W)$ does not change k, it can only act on the spin degree of freedom. On the other hand, $U[L(\Lambda p)]$ transforms according to (2.16), leaving spin alone. We can then write Equation (2.17) as follows,

$$U(\Lambda)\,|\mathbf{p},\sigma\rangle = U[W(\Lambda,\mathbf{p})]\,|\Lambda\mathbf{p},\sigma\rangle \ . \tag{2.20}$$

Comparing with (2.13) shows this can be rewritten as

$$U(\Lambda)\,|\mathbf{p},\sigma\rangle = \sum_\lambda D_{\lambda\sigma}[W(\Lambda,\mathbf{p})]\,|\Lambda\mathbf{p},\lambda\rangle \ , \tag{2.21}$$

where D is a representation of the little group element W. For massive particles, the little group for the standard momentum is the usual group of ordinary rotations in three dimensions, $\mathrm{SO}(3)$. The corresponding representation D for spin-$1/2$ particles that we are interested in is given by $\mathrm{SU}(2)$, whose elements have the generic form

$$R_{\mathbf{n}}(\phi) = \exp\left(-\mathrm{i}\frac{\phi}{2}\boldsymbol{\sigma}\cdot\mathbf{n}\right) \ , \tag{2.22}$$

where ϕ is an angle of rotation, $\mathbf{n} = (n_x, n_y, n_z)$ a real unit vector in three dimensions and $\boldsymbol{\sigma} = (\sigma_x, \sigma_y, \sigma_z)$ denotes the three component vector of Pauli matrices.

For subsequent calculations, it is useful to obtain a representation of the little group matrix for spin-$1/2$ systems as a function of momentum and rapidity. We will follow the exposition given in [75] in finding this. The desired representation can be determined directly from expression (2.18) by writing each factor in the 2×2 representation of the Lorentz group [66], and then calculating the product.

We begin by writing the boost $L(p)$, which takes the standard momentum k to an arbitrary p, in the 2×2 representation,

$$C\left[L(p)\right] = \left(\frac{E(\mathbf{p})+m}{2m}\right)^{\frac{1}{2}} + \left(\frac{E(\mathbf{p})-m}{2m}\right)^{\frac{1}{2}} \frac{\boldsymbol{\sigma}\cdot\mathbf{p}}{|\mathbf{p}|} \ , \tag{2.23}$$

where $\mathbf{p}$ is the spatial part of p. Next, the pure Lorentz transformation $K(\Lambda)$ with rapidity ξ in the direction $\mathbf{e} = (e_x, e_y, e_z)$ takes the form

$$K(\Lambda) = \cosh\frac{\xi}{2} + \sinh\frac{\xi}{2}(\boldsymbol{\sigma}\cdot\mathbf{e}) \ . \tag{2.24}$$

Lastly, the transformation $C[L(\Lambda p)]$ is given by

$$C[L(\Lambda p)] = \left(\frac{E(\mathbf{p}')+m}{2m}\right)^{\frac{1}{2}} + \left(\frac{E(\mathbf{p}')-m}{2m}\right)^{\frac{1}{2}} \frac{\boldsymbol{\sigma}\cdot\mathbf{p}'}{|\mathbf{p}'|} \ . \tag{2.25}$$

with $\mathbf{p}'$ and $E(\mathbf{p}')$ given by Λp,

$$\begin{aligned} E(\mathbf{p}') &= E(\mathbf{p})\cosh\xi + \mathbf{p}\cdot\mathbf{e}\sinh\xi \ , \\ \mathbf{p}' &= [\mathbf{p} - (\mathbf{p}\cdot\mathbf{e})\mathbf{e}] + [E(\mathbf{p})\sinh\xi + \mathbf{p}\cdot\mathbf{e}\cosh\xi]\,\mathbf{e} \ . \end{aligned} \tag{2.26}$$

The rotation $U(\Lambda,\mathbf{p}) \equiv U[W(\Lambda,\mathbf{p})]$ we are seeking is given by the product (2.18) in the 2×2 representation,

$$U\left[W(\Lambda,\mathbf{p})\right] = C^{-1}[L(\Lambda p)]K(\Lambda)C[L(p)] \ . \tag{2.27}$$

By substituting the expressions of the three factors C^{-1}, K and C from the above equations one obtains the desired expression. We will omit the somewhat long but straightforward algebraic manipulations and display the final result,[4]

$$\begin{aligned} U(\Lambda,\mathbf{p}) =& \frac{1}{\sqrt{(E(\mathbf{p})+m)\,(E(\mathbf{p}')+m)}} \\ & \times \left\{\cosh\frac{\xi}{2}\,(E(\mathbf{p})+m) + \sinh\frac{\xi}{2}(\mathbf{p}\cdot\mathbf{e}) - \mathrm{i}\sinh\frac{\xi}{2}\boldsymbol{\sigma}\cdot(\mathbf{p}\times\mathbf{e})\right\} \end{aligned} \tag{2.28}$$

Both expressions (2.22) and (2.28) will be used in the following to describe the Thomas-Wigner rotation, but in slightly different contexts.

2.3 Properties of the Thomas-Wigner rotation

We will next review the properties of Thomas-Wigner rotation by relating it to a particular physical scenario, describing what the rotation angle depends on and what its magnitude is.

For concreteness, consider three inertial observers O, O' and O'' where O' has velocity v_1 relative to O and O'' has v_2 relative to O'. Above we learned that the combination of two boosts $\Lambda(v_1)$ and $\Lambda(v_2)$ that relates O to O'' is in general a boost and a rotation,

$$\Lambda(v_2)\Lambda(v_1) = R(\omega)\Lambda(v_3) \ , \tag{2.29}$$

[4] See [75], appendix 3 for details.

where $R(\omega)$ is the Thomas-Wigner rotation with angle ω. To an observer O, the frame of O'' appears to be rotated by ω. Perhaps the simplest formula for the angle of rotation is given by [70, 75],

$$\tan\frac{\omega}{2} = \frac{\sin\theta}{\cos\theta + D}\,, \tag{2.30}$$

where θ is the angle between two boosts or, equivalently, v_1 and v_2, and

$$D = \sqrt{\left(\frac{\gamma_1+1}{\gamma_1-1}\right)\left(\frac{\gamma_2+1}{\gamma_2-1}\right)}\,, \tag{2.31}$$

with $\gamma_{1,2} = (1-v_{1,2}^2)^{-1/2}$. The axis of rotation specified by $\hat{n} = \hat{v}_2 \times \hat{v}_1$ is orthogonal to the plane defined by v_1 and v_2. The dependence of Thomas-Wigner rotation on the angle between two boosts is shown in Figure 2.1.

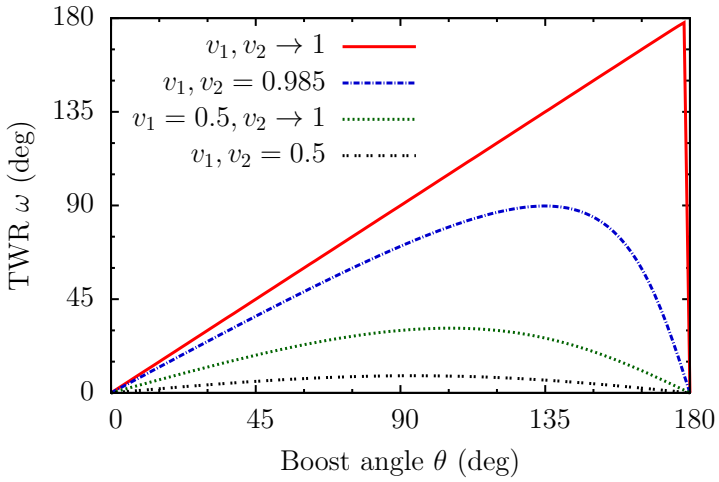

Figure 2.1. Dependence of Thomas-Wigner rotation (TWR) on the angle θ between two boosts.

Several interesting characteristics are immediately noticeable. First, for any two boosts with velocities v_1, v_2 at an angle θ, the Thomas-Wigner rotation increases with both v_1, v_2, approaching the maximum value 180° as v_1, v_2 approach the speed of light. Second, the maximum value of ω is bounded by the smaller boost. If $v_1 = 0.5$, then even if v_2 becomes arbitrarily close to the speed of light, ω will be considerably lower than in the case when both boosts approach the speed of light. Third, the angle θ at which the maximum Thomas-Wigner rotation occurs depends on the magnitudes of both v_1 and v_2. It is worth noting that ω approaches the maximum value 180° when both boosts are almost opposite and both $v_1, v_2 \to 1$. At lower velocities, maximum rotation occurs earlier. We will see below that all

these features play an important role in explaining the behaviour of entanglement in boosted frames.

The foregoing highlights the crucial fact that the Thomas-Wigner rotation is highly dependent on the *boost scenario* or *boost geometry* in question, by which we mean the specification of the magnitudes of boosts and the boost angle, denoted by the triple (v_1, v_2, θ). Alternatively, since velocities and rapidities are in one-one correspondence, the same can be specified by (ξ_1, ξ_2, θ). When working with the representation (2.28) in terms of momentum, rapidity and boost angle, we will use the quantities $(\mathbf{p}, \xi, \theta)$ for the same purpose.

For future reference, it is useful to visualise the relationships between ω, θ and the pair of boosts in a three dimensional manner. To this end, we express boosts in terms of rapidities for later convenience, (ξ_1, ξ_2), and subsume them under a single parameter by setting $\xi = \xi_1 = \xi_2$. Using Equation (2.30), ω can be expressed as a function of ξ and θ,

$$\omega = 2 \arctan \left(\frac{\sin \theta}{\cos \theta + D(\xi)} \right) , \tag{2.32}$$

where

$$D(\xi) = \frac{\cosh^2 \xi/2}{\sinh^2 \xi/2} . \tag{2.33}$$

The plot is shown in Figure 2.2, and it is related to Figure 2.1 in a simple way. We

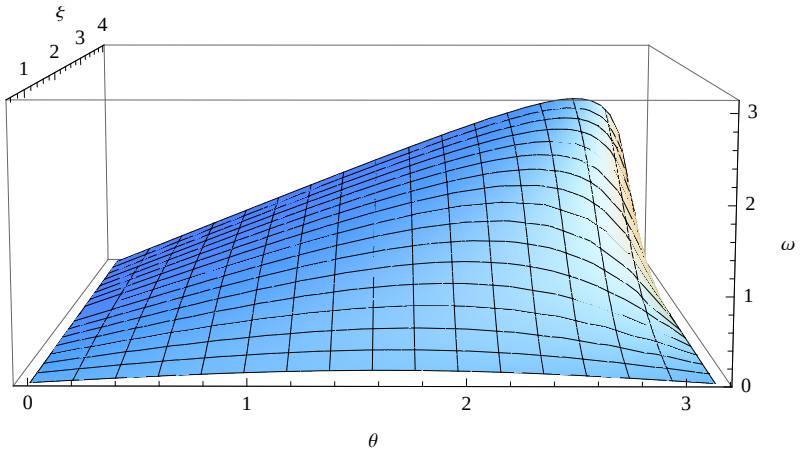

Figure 2.2. TWR ω as a function of rapidity ξ and boost angle θ. Angles are measured in radians.

saw above that the smaller boost sets a bound to the maximum Thomas-Wigner angle. Hence the curves characterising different pairs of boosts in Figure 2.1 correspond to different intersections of $\theta - \omega$-planes with a fixed $\xi = \text{const}$ and the

surface describing the Thomas-Wigner rotation.

2.4 Entanglement

Quantum entanglement has puzzled physicists since the early days of the theory and sparked a lot of discussion about the nature of the quantum world as pointed out in the Introduction. With the birth of quantum information theory, it was realised that this weird quantum phenomenon could be harnessed to power technology that goes beyond what can be achieved using any classical theory [78]. This has led to a renewed interest in the research of entanglement, whose ultimate goal is to create a comprehensive theory of the phenomenon.

Formally, while in classical theory we use the Cartesian product to combine the state spaces of n systems into the space describing the total system, in quantum theory we must use the tensor product. The total Hilbert space $\mathcal{H}$ is given by $\mathcal{H} = \otimes_{k=1}^{n} \mathcal{H}_k$, where $\mathcal{H}_k$ is the Hilbert space of a subsystem [79]. Due to the superposition principle, a generic pure state has the form,

$$|\psi\rangle = \sum_{k_1,\ldots,k_n} c_{k_1,\ldots,k_n} |i_1\rangle \otimes |i_2\rangle \otimes \cdots \otimes |i_n\rangle \ , \tag{2.34}$$

implying that in general the state cannot be written as a tensor product of the states of individual systems,

$$|\psi\rangle \neq |i_1\rangle \otimes |i_2\rangle \otimes \cdots \otimes |i_n\rangle \ . \tag{2.35}$$

Pure states that cannot be written as products are entangled, while those that can be are separable. For brevity of notation, we will use $|i_1\rangle\,|i_2\rangle \cdots |i_n\rangle$ or $|i_1, i_2, \cdots, i_n\rangle$ in the following instead of $|i_1\rangle \otimes |i_2\rangle \otimes \cdots \otimes |i_n\rangle$.

For mixed states, entanglement does not mean the system is a non-product state. Instead, a mixed state is said to be entangled if it cannot be described by a convex combination of product states [80],

$$\rho \neq \sum_{p_k} p_k \, \rho_1^k \otimes \rho_2^k \otimes \cdots \otimes \rho_n^k \ . \tag{2.36}$$

By way of illustration, in this thesis we will be mostly concerned with bipartite systems for which the most prominent examples of entangled states are the Bell

states,

$$\left|\Phi^{\pm}\right\rangle = \frac{1}{\sqrt{2}}\left(|00\rangle \pm |11\rangle\right) \ , \qquad \left|\Psi^{\pm}\right\rangle = \frac{1}{\sqrt{2}}\left(|01\rangle \pm |10\rangle\right) \ . \tag{2.37}$$

They represent the simplest yet highly non-trivial cases of entanglement. Determining whether or not, or how much a given state is entangled is in general a difficult task and subject to ongoing research. For two-level bipartite states, however, we have satisfactory measures of entanglement, which we will review next.

2.4.1 Entropy of entanglement

For pure bipartite states ρ_{AB} describing a composite system AB, one can measure the entanglement using the entropy of entanglement [81]. It is defined in terms of the von Neumann entropy of the reduced density matrix of either of the subsystem A or B,

$$S(\rho_i) = -\mathsf{Tr}(\rho_i \log \rho_i) \ , \quad i \in \{A, B\} \ , \tag{2.38}$$

where $\rho_i = \mathsf{Tr}_j(\rho_{AB})$, $i, j \in \{A, B\}$, $i \neq j$ is the state of the subsystem. If the state of the subsystem is maximally mixed, then $S(\rho_i) = 1$ and the total state is maximally entangled. If the state of the subsystem is pure, then $S(\rho_i) = 0$ and the total state is a product state. Other cases lie between these extreme values. This allows us to quantify the degree of entanglement of the total state of the system based on how mixed the state of the subsystem is.

The Bell states given above in (2.37) have $S(\rho_A) = 1$ and thus describe states of maximal entanglement.

Unfortunately, the utility of entropy is restricted to pure states. This is because entropy quantifies the degree of mixedness of the subsystem and thus it fails to correctly distinguish classical and quantum correlations for mixed states. Also, it is applicable only to bipartite systems. It is nevertheless a useful measure and we will employ it in chapter 3 to characterise the entanglement between different degrees of freedom of a single spin-$1/2$ particle.

2.4.2 Concurrence

Since the state of a two particle system is in general mixed we will use concurrence to quantify entanglement. Although initially introduced for pure states, it was later generalised to mixed states as well [82, 83]. Concurrence C of a bipartite state ρ is

defined as

$$C(\rho) = \max\{0, \lambda_1 - \lambda_2 - \lambda_3 - \lambda_4\} \ , \tag{2.39}$$

where the λ_i are square roots of eigenvalues of a non-Hermitian matrix $\rho\widetilde{\rho}$ in decreasing order and

$$\widetilde{\rho} = (\sigma_y \otimes \sigma_y)\, \rho^* \, (\sigma_y \otimes \sigma_y) \ , \tag{2.40}$$

with σ_y a Pauli matrix, is the spin-flipped state with the complex conjugate * taken in the standard basis [83].

2.5 Orbit

In order to study the behaviour of a quantum state ρ under Lorentz boosts for two particle systems, we will investigate the *orbit* of a state. By this we simply mean the set of images of a given state under a family of one or two-parameter maps. Formally, suppose we have a family of one-parameter maps $\Phi_\omega : \rho \mapsto \rho'$ where ω takes values in a subset Ω of reals. We then define the orbit $t(\omega)$ of the state ρ as the range of Φ_ω for all ω,

$$t(\omega) = \{\Phi_\omega(\rho) \mid \omega \in \Omega\} \ . \tag{2.41}$$

The same definition applies when $\Phi_{\omega,\lambda} : \rho \mapsto \rho'$ has two real parameters ω and λ. We will typically keep one parameter, e.g. λ, fixed and compute the orbit by varying ω as given in (2.41).

Chapter 3

Single particle

3.1 Introduction

In this chapter, we are going to explore the simplest nontrivial system of interest: a single massive spin-$1/2$ particle with momentum. This constitutes the qubit in the context of relativistic quantum information, studying which is a prerequisite to the understanding the behaviour of multiparticle systems.

One of the first works on the topic is the seminal paper [18], where the authors establish an intriguing phenomenon: the reduced density matrix of a massive free spin-$1/2$ particle is not covariant under Lorentz transformations, implying that spin entropy has no invariant meaning in relativity. This stands in stark contrast to the non-relativistic regime where no such phenomenon occurs. Later, [8] investigate a particle in a superposition of two different velocities and show that an observer in a relativistically boosted inertial frame sees the system entangled up to the speed of light.

Our treatment builds on these works. We begin by deriving the transformation of the particle's state under Lorentz transformations. Thereafter we will revisit two idealised models discussed in the literature. This is followed by a construction of a model involving Gaussian momenta, which we will study in a large variety of boost scenarios. We will then analyse the behaviour of entanglement from the geometric point of view, and conclude with the results obtained.

3.2 The state of a Lorentz boosted particle

We begin by calculating the general transformation of the single massive spin-$1/2$ particle state under a Lorentz boost. Consider an observer O who sees the particle

in motion with constant momentum. Using basis vectors of the form $|\mathbf{p}, \lambda\rangle$, where $\mathbf{p}$ labels momentum and $\lambda = \pm\frac{1}{2}$ is spin, we can write a generic pure state of the particle as

$$|\psi\rangle = \sum_{\lambda} \int \mathrm{d}\mu(p)\, \psi_\lambda(\mathbf{p})\, |\mathbf{p}, \lambda\rangle \ , \tag{3.1}$$

where

$$\mathrm{d}\mu(p) = \frac{1}{2E(\mathbf{p})} \mathrm{d}p_1\, \mathrm{d}p_2\, \mathrm{d}p_3 \tag{3.2}$$

is the integration measure which remains invariant under Lorentz transformations Λ [76],

$$\mathrm{d}\mu(\Lambda p) = \mathrm{d}\mu(p) \ . \tag{3.3}$$

The wave function satisfies the normalisation condition,

$$\sum_{\lambda} \int \mathrm{d}\mu(p)\, |\psi_\lambda(\mathbf{p})|^2 = 1 \ . \tag{3.4}$$

To an observer O'' who is Lorentz boosted relative to O by Λ^{-1} the state of the particle $|\psi\rangle$ appears transformed by $U(\Lambda)$. The action of $U(\Lambda)$ on a basis vector is given by

$$U(\Lambda)\, |\mathbf{p}, \lambda\rangle = \sum_{\kappa} U_{\kappa\lambda}(R(\Lambda, \mathbf{p}))\, |\Lambda\mathbf{p}, \kappa\rangle \ , \tag{3.5}$$

where $U(R) \in \mathrm{SU}(2)$ is the spin-$1/2$ representation of the Thomas-Wigner rotation R. This means that to the observer O'' the boosted spin appears rotated by $U(R)$. We calculate the transformation of the state $|\psi''\rangle = U(\Lambda)\, |\psi\rangle$ as follows,

$$\begin{aligned} \big|\psi''\big\rangle &= \sum_{\lambda} \int \mathrm{d}\mu(p)\, \psi_\lambda(\mathbf{p})\, |\Lambda\mathbf{p}\rangle \otimes \sum_{\kappa} U_{\kappa\lambda}(R(\Lambda, \mathbf{p}))\, |\kappa\rangle \\ &= \sum_{\lambda} \int \mathrm{d}\mu(\Lambda^{-1}p'')\, \psi_\lambda(\Lambda^{-1}\mathbf{p}'')\, \big|\mathbf{p}''\big\rangle \otimes \sum_{\kappa} U_{\kappa\lambda}(R(\Lambda, \Lambda^{-1}\mathbf{p}''))\, |\kappa\rangle \\ &= \sum_{\kappa} \int \mathrm{d}\mu(p)\, \psi''_\kappa(\mathbf{p})\, |\mathbf{p}, \kappa\rangle \ , \end{aligned} \tag{3.6}$$

where in the last line we have changed the dummy variable $\mathbf{p}'' \mapsto \mathbf{p}$ and signified

$$\psi''_\lambda(\mathbf{p}) = \sum_\kappa U_{\lambda\kappa}(R(\Lambda, \Lambda^{-1}\mathbf{p}))\psi_\kappa(\Lambda^{-1}\mathbf{p}) \ . \tag{3.7}$$

The above expression shows the transformation that $U(\Lambda)$ induces on the wave function of the system. Since we are interested in knowing the spin state ρ''_S according to O'', we trace out the momentum degrees of freedom,

$$\begin{aligned}
\rho''_S &= \mathsf{Tr}_P\left(|\psi''\rangle\langle\psi''|\right) = \int \mathrm{d}\mu(p)\ \langle\mathbf{p}|\psi''\rangle\langle\psi''|\mathbf{p}\rangle \\
&= \sum_{\sigma,\lambda}\int \mathrm{d}\mu(p)\int \mathrm{d}\mu(q)\int \mathrm{d}\mu(k)\,\delta^3(\mathbf{p}-\mathbf{q})\delta^3(\mathbf{k}-\mathbf{p})\psi''_\sigma(\mathbf{q})\psi''^*_\lambda(\mathbf{k})\,|\sigma\rangle\langle\lambda| \\
&= \sum_{\sigma,\lambda}\int \mathrm{d}\mu(p)\,\psi''_\sigma(\mathbf{p})\psi''^*_\lambda(\mathbf{p})\,|\sigma\rangle\langle\lambda| \ ,
\end{aligned} \tag{3.8}$$

where we used

$$\left\langle \mathbf{p}', \sigma' | \mathbf{p}, \sigma \right\rangle = 2E(\mathbf{p})\delta^3(\mathbf{p}-\mathbf{p}')\delta_{\sigma\sigma'} \ . \tag{3.9}$$

Finally, to quantify how much the entanglement has changed between the spin and momentum degrees of freedom, we calculate the von Neumann entropy

$$S(\rho''_S) = -\mathsf{Tr}(\rho''_S \log \rho''_S) \tag{3.10}$$

of the boosted spin state ρ''_S.

3.3 Two models

In this section we will discuss two models of single particle systems that have appeared in the literature and which form a prequel to our investigations in the next section.

One of the first studies of single particle systems was carried out in [18]. The authors consider a particle with mass m whose momentum wave function in the rest frame is given by a Gaussian,

$$\psi(\mathbf{p}) = \exp\left(\frac{-\mathbf{p}^2}{2\sigma^2}\right) \ , \tag{3.11}$$

where σ is width of the wave packet. This is a state of minimum uncertainty. The spin of the particle points in the z-direction, and spin and momentum degrees fac-

torise. Hence the corresponding Bloch vector has only one non-zero component $n_z = 1$ and the von Neumann entropy is zero. Suppose now the system is boosted in the x-direction with rapidity ξ, then the z-component of the new Bloch vector is described by

$$n_z' = 1 - \left(\sigma \tanh \frac{\xi}{2} \Big/ 2m\right)^2 , \tag{3.12}$$

where it has been assumed that $\sigma/m \ll 1$ and only the leading order has been taken into account. Importantly, the corresponding entropy is now generally larger than in the rest frame,

$$S \simeq t(1 - \ln t) , \tag{3.13}$$

where $t = \sigma^2 \tanh^2 \frac{\xi}{2}/8m^2$. The novel consequence is that whereas in the rest frame spin and momentum factorise, the boosted state in general shows entanglement between these two degrees of freedom. This is in contrast to the non-relativistic regime, where no such phenomenon occurs. A Galilei boosted particle with spin and momentum does not change its degree of entanglement in the boosted frame. Note that it is not the familiar kind of entanglement encountered in quantum information theory, where one typically considers entanglement between two spins or other degrees of freedom that can be represented as two level systems and thus correspond to qubits.

Figure 3.1 shows the dependency of entropy given by (3.13) for different values of parameter σ/m. We see that for $\sigma/m = 0.1$, entropy increases by approximately 10^{-2} when boosts become comparable to the speed of light. At smaller values of the parameter, $\sigma/m = 0.01$, increase of entropy is about two orders of magnitude smaller, saturating at 1.5×10^{-4} when boosts approach the speed of light. As σ/m decreases further to 0.001, saturation occurs at 2.1×10^{-6}. So while spin entropy does indeed increase for a relativistic observer, the effect is of the order of 10^{-2} or less for widths that satisfy the approximation $\sigma/m \ll 1$. This raises the question of whether larger changes of entropy might be observed if the calculation is carried through without approximation. For instance, a similar model involving origin centred Gaussian momenta for a two particle system studied in [15] without approximation displays changes from maximal to zero entanglement. While we will address this query in the next section, for now we focus on a slightly different problem: what happens if one alters the momentum state, for instance by replacing the Gaussian with a superposition of momenta?

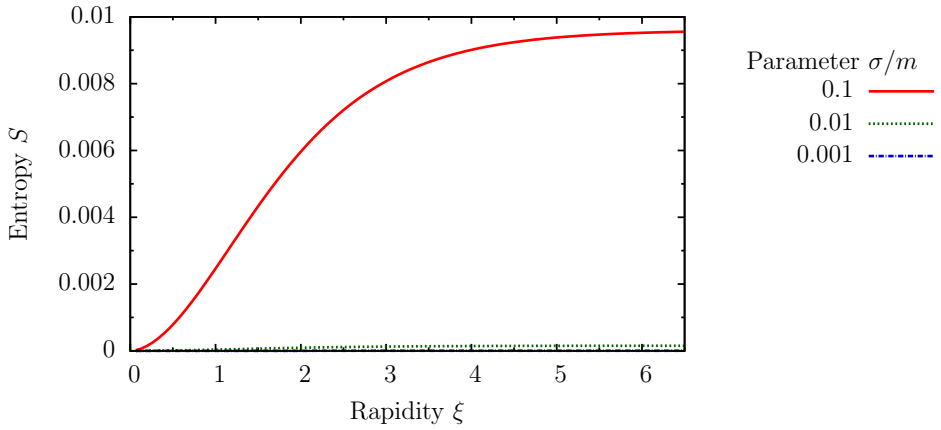

Figure 3.1. Dependence of spin entropy of a Lorentz boosted single spin-1/2 particle on rapidity. Momentum is given by an origin centered Gaussian momentum. To demonstrate the scale of entropy in different regimes, data is shown for three values of the parameter σ/m. The shape of entropy for $\sigma/m = 0.01$ and $\sigma/m = 0.001$ can be seen in detail in Figures 3.4 and 3.5 below.

This leads to the second model, which was studied in [8]. The particle is assumed to be in a superposition of two momentum eigenstates aligned in the positive and negative direction of the y-axis[1]

$$|\psi\rangle = \frac{1}{\sqrt{2}} \left(|\mathbf{p}\rangle + |-\mathbf{p}\rangle\right) |0\rangle \ . \tag{3.14}$$

Spin $|0\rangle$ points in the z-direction, with spin and momentum again in product state in the rest frame. Suppose an observer is moving in the $x-z$-plane perpendicular to the momentum of the particle, making an angle ϕ relative to the z-axis. Since the momenta of the particle and the observer are not collinear, the observer sees the spin transformed by

$$D = \sigma_0 \cos\frac{\omega}{2} + \mathrm{i} \sin\frac{\omega}{2} \left(\cos\phi\, \sigma_x - \sin\phi\, \sigma_z\right) \ , \tag{3.15}$$

where ω is the angle of Thomas-Wigner's rotation given by

$$\sin\frac{\omega}{2} = \sqrt{\frac{(\gamma_1 - 1)(\gamma_2 - 1)}{2(1 + \gamma_1\gamma_2)}} \ , \tag{3.16}$$

and $\gamma_{1,2} = (1 - (v_{1,2}/c)^2)^{-(1/2)}$. Because the Thomas-Wigner rotation is momentum dependent, spins at different momenta are rotated by the same angle but in

[1] The authors use velocity eigenstates in their treatment. We will change the notation slightly and use momenta in the following to be in line with the foregoing discussion. This changes neither the quantitative results nor the conceptual structure.

opposite directions, and the final state is described by

$$\begin{aligned}|\psi'\rangle =& \frac{1}{\sqrt{2}}|\mathbf{p}'\rangle\left(\left(\cos\frac{\omega}{2}-\mathrm{i}\sin\frac{\omega}{2}\sin\phi\right)|0\rangle+\mathrm{i}\sin\frac{\omega}{2}\cos\phi\,|1\rangle\right)\\ &+\frac{1}{\sqrt{2}}|-\mathbf{p}'\rangle\left(\left(\cos\frac{\omega}{2}+\mathrm{i}\sin\frac{\omega}{2}\sin\phi\right)|0\rangle-\mathrm{i}\sin\frac{\omega}{2}\cos\phi\,|1\rangle\right)\,,\end{aligned} \tag{3.17}$$

where $|\pm\mathbf{p}'\rangle$ stand for the boosted momenta. We see again the intriguing phenomenon encountered above, namely, that while in the rest state spin and momentum factorise, the boosted state in general contains spin-momentum entanglement. The degree of entanglement depends on the parameters ω and ϕ. In order obtain the spin state, we trace out the momentum degrees of freedom,

$$\rho''_S=\begin{pmatrix}\cos^2\frac{\omega}{2}+\sin^2\frac{\omega}{2}\sin^2\phi & \sin^2\frac{\omega}{2}\sin 2\phi\\ \sin^2\frac{\omega}{2}\sin 2\phi & \sin^2\frac{\omega}{2}\cos^2\phi\end{pmatrix}\,. \tag{3.18}$$

Let us first concentrate on the situation where $\phi=0$, which corresponds to the boost in the z-direction.[2] Then the spins lie entirely in the boost plane and the generic expression (3.18) reduces to

$$\rho''_S=\begin{pmatrix}\cos^2\frac{\omega}{2} & 0\\ 0 & \sin^2\frac{\omega}{2}\end{pmatrix}\,. \tag{3.19}$$

The eigenvalues are $\cos^2\frac{\omega}{2}$ and $\sin^2\frac{\omega}{2}$, thus the von Neumann entropy of ρ''_S takes a form,

$$S(\rho''_S)=-\cos^2\frac{\omega}{2}\,\log\left(\cos^2\frac{\omega}{2}\right)-\sin^2\frac{\omega}{2}\,\log\left(\sin^2\frac{\omega}{2}\right)\,, \tag{3.20}$$

where base of $\log$ is 2. The plot is shown in Figure 3.2 and it displays interesting phenomena. Initially when spin and momentum factorise, the spin entropy is zero. As boosts grow larger, spin and momentum become entangled, leading to monotonic increase of spin entropy. However, in contrast to the previous model, we now observe significantly larger changes of spin entropy, ranging from zero to the maximal value 1 when $\omega=\pi/2$. The latter corresponds to boosts that approach the speed of light.

Let us also consider the boost scenario where $\phi=\pi/2$. The spins are then

[2] The discussion to follow will deviate slightly from [8]. While the authors focus on the entanglement of the momentum degree of freedom, our interest lies in the behaviour of spin entanglement.

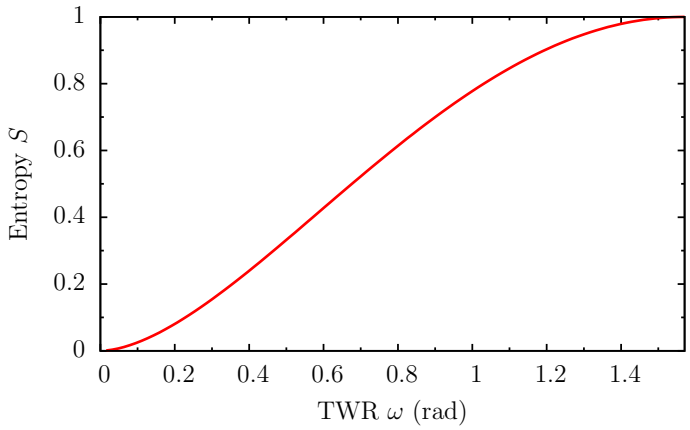

Figure 3.2. Dependence of spin entropy of a Lorentz boosted single spin-1/2 particle on the Thomas-Wigner angle. Momentum is given by a y-symmetric superposition of momentum eigenstates.

orthogonal to the boost plane and the generic state (3.18) reduces to

$$\rho_S'' = \begin{pmatrix} 1 & 0 \\ 0 & 0 \end{pmatrix} , \tag{3.21}$$

describing the pure spin z-up state. The corresponding entropy $S = 0$ at all boosts, implying that spin and momentum remain factorised for the moving observer. This is in stark disagreement with the cases examined so far, demonstrating that while boost-induced entanglement is a common phenomenon in many geometries, it is not a universal property of every boost situation.

Summarising the discussion so far, each of the models discussed contains boost scenarios which exhibit the phenomenon that spin and momentum degrees of freedom become entangled for a Lorentz boosted observer. At the same time, each contains either an approximation or idealisation, thereby limiting the results to certain parameter regimes, and raising questions of both quantitative and qualitative nature. Regarding the former, it should be asked how spin entropy is affected when origin centred Gaussians are not restricted to the approximation $\sigma/m \ll 1$. In the same vein, it should be investigated whether one would see as large changes of entropy if the superposed momenta are extended to involve wave packets of finite width instead of plain waves? In the course of pursuing these quantitative goals, we would also like to gain conceptual insight. The discrete model involving delta momenta showed two types of extreme behaviour. For spins lying in the boost plane, we saw the same qualitative behaviour—increase of entropy in the boosted frame—as the system consisting of continuous Gaussian momentum state. On the other hand, the scenario with spins orthogonal to the boost plane lacked any pres-

ence of boost-induced entanglement. This suggests that the discrete model might serve as a basis for studying the behaviour of the continuous model as well as the sensitivity of spin-momentum entanglement to the boost geometry.

3.4 The continuous model

In order to answer the queries raised at the end of the previous section, we will next develop a model of a single particle system involving continuous momenta with no approximations, and study both origin centred and symmetric states.

In analogy to the foregoing discussion, we will assume that spin and momentum are initially in the product state,

$$|\psi\rangle = \int \mathrm{d}\mu(p)\, f_0(\mathbf{p}, \mathbf{p}_0)\, |\mathbf{p}, 0\rangle \ , \tag{3.22}$$

where $|0\rangle$ denotes z-up spin and $f_0(\mathbf{p}, \mathbf{p}_0)$ signifies a superposition of Gaussian distributions centred at $\pm\mathbf{p}_0 = (\pm p_{x0}, p_{y0}, p_{z0})$,

$$f_0(\mathbf{p}, \mathbf{p}_0) = [N(\sigma)]^{-\frac{1}{2}} \left(g(\mathbf{p}, \mathbf{p}_0) + g(\mathbf{p}, -\mathbf{p}_0)\right) \ , \tag{3.23}$$

with $N(\sigma)$ the normalisation and $g(\mathbf{p}, \mathbf{p}_0)$ a Gaussian of width σ

$$g(\mathbf{p}, \mathbf{p}_0) = \exp\left(\frac{(p_x - p_{x0})^2}{2\sigma^2}\right) \exp\left(\frac{(p_y - p_{y0})^2}{2\sigma^2}\right) \exp\left(\frac{(p_z - p_{z0})^2}{2\sigma^2}\right) \ . \tag{3.24}$$

In order to compare with the models above, we will consider two boost scenarios, in the y-direction and in the z-direction. In the former case the unit vector in the boost direction is $\mathbf{e} = (0, 1, 0)$, hence the boost matrix $\Lambda_y \equiv \Lambda_y(\xi)$ given by (2.7) is

$$\Lambda_y = \begin{pmatrix} \cosh\xi & 0 & \sinh\xi & 0 \\ 0 & 1 & 0 & 0 \\ \sinh\xi & 0 & \cosh\xi & 0 \\ 0 & 0 & 0 & 1 \end{pmatrix} \ . \tag{3.25}$$

In the latter case the unit vector is $\mathbf{e} = (0, 0, 1)$ and we have $\Lambda_z \equiv \Lambda_z(\xi)$,

$$\Lambda_z = \begin{pmatrix} \cosh\xi & 0 & 0 & \sinh\xi \\ 0 & 1 & 0 & 0 \\ 0 & 0 & 1 & 0 \\ \sinh\xi & 0 & 0 & \cosh\xi \end{pmatrix} \ . \tag{3.26}$$

To calculate the boosted spin state given in Equation (3.8), we need the unitary representation of the Thomas-Wigner rotation $U(\Lambda, \mathbf{p})$. We write the particles' three momentum in Cartesian coordinates, $\mathbf{p} = (p_x, p_y, p_z)$ and $v_1 = |\mathbf{p}|/E(\mathbf{p})$. Then in case boost is in the y-direction, the generic expression for $U(\Lambda, \mathbf{p})$ given in (2.28) takes the form,

$$U(\Lambda_y, \mathbf{p}) = \begin{pmatrix} \delta & \nu \\ \nu & \delta^* \end{pmatrix} , \tag{3.27}$$

with

$$\delta = \sqrt{\frac{E+m}{E''+m}} \left(\cosh \frac{\xi}{2} + \frac{p_y - \mathrm{i}p_x}{E+m} \sinh \frac{\xi}{2} \right) ,$$

$$\nu = \frac{p_z}{\sqrt{(E+m)(E''+m)}} \sinh \frac{\xi}{2} , \tag{3.28}$$

where $\xi = \operatorname{arctanh} v_2$ is the rapidity of the boost in the y-direction, and

$$E'' = E \cosh \xi + p_y \sinh \xi . \tag{3.29}$$

By substituting into the expression (3.8), we obtain the traced out spin state,

$$\rho''_S(\xi) = \int \mathrm{d}\mu(p)\, \rho''(\xi, \Lambda_y^{-1}\mathbf{p}) \left| f_0 \left(\Lambda_y^{-1}\mathbf{p}, \mathbf{p}_0 \right) \right|^2 . \tag{3.30}$$

with

$$\rho''(\xi, \mathbf{p}) = \begin{pmatrix} |\delta|^2 & \delta\nu^* \\ \delta^*\nu & |\nu|^2 \end{pmatrix} . \tag{3.31}$$

In a similar fashion, we calculate $U(\Lambda, \mathbf{p})$ for the boost in the z-direction,

$$U(\Lambda_z, \mathbf{p}) = \begin{pmatrix} \alpha & \beta(p_x - \mathrm{i}p_y) \\ -\beta(p_x + \mathrm{i}p_y) & \alpha \end{pmatrix} , \tag{3.32}$$

where we have signified

$$\alpha = \sqrt{\frac{E+m}{E''+m}} \left(\cosh \frac{\xi}{2} + \frac{p_z}{E+m} \sinh \frac{\xi}{2} \right) ,$$

$$\beta = \frac{1}{\sqrt{(E+m)(E''+m)}} \sinh \frac{\xi}{2} , \tag{3.33}$$

and ξ is the rapidity of the boost in the z-direction, with

$$E'' = E\cosh\xi + p_z\sinh\xi\ . \tag{3.34}$$

Next, substituting into (3.8), we get the traced out spin state,

$$\rho''_S(\xi) = \int \mathrm{d}\mu(p)\,\rho''(\xi,\Lambda_z^{-1}\mathbf{p})\left|f_0\left(\Lambda_z^{-1}\mathbf{p},\mathbf{p}_0\right)\right|^2\ . \tag{3.35}$$

where

$$\rho''(\xi,\mathbf{p}) = \begin{pmatrix} \alpha^2 & -\alpha\beta\left(p_x - \mathrm{i}p_y\right) \\ -\alpha\beta\left(p_x + \mathrm{i}p_y\right) & \beta^2\left(p_x^2 + p_y^2\right) \end{pmatrix}\ . \tag{3.36}$$

To quantify entanglement between spin and momentum we compute the von Neumann entropy of ρ''_S. Unfortunately, neither of the expressions (3.30) or (3.35) can be integrated analytically when no approximations are made, so we will resort to numerical methods. The code that has been used to obtain the numerical results in the following sections is described in appendix A.

3.4.1 Origin centred Gaussian momenta

We will first return to examine the first model which was treated in terms of analytic approximation above in section 3.3. The system consists of an origin centred Gaussian momentum and constant spin field in the z-direction, with spin and momentum factorising in the rest frame. The particle's state in the rest frame is given by (3.22) with $\mathbf{p}_0 = 0$ and boost is in the y-direction. The plots comparing the results of numerical computation with the ones obtained analytically by approximation (3.13), cf. Figure 3.1, are depicted in Figures 3.3, 3.4 and 3.5. We see that while there is a slight quantitative difference between the analytical and numerical results, they are in good agreement on the the qualitative behaviour of spin entropy in different scales of parameter σ/m.

Since our numerical treatment is not restricted to narrow distributions, we will next attend to the question of what happens if the width of Gaussian lies in the regimes $\sigma/m = 1$ and $\sigma/m = 4$ studied in [15]. We will also generalise the model in another way. While the origin centred Gaussians provide interesting insight into relativistic entanglement, they represent a special case. As is evident in Figure 2.1, the geometry of the Thomas-Wigner rotation is much richer. Boosts at smaller angles tend to result in less Thomas-Wigner rotation, while larger boost angles produce larger rotation angles; and the magnitude of either boost plays a role as well.

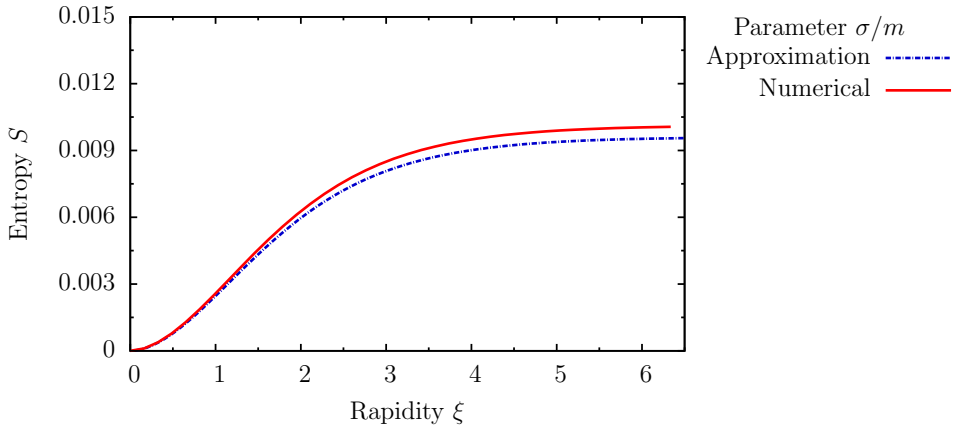

Figure 3.3. Comparison of dependence of spin entropy on rapidity obtained by numerical computation (red) and analytic approximation (blue). Momentum is given by origin centred Gaussian with $\sigma/m = 0.1$.

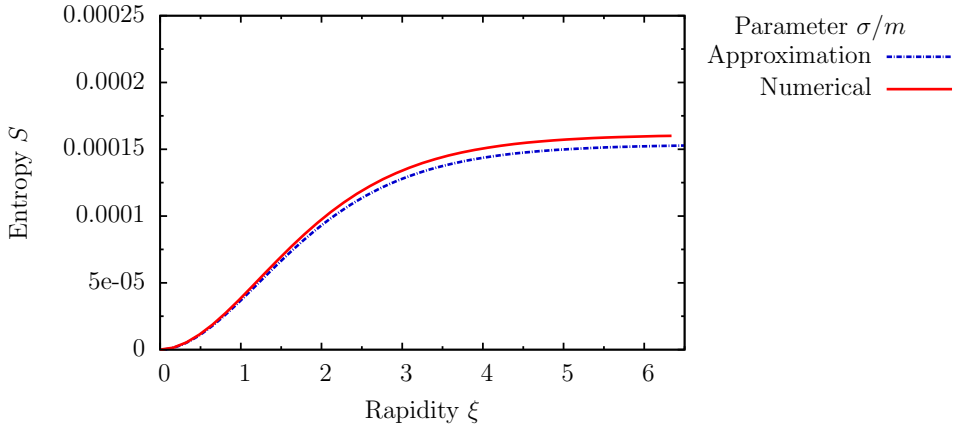

Figure 3.4. Comparison of dependence of spin entropy on rapidity obtained by numerical computation (red) and analytic approximation (blue). Momentum is given by origin centred Gaussian with $\sigma/m = 0.01$.

This suggests that the behaviour of entanglement also depends on whether the particle is moving in the same direction as the observer, or in the opposite direction. In order to study this dependency, we will consider three different boost scenarios as follows. In the first, the particle's state in the rest frame has a momentum component in the same direction as the boost in the y-direction, $\mathbf{p}_0 = (0, 4, 0)$. The second scenario involves the origin centred momentum with $\mathbf{p}_0 = (0, 0, 0)$. Thirdly, we consider the situation where the momentum component is opposite to the direction of boost, $\mathbf{p}_0 = (0, -4, 0)$. The results for $\sigma/m = 1$ and $\sigma/m = 4$ are plotted in Figures 3.6 and 3.7, respectively.

While all the scenarios show the qualitative pattern already encountered in the model obtained by analytic approximation, it is intriguing that the increase of en-

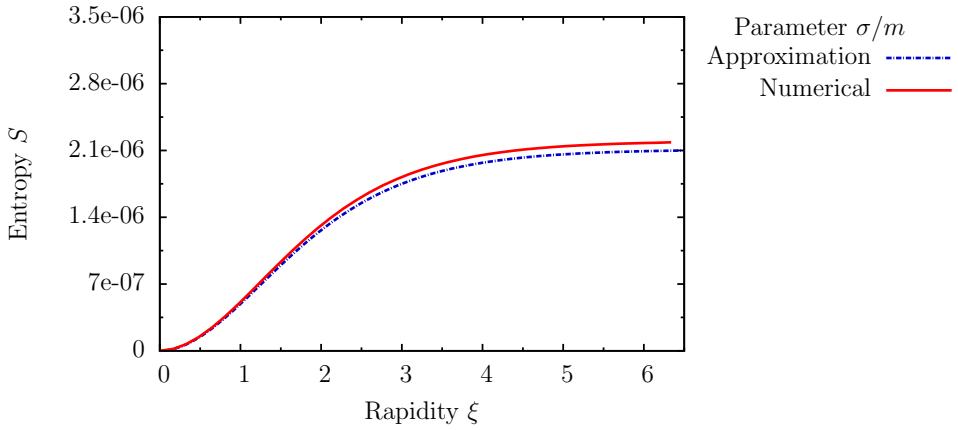

Figure 3.5. Comparison of dependence of spin entropy on rapidity obtained by numerical computation (red) and analytic approximation (blue). Momentum is given by origin centred Gaussian with $\sigma/m = 0.001$.

tropy is significantly larger, ranging between 0.1 and 0.8. We also discern a distinctive dependence on whether the particle's initial velocity is in the same or the opposite direction as the boost: spin entropy is largest if they are opposite and lowest if they coincide. Thirdly, the increase of spin entropy depends on the width of the momentum distribution. Gaussians with larger widths result in higher spin entropy.

So far we have assumed that the spin field of the system is orthogonal to the direction of boost. Let us next study the case where the spin field and the boost both point in the same direction. With no restriction to generality we choose both to be aligned along the z-direction. In analogy to the above, we consider three scenarios with different initial momenta, $\mathbf{p}_0 = (0, 0, 4)$, at the origin, $\mathbf{p}_0 = (0, 0, 0)$, and opposite to the direction of boost, $\mathbf{p}_0 = (0, 0, -4)$. The results for $\sigma/m = 1$ and $\sigma/m = 4$ are shown in Figures 3.8 and 3.9. Amongst the non-idealised models, these display the largest increase of entropy so far. For a Gaussian of given width, entropy always saturates at a higher level if spin field points in the same direction as boost. Also, for the first time entropy reaches the maximum value 1, this occurs for $\sigma/m = 4$ and $\mathbf{p}_0 = (0, 0, -4)$. The system with $\sigma/m = 1$ and the same momentum achieves a near maximum value at 0.97 as well.

3.4.2 Symmetric Gaussian momenta

We will next turn to the second idealised model considered above, which involves superposed momenta in opposite directions. This can be generalised along same lines as the origin centred system. While the idealised model in [8] assumed that the

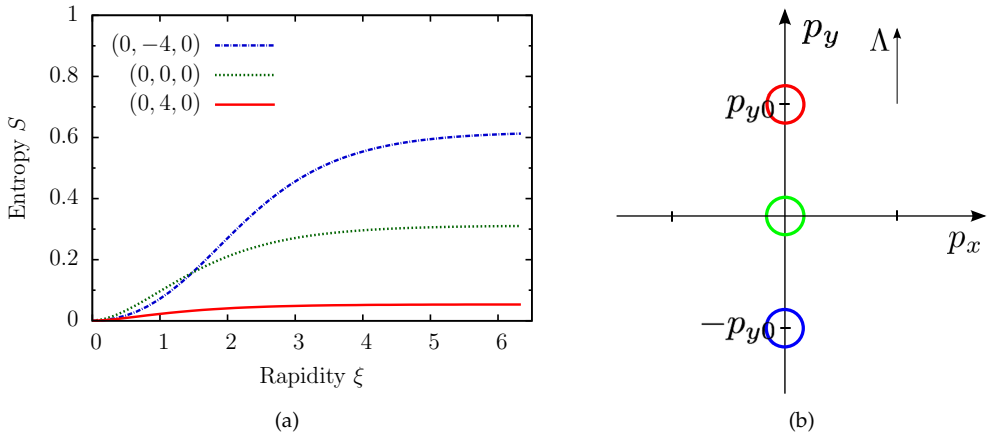

Figure 3.6. Spin entropy and boost geometry of a single particle with origin centred Gaussian momenta for $\sigma/m = 1$. Boost $\Lambda \equiv \Lambda_y(\xi)$ is in the positive y-direction. (a) Entropy of Gaussian centred at $(0,-4,0)$ is shown blue, $(0,0,0)$ green and $(0,4,0)$ red. (b) Schematic representation of Gaussians in the rest frame, centered at different $\mathbf{p}_0 = (0, p_{y0}, 0)$ in the momentum space. The width of the Gaussians shown is not to scale.

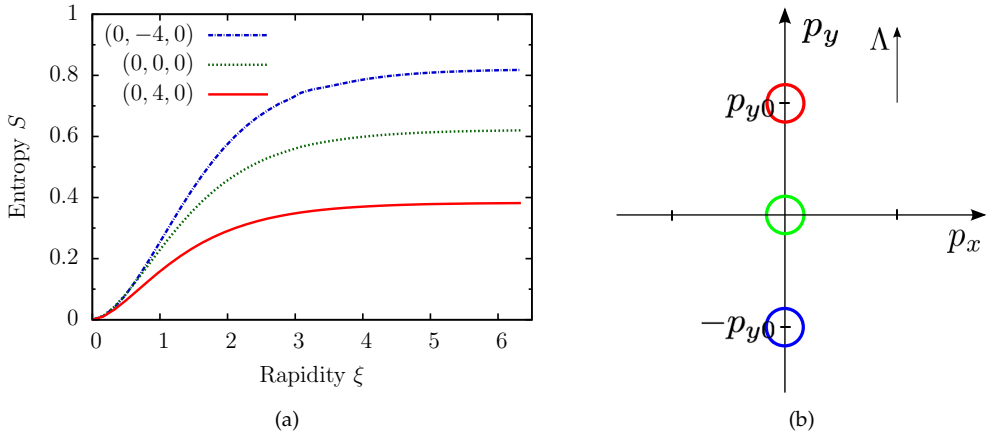

Figure 3.7. Spin entropy and boost geometry of a single particle with origin centred Gaussian momenta for $\sigma/m = 4$. Boost $\Lambda \equiv \Lambda_y(\xi)$ is in the positive y-direction. (a) Entropy of Gaussian centred at $(0,-4,0)$ is shown blue, $(0,0,0)$ green and $(0,4,0)$ red. (b) Schematic representation of Gaussians in the rest frame, centered at different $\mathbf{p}_0 = (0, p_{y0}, 0)$ in the momentum space. The width of the Gaussians shown is not to scale.

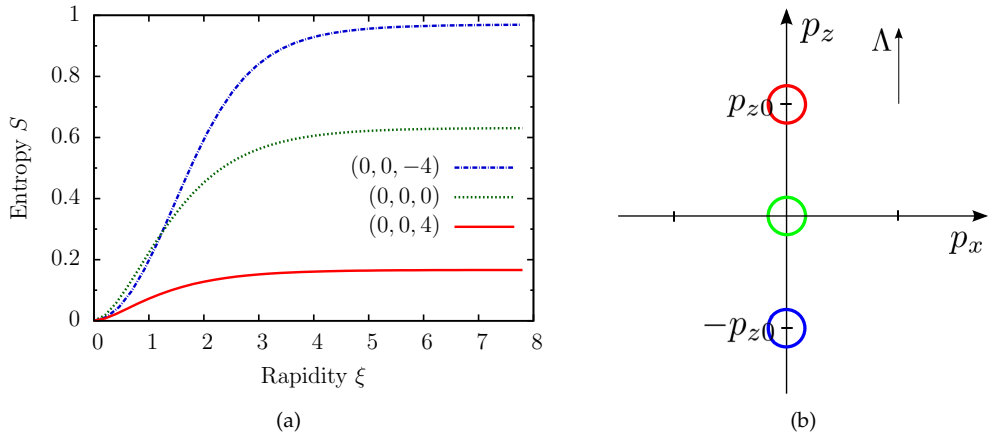

Figure 3.8. Spin entropy and boost geometry of a single particle with origin centred Gaussian momenta for $\sigma/m = 1$. Boost $\Lambda \equiv \Lambda_z(\xi)$ is in the positive z-direction. (a) Entropy of Gaussian centred at $(0, 0, -4)$ is shown blue, $(0, 0, 0)$ green and $(0, 0, 4)$ red. (b) Schematic representation of Gaussians in the rest frame, centered at different $\mathbf{p}_0 = (0, 0, p_{z0})$ in the momentum space. The width of the Gaussians shown is not to scale.

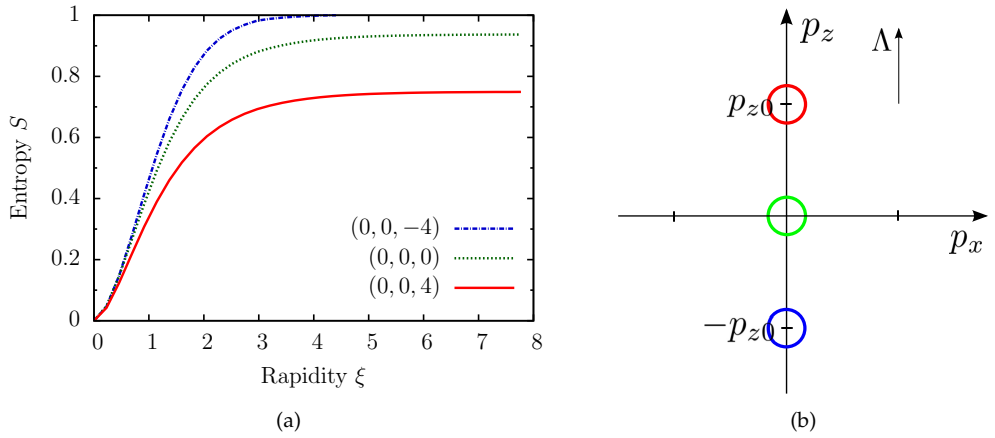

Figure 3.9. Spin entropy and boost geometry of a single particle with origin centred Gaussian momenta for $\sigma/m = 4$. Boost $\Lambda \equiv \Lambda_z(\xi)$ is in the positive z-direction. (a) Entropy of Gaussian centred at $(0, 0, -4)$ is shown blue, $(0, 0, 0)$ green and $(0, 0, 4)$ red. (b) Schematic representation of Gaussians in the rest frame, centered at different $\mathbf{p}_0 = (0, 0, p_{z0})$ in the momentum space. The width of the Gaussians shown is not to scale.

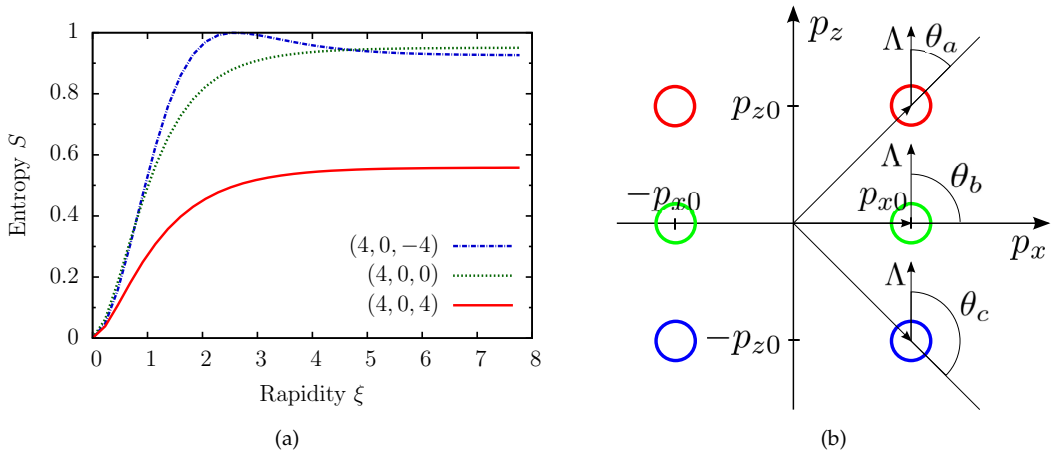

(a) (b)

Figure 3.10. Spin entropy and boost geometry of a single particle with x-symmetric Gaussian momenta for $\sigma/m = 1$. Boost $\Lambda \equiv \Lambda_z(\xi)$ is in the positive z-direction. (a) Entropy of Gaussians centred at $(\pm 4, 0, -4)$ is shown blue, $(\pm 4, 0, 0)$ green and $(\pm 4, 0, 4)$ red. (b) Schematic representation of Gaussians in the rest frame, centered at different $\pm\mathbf{p}_0 = (\pm\mathbf{p}_{x0}, 0, p_{z0})$ in the momentum space. Boost angles $\theta_a < 90°$, $\theta_b = 90°$ and $\theta_c > 90°$ correspond to rest frame momenta $\mathbf{p}_0$ and are shown for one peak of each state. The width of the Gaussians shown is not to scale.

particle's velocity and boost are orthogonal, we have learned that this represents a special case. The behaviour of entanglement is sensitive to the boost angle θ. To study this dependency for superposed momenta, we will again consider three cases, in all of which spins are assumed to lie entirely in the boost plane. The reason is that we would like to study maximal changes of entropy, which as we observed above occurred for spin fields aligned to the direction of boost.

In the first scenario, the particle has a momentum component p_{z0} in the same direction as the boost in the z-direction. Thus the centers of Gaussian wave packets at $\pm\mathbf{p}_0 = (\pm p_{x0}, 0, p_{z0})$ make angles of $\theta_a < 90°$ to the direction of boost, see Figure 3.10b. In the second scenario, the initial momenta $\pm\mathbf{p}_0 = (\pm p_{x0}, 0, 0)$ are orthogonal to the boost, so $\theta_b = 90°$. In the third, the particle's momentum has a p_{z0} component opposite to the boost direction, hence $\theta_c > 90°$ and $\pm\mathbf{p}_0 = (\pm p_{x0}, 0, -p_{z0})$. Plots for $\sigma/m = 1$ and $\sigma/m = 4$ are shown in Figures 3.10 and 3.11.

Curiously, although for $\sigma/m = 4$ the entropy saturates at a marginally higher value than for the origin centred momenta, the increase is quite pronounced for $\sigma/m = 1$. The latter reveals strong dependence of entropy increase on the boost angle. It also shows novel behaviour. When the particle's velocity has a component in the direction opposite to the boost, i.e. when boost angle $\theta > 90°$, entropy reaches the maximum value 1 at $\xi = 2.3$ and decreases thereafter as boosts grow larger, saturating at a lower than maximum value when boosts approach the speed of light.

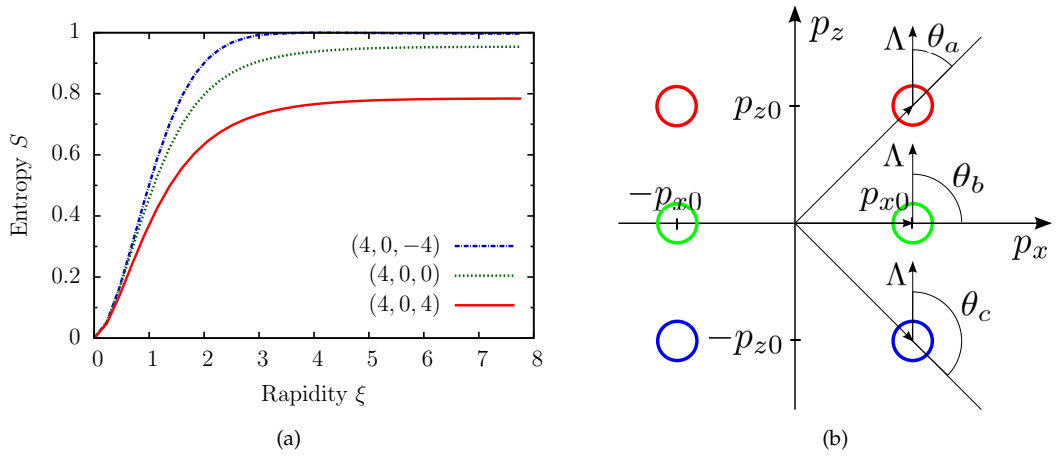

Figure 3.11. Spin entropy and boost geometry of a single particle with x-symmetric Gaussian momenta for $\sigma/m = 4$. Boost $\Lambda \equiv \Lambda_z(\xi)$ is in the positive z-direction. (a) Entropy of Gaussians centred at $(\pm 4, 0, -4)$ is shown blue, $(\pm 4, 0, 0)$ green and $(\pm 4, 0, 4)$ red. (b) Schematic representation of Gaussians in the rest frame, centered at different $\pm\mathbf{p}_0 = (\pm\mathbf{p}_{x0}, 0, p_{z0})$ in the momentum space. Boost angles $\theta_a < 90°$, $\theta_b = 90°$ and $\theta_c > 90°$ correspond to rest frame momenta $\mathbf{p}_0$ and are shown for one peak of each state. The width of the Gaussians shown is not to scale.

The latter suggests that such a pattern might become even more marked at larger boost angles. To verify this hypothesis, we compute two scenarios for the system with $\sigma/m = 1$, where in the first the particle's momentum in the rest frame is described by $\pm\mathbf{p}_0 = (\pm 7.05, 0, -21.20)$, which corresponds to the boost angle and the particle's speed $(\theta_e = 161°, v_1 = 0.999)$. The second involves momentum $\mathbf{p}_0 = (\pm 17.13, 0, -98.5)$ or equivalently $(\theta_f = 170°, v_1 = 0.99995)$. The results shown in Figure 3.12 indeed confirm the pattern, displaying remarkable decrease of entanglement as rapidity crosses a critical value at about 2.4 when $\theta = 161°$, and at about 2.6 when $\theta = 170°$. Also, entropy saturates at a significantly lower value, at about 0.15 for the larger boost angle, compared to 0.41 when the angle is smaller.

3.5 Momenta as control qubits

In the foregoing discussion we have repeatedly said that spin rotations are momentum dependent. It turns out that the sense of dependence at work here can be made more precise using concepts from quantum information theory. The analogy we will describe was first mentioned in [84].

In quantum computation, a prominent multi-qubit gate is the so-called controlled NOT or CNOT gate [85]. The gate has two input qubits, where the first is called the *control* qubit and the second is the *target* qubit. The action of the gate is to change the target qubit depending on the value of the control qubit. If the control

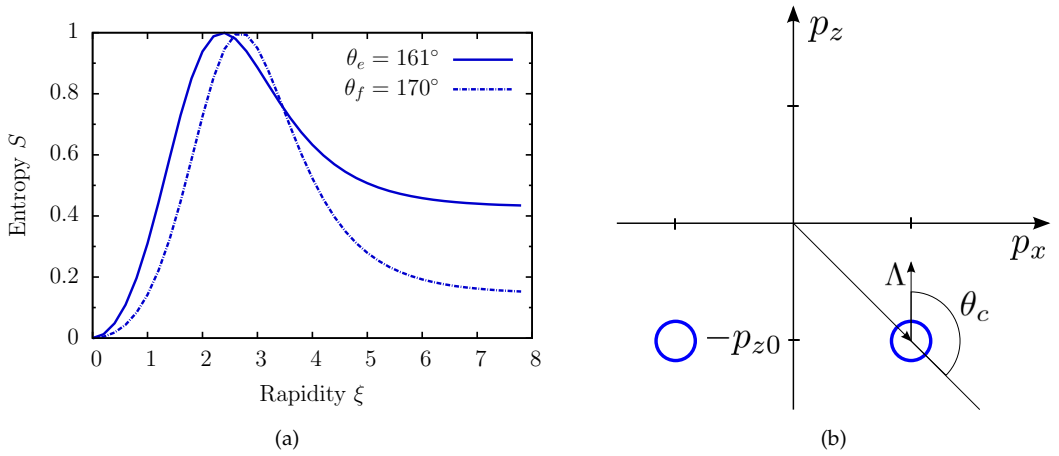

(a) (b)

Figure 3.12. Spin entropy and boost geometry of a single particle with x-symmetric Gaussian momenta for $\sigma/m = 1$ and large boost angles. Boost $\Lambda \equiv \Lambda_z(\xi)$ is in the positive z-direction. (a) Entropy for two boost geometries ($\theta_e = 161°, v_1 = 0.999$) and ($\theta_f = 170°, v_1 = 0.99995$). (b) Schematic representation of Gaussians in the rest frame, centered at different $\pm\mathbf{p}_0 = (\pm\mathbf{p}_{x0}, 0, p_{z0})$ in the momentum space. Boost angle $\theta_c > 90°$ corresponds to rest frame momenta $\mathbf{p}_0$ and is shown for one peak of the state. The width of the Gaussians shown is not to scale.

qubit is set to 0, then the target qubit is left alone. If the control qubit is 1, then the target qubit is flipped. This can be described in equations,

$$|00\rangle \mapsto |00\rangle \ , \quad |01\rangle \mapsto |01\rangle \ , \quad |10\rangle \mapsto |11\rangle \ , \quad |11\rangle \mapsto |10\rangle \ . \tag{3.37}$$

Alternatively, it can be written in the operator form,

$$U_{\text{CN}} = \mathbf{1} \otimes |0\rangle\langle 0| + \sigma_x \otimes |1\rangle\langle 1| \ , \tag{3.38}$$

where σ_x is the Pauli operator which performs spin flip in the computational basis. The significance of CNOT for quantum computation lies in the universality result, according to which any multiple qubit logic gate may be composed from CNOT and single qubit gates [85].

A natural extension of the CNOT gate is a controlled-U gate. It has a single control qubit and n target qubits, which are transformed by U depending on the value of the control qubit. It can be represented as an operator,

$$U_{\text{CU}} = \mathbf{1} \otimes |0\rangle\langle 0| + U^{\otimes n} \otimes |1\rangle\langle 1| \ , \tag{3.39}$$

where $U^{\otimes n}$ is an operator on n qubits. CNOT appears as a special case when there is only a single target qubit and $U = \sigma_x$.

Now it is pointed out in [84] that we can conceive of a Lorentz boost as a kind of controlled operation in analogy to controlled-U operations. Momenta play the

role of control qubits and spins are the target qubits. Boosting generates a unitary operation, the Thomas-Wigner rotation, on the target qubits, i.e. the spins. For instance, when an idealised system whose momenta are given by the superposition $(|\mathbf{p}_0\rangle + |\mathbf{p}_1\rangle)$ is boosted with $\Lambda \equiv \Lambda(\xi)$, the state undergoes a transformation described by an operator

$$U(\Lambda, \mathbf{p}_0) \otimes |\Lambda\mathbf{p}_0\rangle\langle\mathbf{p}_0| + U(\Lambda, \mathbf{p}_1) \otimes |\Lambda\mathbf{p}_1\rangle\langle\mathbf{p}_1| \ . \tag{3.40}$$

This can be generalised to finitely many momenta,

$$\sum_{\mathbf{p}} U(\Lambda, \mathbf{p}) \otimes |\Lambda\mathbf{p}\rangle\langle\mathbf{p}| \ , \tag{3.41}$$

and formally also to continuous momenta,

$$\int \mathrm{d}\mu(p)\, U(\Lambda, \mathbf{p}) \otimes |\Lambda\mathbf{p}\rangle\langle\mathbf{p}| \ . \tag{3.42}$$

However, in the subsequent discussion the latter forms will not be used. For us the main import lies in the conceptualisation of momenta as control qubits. This, accompanied with the geometric view of how the boosts affect spin entropy in the next section, forms the basis of the conceptual framework that we will use to explain the phenomena both for the single and two particle systems.

3.6 The geometric point of view

To understand the behaviour of entanglement, it is useful to adopt a geometric perspective. One can think of vectors $|\mathbf{p}, \lambda\rangle$ in Hilbert space as vector fields $\lambda(\mathbf{p})$ on the mass-shell of a particle with mass m [67]. Whereas the geometric picture applies to both the continuous and discrete case, the essential qualitative behaviour can be understood in terms of a discrete model of four spins in Figure 3.13 which we will use from now on. The spin state ρ''_S, found by tracing out momentum, can be viewed as taking a (possibly infinite) convex sum of spin projection operators $|\lambda(\mathbf{p})\rangle\langle\lambda(\mathbf{p})| = \Pi_\lambda(\mathbf{p})$ over the support of the Gaussian. In our discrete example this reduces to

$$\begin{aligned}\rho''_S = \alpha(-\mathbf{p}_2)\Pi_\lambda(-\mathbf{p}_2) + \alpha(-\mathbf{p}_1)\Pi_\lambda(-\mathbf{p}_1) \\ + \alpha(\mathbf{p}_1)\Pi_\lambda(\mathbf{p}_1) + \alpha(\mathbf{p}_2)\Pi_\lambda(\mathbf{p}_2) \ ,\end{aligned} \tag{3.43}$$

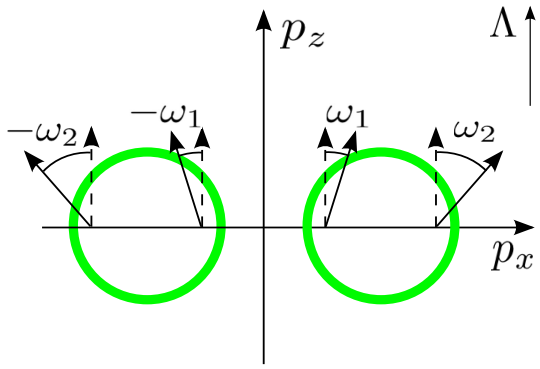

Figure 3.13. In the rest frame, the Gaussian spin field (circle) is given by a constant field of z-up spins (dashed). In the boosted frame, each spin $\lambda(\mathbf{p}_i)$ of the field is Thomas-Wigner rotated by a particular $\omega_i \equiv \omega(\mathbf{p}_i)$. For a fixed boost ξ, rotation angle increases with $|\mathbf{p}_i|$. Boost $\Lambda \equiv \Lambda_z(\xi)$ is in the positive z-direction.

where the coefficients satisfy $\sum_i \alpha(\mathbf{p}_i) = 1$.

It is now relatively easy to see how entanglement between spin and momentum arises. Suppose the rest frame state is given by a product of spin and momentum as in Equation (3.22). This corresponds to a constant spin (operator) field in the momentum space, depicted by dashed arrows in Figure 3.13. When the field is Lorentz boosted, each individual spin $\lambda(\mathbf{p})$ in Figure 3.13 is rotated by a different Thomas-Wigner angle ω_i, whose magnitude is determined by $|\mathbf{p}_i|$, boost ξ and the angle θ between $\mathbf{p}$ and the boost direction. Hence after the boost each spin in the momentum space points in a different direction and the total state does not factorize any more: spin and momentum have become entangled. This means the spin operators $\Pi_\lambda(\mathbf{p}_i)$ on the Bloch sphere in Figure 3.14 also point to different directions and summing them up yields in general a mixed state ρ''_S. Combined with the

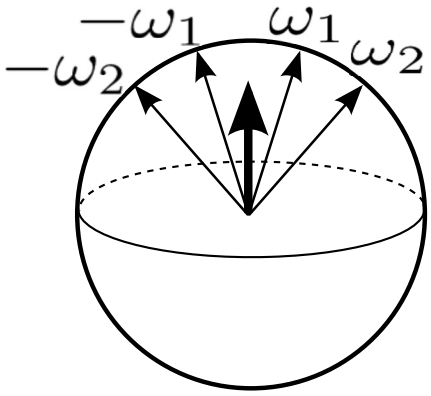

Figure 3.14. Tracing out momentum amounts to forming a convex sum of spins $\Pi_\lambda(\mathbf{p}_i)$ that are Thomas-Wigner rotated by $\omega_i \equiv \omega(\mathbf{p}_i)$, here represented on the Bloch sphere. The resulting spin state ρ''_S (boldface arrow) is generally mixed.

properties of Thomas-Wigner rotation, we can now explain all the qualitative features of spin-momentum entanglement shown in the Figures of sections 3.4.1 and 3.4.2—saturation, its level, and whether or not there is a bump.

3.7 Discussion

Saturation was first noted in [15] where the authors study two spin-$1/2$ particles in a Bell state with a Gaussian product momentum as an initial state. Our results confirm that saturation occurs for a single particle with a Gaussian product momentum. The reason can be traced back to the properties of Thomas-Wigner rotation. Given any two boosts at a particular angle θ, when both boosts approach the speed of light, Thomas-Wigner rotation asymptotically approaches a particular maximum value ω_m (see, for example, Figure 2.1). This implies that each individual spin of the field asymptotically approaches a particular $\mathbf{p}$-dependent maximum rotation angle $\omega_m(\mathbf{p})$ as both boosts approach the speed of light. Since entropy is a monotonic function of spin, its behaviour follows the same pattern: entropy approaches asymptotically a particular level as rapidity grows arbitrarily large.

Although this explains why saturation occurs, it requires some qualification to account for why saturation reaches *different levels* for Gaussians initially centered at different p_{z0}. This originates in the fact that the maximum value of Thomas-Wigner rotation ω_m depends on the angle θ between two boosts. In our boosting schemes depicted above, the boost angle θ is determined by the center $\mathbf{p}_0$ of the Gaussian wave packet. However, specifying θ amounts to setting a bound on the maximum value of rotation, that is, specifying ω_m. The latter, in turn, sets a bound to the maximum rotation of spin operators on the Bloch sphere in Figure 3.14 or, equivalently, entropy. As a result, for two Gaussians with angles θ_a and θ_b, where $\theta_a < \theta_b$, entanglement saturates at a lower level for θ_a than for θ_b.

For boost geometries with $\theta \geq 90^\circ$ entanglement initially reaches a maximum value and thereafter saturates at a lower value. It might seem that this contradicts what we just said about saturation. In light of the spin field picture, however, the bump is to be expected in such boost geometries. By way of example, consider the scenario with $v_1 = 0.999$, $\theta = 161^\circ$ in Figure 3.12. Initially, as rapidity starts to grow, spins start to rotate in opposite directions at either Gaussian and so entanglement starts to increase in line with the explanation above. At $\xi = 2.4$, the effective spin of either Gaussian in Figure 3.14 has rotated by $|\omega| = 90^\circ$, hence the spins of the left and right Gaussians become orthogonal and entanglement attains the maximum

value 1. Now as rapidity increases further, spins 'over-rotate', becoming again non-orthogonal and spin entropy starts to decrease. As rapidity grows even larger, the Thomas-Wigner rotation attains a maximum value ω_m and entropy saturates at a value less than 1. The larger the θ, the larger is ω_m and the lower is the final level of saturation as is seen in Figure 3.12. In the limiting case of large boosts $v_1, v_2 \to 1$, narrow Gaussians, $\sigma \to 0$ and boost angles $\theta \to 180^\circ$, the boosted state approaches a product state and entanglement vanishes.

3.8 Conclusion

In this chapter, we studied the behaviour of a single massive spin-$1/2$ particle under Lorentz boosts. We confirm the general conclusion that boosts change the entanglement of the spin and momentum degrees of freedom, implying that the spin state transforms in general non-trivially for a moving observer. While previous works in the literature focussed on systems involving various idealisations, the importance of this study lies in generalising the treatment in three ways, which to the best of our knowledge had not been done before. First, we have extended the discussion to realistic systems described by Gaussian wavepackets with finite width. We have secondly generalised the analysis to geometries involving a large variety of boost angles and established that the behaviour of entanglement is sensitive to the boost geometry. Maximal entanglement between spin and momentum components of a single particle can be achieved with sub-luminal boosts. However, due to rich geometric setting, boost parameters must be chosen carefully as too large boosts lead to deterioration of entanglement. The effect persists for wave packets. Lastly, we have provided a natural geometric explanation, in terms of which all the diverse qualitative features of entanglement behaviour of systems with discrete and continuous momenta can be understood in a simple manner.

Chapter 4

Two particles I: discrete momenta

4.1 Introduction

In the previous chapter we investigated the behaviour of a single particle under Lorentz boosts. This laid groundwork for the current chapter, where we turn to two particle systems with spin and momenta. Our focus will now shift importantly. Whereas in the previous chapter we were concerned with how boosts entangle spin and momenta of a single particle, in this chapter we will look at how boosts affect the entanglement of the spin degree of freedom of a two particle system. It is in this sense that single particle systems provided a foundation: the physical mechanism which leads to nontrivial transformations of two spins is precisely the one that causes entanglement between momentum and spin of a single particle. Yet the characterisation of composite spin behaviour is considerably less straightforward because the geometry of the two particle state space is much more complicated.

The behaviour of entanglement in massive spin-$1/2$ two particle systems in the relativistic setting has been subject to extensive research. Early work on the topic found that although the particles undergo rotations under Lorentz boosts, the entanglement fidelity of the bipartite state remains invariant [17]. Almost simultaneously it was reported in [15] that the entanglement of a relativistic bipartite spin system *does not* remain invariant. These results produced a flurry of papers [9, 14, 16, 24, 86], some of which confirm the invariance of entanglement while others claim entanglement depends on the magnitude of boost.

A key aspect one notices is that the (sometimes seemingly contradictory) results in the literature rely on different boost scenarios, that is, the momentum states and geometries assumed. This confirms what we discovered in our investigation of single particle systems: entanglement under Lorentz boosts is highly dependent

on the boost scenario in question. We also learned that in the relativistic context it is fruitful to view momenta as qubits that perform controlled unitary operations on spins. These considerations lead to the question, how do different momentum states and boost geometries affect the entanglement of a bipartite spin state under Lorentz boosts? In order to tackle the issue, we will systematically survey the structure of maps that momenta induce on the spin degree of freedom under Lorentz boosts. By making progress on the question, one might hope to clarify at least some of the questions posed in the literature. We proceed in two stages. In this chapter we focus on an idealised model involving discrete momentum states. This provides a convenient framework to analyse entanglement in a simplified setting. However, realistic systems involve wave packets, so in the next chapter we extend treatment to continuous momenta.

The chapter is organised as follows. We begin by characterising the model to be used throughout the chapter. Sections 4.3 and 4.4 describe the momenta and boost scenarios, and spin states, respectively, of the bipartite system. Thereafter we turn to studying the behaviour of pure and the mixed spin states in different boost scenarios. We conclude with an analysis of the results obtained.

4.2 The discrete model

Our aim in this chapter is to study the landscape of maps that Lorentz boosts induce on the spin degree of freedom of a two particle system. To achieve this, we will make a number of simplifications about momenta. One of the most important is that throughout the chapter momenta are regarded as discrete. We will assume that momentum states are sufficiently narrow so we can use orthogonal state vectors at different momentum values, formally satisfying the relationship

$$\langle \mathbf{p}_i | \mathbf{p}_j \rangle = \delta_{ij} \ , \tag{4.1}$$

allowing us to treat momenta as a discrete basis. Each $|\mathbf{p}_i\rangle$ will then generate a single Thomas-Wigner rotation $R(\mathbf{p}_i)$. In essence, as highlighted in the discussion of single particle systems, we view momenta as control qubits that generate transformations on spins [84]. We acknowledge that such narrow momenta are an idealisation; but for several reasons it constitutes a system worthwhile studying. Discrete momenta are computationally easier to deal with than continuous ones but display qualitative features that carry over to systems with continuous momenta. We will encounter examples of this in the next chapter where we are concerned with

continuous systems. Secondly, and relatedly, continuous momenta can be approximated by a finite (but possibly large) number of discrete momenta. Indeed, part of our strategy is to investigate, and model, continuous Gaussian systems by first studying simpler, discrete systems.

We will next assume that spin and momentum are initially, i.e. in the rest frame, in a product state, so the total state of the system is given by

$$|\psi\rangle = |M\rangle \otimes |\Psi\rangle \ , \tag{4.2}$$

where $|\Psi\rangle \in \mathcal{H}_S \otimes \mathcal{H}_S$ is the spin state of the particles, and $|M\rangle \in \mathcal{H}_P \otimes \mathcal{H}_P$, is momentum,

$$|M\rangle = \sum_{|\mathbf{p}_i,\mathbf{q}_j\rangle \in Q} \psi(\mathbf{p}_i, \mathbf{p}_j)\, |\mathbf{p}_i, \mathbf{q}_j\rangle \tag{4.3}$$

where $|\mathbf{p}_i, \mathbf{q}_j\rangle \in \mathcal{H}_P \otimes \mathcal{H}_P$ denote pairs of particles' momenta given by the set Q. In order to calculate how the state appears to an observer O'' who is boosted by Λ^{-1} relative to the rest frame, we note that the action of the boost $\Lambda \equiv \Lambda(\xi, \phi)$ on the composite system is given by the direct product of single particle transforms $U(\Lambda) \otimes U(\Lambda)$,

$$|\psi\rangle \longmapsto \left|\psi''\right\rangle = U(\Lambda) \otimes U(\Lambda)\, |\psi\rangle \ . \tag{4.4}$$

Combining (4.2), (4.3) and (4.4) we get

$$\left|\psi''\right\rangle = \sum_{|\mathbf{p}_i,\mathbf{q}_j\rangle \in Q} \psi(\mathbf{p}_i, \mathbf{q}_j)\, |\Lambda\mathbf{p}_i, \Lambda\mathbf{q}_j\rangle \otimes U(\Lambda, \mathbf{p}_i, \mathbf{q}_j)\, |\Psi\rangle \ , \tag{4.5}$$

where $U(\Lambda, \mathbf{p}_i, \mathbf{q}_j)$ stands for a product of spin-$1/2$ rotations,

$$U(\Lambda, \mathbf{p}_i, \mathbf{q}_j) \equiv U(\Lambda, \mathbf{p}_i) \otimes U(\Lambda, \mathbf{q}_j) \ . \tag{4.6}$$

For brevity of notation we will use the shorthand

$$R(\omega_i) \equiv U(\Lambda, \mathbf{p}_i) \tag{4.7}$$

for single particle rotations, assuming that a rotation by angle $\omega_i \in [0, \pi]$ is realised by a particular geometry encoded in either momenta, rapidity and boost angle, $(\mathbf{p}_i, \xi, \phi)$, or equivalently, velocities $v_i = |\mathbf{p}_i|/E(\mathbf{p}_i), v_2 = \tanh \xi$ and boost angle, (v_i, v_2, ϕ). In the same vein we will write $R(\omega_i, \chi_j)$ instead of $U(\Lambda, \mathbf{p}_i, \mathbf{q}_j)$ for two

particle rotations.

The latter provides a significant layer of abstraction in our treatment in this chapter. In essence, in the following calculations we will hide away the particular geometry which is given in terms of momenta, rapidity and boost angle. Instead, we will use the Thomas-Wigner angle ω as a parameter that takes values in the range $[0, \pi]$, assuming that some actual geometry, not necessarily a unique one, realises such a rotation. A worry might be raised that no actual boost scenario exists that realises a rotation by a given angle. This will be addressed in two stages. The next section elaborates on the boost scenarios that we will study below, showing how each arises and what momentum state implements a given scenario. Second, in the next chapter where we study realistic, Gaussian momentum states, we will perform calculations using concrete momentum states, so spin rotations $R(\omega_i, \chi_j)$ that we take as primitive in this chapter arise there as a result of boosting the particles in a particular geometry $(\mathbf{p}_i, \xi, \phi)$. In other words, in the next chapter we take a step from the abstract level down to the level of implementation. Since the two different calculations, in terms of angles in this chapter and in terms of concrete momenta in the next, are in agreement, the abstraction we use here is justified.

Note that whereas the rest frame state (4.2) factorises between spin and momentum, the boosted state (4.5) does not. This entails that the assumption made at the beginning, namely that spin and momentum factorise, is less restricting than seems at first sight. By studying how spin–momentum product states are transformed to entangled states, we are also investigating the dual situation where entangled states are mapped to product states. This is simply because we can regard either frame as rest frame and the other a moving frame since all inertial frames are on equal footing. Neither can be singled out as *the* rest frame or *the* moving frame. Also, we are always guaranteed to have inverses of maps since Lorentz boosts form a group. In this thesis however we will be concerned mostly with the analysis of spin–momentum product states, proper analysis of spin–momentum entanglement is beyond the scope of this thesis and will be left for another occasion.

Since we are interested in how the spin state changes under boosts, we trace out momenta in Equation (4.5), obtaining the spin state $\rho''_S = \mathsf{Tr}_{\mathbf{p},\mathbf{q}} \left(|\psi''\rangle \langle\psi''| \right)$,[1]

$$\rho''_S = \sum_{\langle \omega_i, \chi_j \rangle} |\psi(\mathbf{p}_i, \mathbf{q}_j)|^2 R(\omega_i, \chi_j) \rho R^\dagger(\omega_i, \chi_j) \ . \tag{4.8}$$

[1] Equation (4.8) is an instance of a separable operation Φ on a bipartite quantum system [79, 87, 88], $\rho' = \Phi(\rho) = \sum_m (A_m \otimes B_m) \rho (A_m^\dagger \otimes B_m^\dagger)$, where the Kraus operators $A_m \otimes B_m$ satisfy the closure condition, $\sum_m A_m^\dagger A_m \otimes B_m^\dagger B_m = \mathbf{1} \otimes \mathbf{1}$. In the present case A_m and B_m are unitary, then Φ is called a *separable random unitary channel* [89].

In general, the evolution of the spin state belongs to the class of maps described in the theory of open quantum systems in the sense that it 'evolves' from a pure state into a mixed state and vice versa. Hence we use concurrence to quantify how much entanglement has changed in the course of the transformation $\rho_S \mapsto \rho_S''$ from frame O to O'', see section 2.4.2.

4.3 Boost scenarios and spin rotations

The behaviour of spin entanglement depends on the map generated by the momenta, hence it will be of interest to study different classes of momentum states. In this section, we will discuss the various forms of momenta to be studied in detail in the rest of the chapter.

We begin with the simplest case,

$$\left|M^1\right\rangle = |\mathbf{p}, \mathbf{q}\rangle \ . \tag{4.9}$$

Momenta of this form represent an oft discussed case in the literature [14, 16, 17, 24, 86]. Setting $\mathbf{q} = -\mathbf{p}$ corresponds to the well-known Bohm version of the Einstein-Podolsky-Rosen setup where the spins are in a Bell state, and the first particle moves in the $\mathbf{p}$-direction while the other particle moves in the opposite direction [90, 91].

In the case of the single particle in the previous chapter, the momentum state was of the form of symmetrically displaced terms $(|\mathbf{p}\rangle + |-\mathbf{p}\rangle)$, and we saw that such a state generated maximal entanglement between spin and momentum. This suggests that similar behaviour for two particles might be observed when momenta contain analogous terms for both particles,

$$\left|M^\Sigma\right\rangle = \frac{1}{2}\left(|\mathbf{p}\rangle + |-\mathbf{p}\rangle\right)\left(|\mathbf{q}\rangle + |-\mathbf{q}\rangle\right) \ . \tag{4.10}$$

where Σ signifies the fact momenta take symmetric values.

Generalising further, we get a momentum state where both particles are in a superposition of momenta along a given direction $|\pm\mathbf{p}\rangle$ and a direction perpendicular to this, $|\pm\mathbf{p}_\perp\rangle$,

$$\left|M^\times\right\rangle = \frac{1}{4}\left(|\mathbf{p}\rangle + |-\mathbf{p}\rangle + |\mathbf{p}_\perp\rangle + |-\mathbf{p}_\perp\rangle\right)\left(|\mathbf{q}\rangle + |-\mathbf{q}\rangle + |\mathbf{q}_\perp\rangle + |-\mathbf{q}_\perp\rangle\right) \ . \tag{4.11}$$

We will see below that momenta of such a form provide a good approximation to the two particle model considered in the seminal paper [15].

Another class of states we would like to study are entangled momenta since they give rise to interesting behaviour in the quantum domain. We assume the generic form of the momenta is given by

$$\left|M_{\pm}^{E}\right\rangle = \frac{1}{\sqrt{2}}\left(|\mathbf{p}_1, \mathbf{q}_1\rangle \pm |\mathbf{p}_2, \mathbf{q}_2\rangle\right) \ , \tag{4.12}$$

where the superscript E stands for 'entangled'. Since we are surveying the logical structure of spin rotations and would like to study the maximal changes that momenta might generate, we will choose momenta to be maximally entangled. For instance, by setting $\mathbf{p}_1 = \mathbf{q}_1 = -\mathbf{p}_2 = -\mathbf{q}_2 = \mathbf{p}$, we get

$$\left|M^{\Phi\pm}\right\rangle = \frac{1}{\sqrt{2}}\left(|\mathbf{p}, \mathbf{p}\rangle \pm |-\mathbf{p}, -\mathbf{p}\rangle\right) \ , \tag{4.13}$$

which correspond to the Bell states $|\Phi^{\pm}\rangle$. Likewise, by choosing $\mathbf{p}_1 = -\mathbf{q}_1 = -\mathbf{p}_2 = \mathbf{q}_2 = \mathbf{p}$, we obtain counterparts of the Bell states $|\Psi^{\pm}\rangle$,

$$\left|M^{\Psi\pm}\right\rangle = \frac{1}{\sqrt{2}}\left(|\mathbf{p}, -\mathbf{p}\rangle \pm |-\mathbf{p}, \mathbf{p}\rangle\right) \ . \tag{4.14}$$

This state has been studied to some extent in [92, 93].

As we will see shortly, in general momenta need not lie along the same axis. For example, specifying that momenta of the first particle are given by $\mathbf{p}_1 = -\mathbf{p}_2 = \mathbf{p}_x$, whereas the second particle has $\mathbf{q}_1 = -\mathbf{q}_2 = \mathbf{p}_y$ leads to states that resemble $|\Phi^{+}\rangle$, so we will signify

$$\left|M^{[\Phi\pm]}\right\rangle = \frac{1}{\sqrt{2}}\left(|\mathbf{p}_x, \mathbf{p}_y\rangle \pm |-\mathbf{p}_x, -\mathbf{p}_y\rangle\right) \ . \tag{4.15}$$

A variant of $|\Psi^{+}\rangle$ like state can be obtained if we choose $\mathbf{p}_1 = -\mathbf{p}_2 = \mathbf{p}_x$ and $\mathbf{q}_1 = -\mathbf{q}_2 = -\mathbf{p}_y$,

$$\left|M^{[\Psi\pm]}\right\rangle = \frac{1}{\sqrt{2}}\left(|\mathbf{p}_x, -\mathbf{p}_y\rangle \pm |-\mathbf{p}_x, \mathbf{p}_y\rangle\right) \ . \tag{4.16}$$

Note that (relative) phases of momenta do not matter as long as spin behaviour is concerned. This is because the expression for the boosted spin state, Equation (4.8), contains only the squared modulus of the momentum wave function, entailing that two momenta $\psi(\mathbf{p})$ and $\psi'(\mathbf{p})$ that are related by a local gauge transformation

$$\psi(\mathbf{p}) \mapsto \psi'(\mathbf{p}) = \mathrm{e}^{\phi(\mathbf{p})}\psi(\mathbf{p}) \tag{4.17}$$

induce the same spin orbits [92]. Thus it suffices when we consider only $\left|M^{\Phi+}\right\rangle$, $\left|M^{\Psi+}\right\rangle$, $\left|M^{[\Phi+]}\right\rangle$ and $\left|M^{[\Psi+]}\right\rangle$, the other Bell states and their counterparts will produce exactly the same spin behaviour.

Although we have specified the general forms that momenta will take, the geometry they might realise is still undetermined. We will now turn to discussing how the generic states are implemented by particular momenta and relate them to different types of rotations generated on spins. This provides the link between two layers: the layer of concrete realisation of boost geometry in terms of momenta and the more abstract layer of rotations that act on spins.

Momenta of both particles can be aligned along the same axes, for instance particle A and B can be in a superposition of momenta along the x-axis, yielding the state,

$$\left|M^{\Sigma}_{XX}\right\rangle = \frac{1}{2}\left(|\mathbf{p}_x\rangle + |-\mathbf{p}_x\rangle\right)\left(|\mathbf{q}_x\rangle + |-\mathbf{q}_x\rangle\right) \ . \tag{4.18}$$

Or momenta of both particles can be aligned along different axes, for instance particle A might be in a superposition of momenta along the x-axis and particle B in a superposition along the y-axis, giving the state,

$$\left|M^{\Sigma}_{XY}\right\rangle = \frac{1}{2}\left(|\mathbf{p}_x\rangle + |-\mathbf{p}_x\rangle\right)\left(|\mathbf{q}_y\rangle + |-\mathbf{q}_y\rangle\right) \ . \tag{4.19}$$

Substituting momentum $\left|M^{\Sigma}_{XX}\right\rangle$ into (4.5) and assuming boost is in the z-direction, we get for the boosted state,

$$\begin{aligned}\left|\psi''\right\rangle =& \frac{1}{2}\big(\,|\Lambda_z\mathbf{p}_x, \Lambda_z\mathbf{q}_x\rangle\ R(\Lambda_z,\mathbf{p}_x)\otimes R(\Lambda_z,\mathbf{q}_x) \\ &+ |\Lambda_z\mathbf{p}_x, -\Lambda_z\mathbf{q}_x\rangle\ R(\Lambda_z,\mathbf{p}_x)\otimes R(\Lambda_z,-\mathbf{q}_x) \\ &+ |-\Lambda_z\mathbf{p}_x, \Lambda_z\mathbf{q}_x\rangle\ R(\Lambda_z,-\mathbf{p}_x)\otimes R(\Lambda_z,\mathbf{q}_x) \\ &+ |-\Lambda_z\mathbf{p}_x, -\Lambda_z\mathbf{q}_x\rangle\ R(\Lambda_z,-\mathbf{p}_x)\otimes R(\Lambda_z,-\mathbf{q}_x)\big)\otimes|\Psi\rangle \ ,\end{aligned} \tag{4.20}$$

or using the shorthand notation of (4.7),

$$\begin{aligned}\left|\psi''\right\rangle =& \frac{1}{2}\big(\,|\Lambda_z\mathbf{p}_x, \Lambda_z\mathbf{q}_x\rangle\ R_Y(\omega)\otimes R_Y(\chi) \\ &+ |\Lambda_z\mathbf{p}_x, -\Lambda_z\mathbf{q}_x\rangle\ R_Y(\omega)\otimes R_Y(-\chi) \\ &+ |-\Lambda_z\mathbf{p}_x, \Lambda_z\mathbf{q}_x\rangle\ R_Y(-\omega)\otimes R_Y(\chi) \\ &+ |-\Lambda_z\mathbf{p}_x, -\Lambda_z\mathbf{q}_x\rangle\ R_Y(-\omega)\otimes R_Y(-\chi)\big)\otimes|\Psi\rangle \ ,\end{aligned} \tag{4.21}$$

where $R_Y(\omega)$ signifies a rotation around the y-axis given by (2.22). Thus we see

that the momenta $\left|M^{\Sigma}_{XX}\right\rangle$ generate rotations of the form

$$R_Y(\pm\omega)\otimes R_Y(\pm\chi)\ , \quad R_Y(\pm\omega)\otimes R_Y(\mp\chi) \tag{4.22}$$

on the spin state. In the same vein, if the momenta are given by $\left|M^{\Sigma}_{XY}\right\rangle$ the z-boosted state will have terms that generate rotations

$$R_Y(\pm\omega)\otimes R_X(\pm\chi)\ , \quad R_Y(\pm\omega)\otimes R_X(\mp\chi) \tag{4.23}$$

on the spin state. Following considerations along these lines we see that by taking momenta along different combinations of axes for both product and entangled momenta, one obtains three different types of rotations that can occur on the spin state,

$$\begin{aligned} &\text{(i)} \ \ R_i\otimes\mathbf{1}\ , \\ &\text{(ii)} \ \ R_i\otimes R_i\ , \\ &\text{(iii)} \ \ R_i\otimes R_j\ , \quad i\neq j\ , \end{aligned} \tag{4.24}$$

where $i,j\in\{X,Y,Z\}$ and each type of rotation can be realised by some set of suitably chosen momenta. For instance, we saw that $R_i\otimes R_i$ is instantiated by $R_Y\otimes R_Y$ when momenta are given by the product state $\left|M^{\Sigma}_{XX}\right\rangle$ and the boost is in the z-direction. Another implementation of the same type is $R_X\otimes R_X$ when momenta are again product but located along the y-axis, $\left|M^{\Sigma}_{YY}\right\rangle$, and the boost is in the z-direction.

To be precise, although we have been speaking as if momenta always lie along some axis, it need not be and typically it is not the case in a general geometry $(\mathbf{p},\xi,\phi)$ as we saw in Chapter 3 in the discussion of single particle systems. To generate maximal spin rotations large boost angles are needed, which are implemented by momentum vectors typically not aligned with an axis. For instance, if boost is in the positive z-direction, then Gaussians centred at $\mathbf{p}_x=(\pm p_{x0},0,-p_{z0})$ realise a state not lying along the x-axis and making an angle to the boost direction which increases as the z-component decreases. However, it is the x-component that determines the boost plane (when boost is assumed to be in the z-direction), and hence the direction of the particular rotation occurring on the spin. We will therefore adopt the convention that we denote by $|\mathbf{p}_i\rangle$, $i\in\{x,y,z\}$ any state that lies in the boost plane, that is, the plane defined by the i-axis and the unit vector $\hat{\mathbf{n}}$ in the direction of boost, but where the boost angle is left unspecified. The reason is that

if we are interested only in whether or not the rotation occurs around a given axis, then any momentum state $|\mathbf{p}_i\rangle$ in the boost plane will do. If we are also interested in specifying the boost angle, then we need to choose a particular vector in the boost plane.

We will next give a few examples of boost geometries that implement the different types of rotations listed in (4.24).

Type $R_i \otimes \mathbf{1}$. In this scenario, only the first particle undergoes rotation. The momentum of the second particle is chosen so that it leaves the spin alone. Denoting such a momentum by $|0\rangle$, the following pairs of boosts and momenta listed on the left hand side generate rotations given on the right hand side,

$$\begin{aligned} &\Lambda_z\,, |\mathbf{p}_y, 0\rangle \longmapsto R_X \otimes \mathbf{1}\ , \\ &\Lambda_z\,, |\mathbf{p}_x, 0\rangle \longmapsto R_Y \otimes \mathbf{1}\ , \\ &\Lambda_y\,, |\mathbf{p}_x, 0\rangle \longmapsto R_Z \otimes \mathbf{1}\ . \end{aligned} \tag{4.25}$$

Type $R_i \otimes R_i$. For scenarios in which both particles are rotated around the same axis but not necessarily in the same direction, we obtain the following boosts and momenta,

$$\begin{aligned} &\Lambda_z\,, |\mathbf{p}_y, \mathbf{q}_y\rangle \longmapsto R_X \otimes R_X\ , \\ &\Lambda_z\,, |\mathbf{p}_x, \mathbf{q}_x\rangle \longmapsto R_Y \otimes R_Y\ , \\ &\Lambda_y\,, |\mathbf{p}_x, \mathbf{q}_x\rangle \longmapsto R_Z \otimes R_Z\ . \end{aligned} \tag{4.26}$$

Type $R_i \otimes R_j$, $i \neq j$. Scenarios where particles undergo rotations around different axes can be realised by

$$\begin{aligned} &\Lambda_y\,, |\mathbf{p}_z, \mathbf{q}_x\rangle \longmapsto R_X \otimes R_Z\ , \\ &\Lambda_z\,, |\mathbf{p}_y, \mathbf{q}_x\rangle \longmapsto R_X \otimes R_Y\ , \\ &\Lambda_x\,, |\mathbf{p}_z, \mathbf{q}_y\rangle \longmapsto R_Y \otimes R_Z\ . \end{aligned} \tag{4.27}$$

In many cases these different implementations of a given type of rotation produce spin orbits that differ only by some symmetry transformation in the state space. They fall in the same equivalence class which we denote using a specific boost scenario specified by the concrete realisation of rotation, the momentum and spin state, for example $[R_X \otimes \mathbf{1}, M^{\Sigma}_{XX}, \Phi^+]$. However, it is in general not true that

different realisations of given type, e.g. $R_i \otimes R_i$, give rise to only one type of spin behaviour. For instance, when the spin state $|\Psi\rangle$ is an eigenstate of operators of the form $R_X(\pm\omega) \otimes R_X(\pm\omega)$ but not of $R_Y(\pm\omega) \otimes R_Y(\pm\omega)$, then the former produces trivial spin behaviour whereas the latter may result in non-trivial state change and thus of concurrence. Thus we expect that both the behaviour of states and of entanglement will fall into a small number of equivalence classes. Finding out what these classes are will occupy us for the rest of the chapter.

4.4 Spin state and its visualisation

Since we are interested in how entanglement changes under boosts, we will begin by assuming that the bipartite spin state $|\Psi\rangle$ is initially maximally entangled, taking the form of one of the Bell states $|\Phi^{\pm}\rangle$, $|\Psi^{\pm}\rangle$. Later in section 4.6 we will relax this condition and extend our investigation to include states whose entanglement varies between maximal entanglement and no entanglement, the so-called Werner states [80].

In order to gain better understanding of dynamics, the state change of a single particle is commonly visualised using the Bloch sphere. We would like to accomplish the same for the bipartite system. Unfortunately, visualisation of a two particle state is in general impossible since $N^2 - 1$ independent real parameters are needed to characterise the density matrix on the Hilbert space with dimension N, which in the current case $N = 4$ equals 15. However, if the orbit of a state is restricted to a lower dimensional space that can be represented in three dimensions, then visualisation is feasible. Fortunately this turns out to be the case for the entangled states that we are going to study.

A boost on a bipartite system will in general map the rest spin state ρ_S into a mixed state ρ''_S, as can be seen in Equation (4.8), so it is useful to work in the Hilbert-Schmidt space of operators $B(\mathcal{H})$, defined on the Hilbert space $\mathcal{H}$ with $\dim = N$ [87]. $B(\mathcal{H})$ becomes a Hilbert space of N^2 complex dimensions when equipped with a scalar product defined as $\langle A|B\rangle = \mathsf{Tr}(A^\dagger B)$, with $A, B \in B(\mathcal{H})$, where the squared norm is $\|A\|^2 = \mathsf{Tr}(A^\dagger A)$. The vector space of Hermitian operators is an N^2 real-dimensional subspace of Hilbert-Schmidt space and can be coordinatized using a basis that consists of identity operator and the generators of $\mathrm{SU}(N)$. For a qubit $N = 2$ and we obtain the familiar Bloch ball. For a bipartite qubit system $N = 4$, $B(\mathcal{H}) = B(\mathcal{H}_A) \otimes B(\mathcal{H}_B)$ where $\mathcal{H}_i$ is the single particle space, and we can use a basis whose elements are tensor products $\{\mathbf{1} \otimes \mathbf{1}, \mathbf{1} \otimes \boldsymbol{\sigma}, \boldsymbol{\sigma} \otimes \mathbf{1}, \boldsymbol{\sigma} \otimes \boldsymbol{\sigma}\}$, where

$\boldsymbol{\sigma} = (\sigma_x, \sigma_y, \sigma_z)$ is the vector of Pauli operators. The density operator for a 2×2 dimensional system can be written in the general form,

$$\rho = \frac{1}{4}\left(\mathbf{1}\otimes\mathbf{1} + \mathbf{r}\boldsymbol{\sigma}\otimes\mathbf{1} + \mathbf{1}\otimes\mathbf{s}\boldsymbol{\sigma} + \sum_{i,j} t_{ij}\sigma_i\otimes\sigma_j\right) , \tag{4.28}$$

where the coefficients $\mathbf{r} = (r_x, r_y, r_z)$, $\mathbf{s} = (s_x, s_y, s_z)$ and t_{ij}, $i, j \in \{x, y, z\}$ are the expectation values of the operators $\boldsymbol{\sigma}\otimes\mathbf{1}$, $\mathbf{1}\otimes\boldsymbol{\sigma}$ and $\sigma_i\otimes\sigma_j$.

For the projectors on the Bell states $s_i = r_i = 0$ and the matrix t_{ij} is diagonal. This implies we only need to consider the values of diagonal components t_{ii} which constitute a vector in 3-dimensional space, allowing us to represent the states in Euclidean three space [94]. The Bell states correspond to vectors,

$$\begin{aligned} t_{\Phi^+} &= (1, -1, \quad 1) \ , \qquad t_{\Phi^-} = (-1, \quad 1, \quad 1) \ , \\ t_{\Psi^+} &= (1, \quad 1, -1) \ , \qquad t_{\Psi^-} = (-1, -1, -1) \ . \end{aligned} \tag{4.29}$$

which, in turn, correspond to the vertices of a tetrahedron $\mathcal{T}$ in Figure 4.1. By taking convex combinations of these, one obtains further diagonal states; the set of all such states is called *Bell-diagonal* and is represented by the (blue) tetrahedron $\mathcal{T}$ in Figure 4.1. The set of separable states forms a double pyramid, an octahedron, in the tetrahedron. The octahedron is given by the intersection of $\mathcal{T}$ with its reflection through the origin, $-\mathcal{T}$. The maximally mixed state $\frac{1}{4}\mathbf{1}_4$ has coordinates $(0, 0, 0)$ and it lies at the origin. The entangled states are located outside the octahedron in the cones of the tetrahedron, see Figure 4.1.

We can now visualise the behaviour of spin by calculating the orbits of Bell states under all types of rotations as functions of the Thomas-Wigner angle ω,

$$t(\omega) = (t_{xx}, t_{yy}, t_{zz}) \quad \text{with} \quad t_{ii} = \mathsf{Tr}(\rho''_S(\omega)\sigma_i\otimes\sigma_i) \ , \ \ i \in \{x, y, z\} \ . \tag{4.30}$$

We will use a single parameter ω to characterise rotations on both particles, making the assumption that momenta of both particles are of equal magnitude, $|\mathbf{p}| = |\mathbf{q}|$, and both are transformed by boosts with the same rapidity ξ. In a more general setting these assumptions may be relaxed, meaning that particles could be subject to different boost geometries, which in turn implies that spins may undergo different rotations. When surveying the topic for the first time, however, we would like to keep the model simple enough in order to gain some insight into how various kinds of momenta affect spin entanglement. In principle, these results can be then

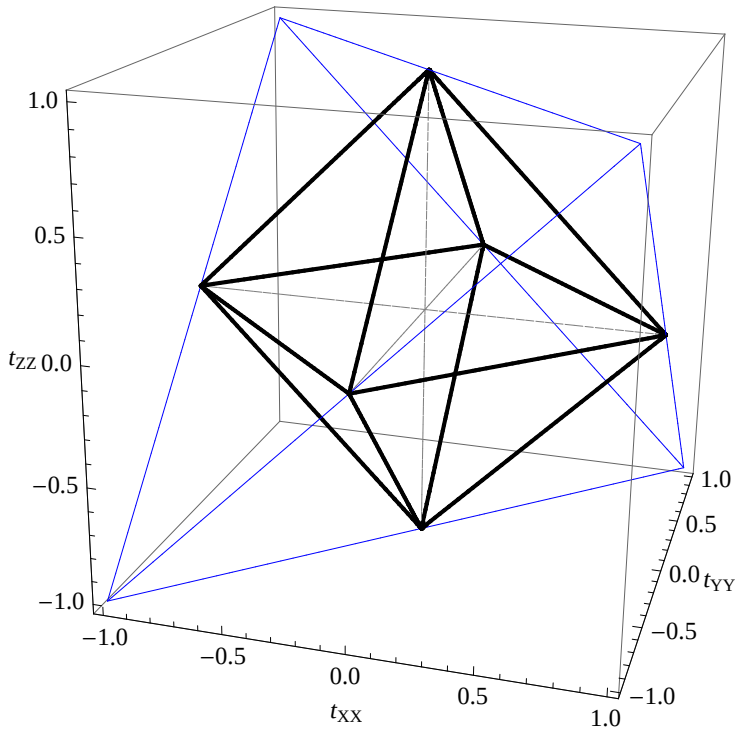

Figure 4.1. The geometry of Bell diagonal states. The vertices of the tetrahedron $\mathcal{T}$ correspond to the four Bell states $|\Phi^+\rangle$, $|\Phi^-\rangle$, $|\Psi^+\rangle$, and $|\Psi^-\rangle$. Convex combinations of projectors on the Bell states, the Bell diagonal states, lie on or in the tetrahedron. A Bell diagonal state is separable iff it lies in the double pyramid formed by the intersection of the tetrahedron $\mathcal{T}$ and its reflection through the origin $-\mathcal{T}$.

later refined by allowing a distinct boost scenario for each particle.

4.5 Entangled pure spins: Bell states

4.5.1 Product momenta $|M^1\rangle$

If momenta are initially in the product state $|M^1\rangle = |\mathbf{p}, \mathbf{q}\rangle$, the boosted state is given by

$$|\psi''\rangle = |\Lambda\mathbf{p}, \Lambda\mathbf{q}\rangle\, R(\Lambda, \mathbf{p}) \otimes R(\Lambda, \mathbf{q})\, |\Psi\rangle \ . \tag{4.31}$$

We see that each particle undergoes a momentum dependent rotation and the final spin state is described by a Bell state that is transformed by a local unitary of the form $U_1 \otimes U_2$. Local unitaries leave the entanglement of Bell states invariant, hence Lorentz boosting momenta of such form does not change entanglement between spins. This was noted first in [17], where the authors carry out a thorough study of both massive spin-$1/2$ particles and massless photons. The conclusion holds for all

three types of rotations because they are all special cases of the form $U_1 \otimes U_2$.

In the context of this work, momenta of such form represent a special case. We will see shortly that in boost scenarios where momenta contain more terms entanglement will in general not remain invariant since spins undergo more complicated transformations.

4.5.2 Product momenta $\left|M^{\Sigma}\right\rangle$

In the following sections 4.5.2.1–4.5.2.3, we will study spin rotations induced by the product momenta of symmetric form

$$\left|M^{\Sigma}\right\rangle = \frac{1}{2}\left(|\mathbf{p}\rangle + |-\mathbf{p}\rangle\right)\left(|\mathbf{q}\rangle + |-\mathbf{q}\rangle\right) \ . \tag{4.32}$$

4.5.2.1 Case $R_i \otimes \mathbf{1}$

Rotations of the form $R_i(\omega) \otimes \mathbf{1}$ can be realised by various geometries as listed in (4.25). For instance, if we choose the boost to be in the z-direction, the rotation $R_X(\omega) \otimes \mathbf{1}$ occurs in a scenario where the momenta of the first particle lie in the $y-z$-plane while the second particle's momentum $|0\rangle$ is located at the origin. The momenta then take the form $\left(|\mathbf{p}_y\rangle + |-\mathbf{p}_y\rangle\right)|0\rangle/\sqrt{2}$. Boosting in the z-direction translates $|0\rangle$ along the z-axis, yielding no rotation. For the initial spin $|\Phi^+\rangle$ the boosted state is given by

$$\begin{aligned}\rho''_S(\omega) &= \frac{1}{4}\left(\mathbf{1}_4 + \sigma_x \otimes \sigma_x - \cos\omega\ \sigma_y \otimes \sigma_y + \cos\omega\ \sigma_z \otimes \sigma_z\right) \\ &= \rho^{\Phi+}\cos^2\frac{\omega}{2} + \rho^{\Psi+}\sin^2\frac{\omega}{2}\ ,\end{aligned} \tag{4.33}$$

This corresponds to the vector

$$t_{X\otimes\mathbf{1}}(\omega) = (1, -\cos\omega, \cos\omega) \ . \tag{4.34}$$

The concurrence is given by

$$C(\omega) = |\cos\omega| \ . \tag{4.35}$$

Plots for the orbit of the state and concurrence are shown in Figure 4.2.

We can now understand the action of boosts on $|\Phi^+\rangle$. As mentioned above, in general a boost maps a pure state into a mixed one. Equation (4.33) shows that the Bell state $|\Phi^+\rangle$ is mapped into a mixture of itself and the projector on $|\Psi^+\rangle$, the states depicted by the red line in Figure 4.2. As boost increases, the state moves

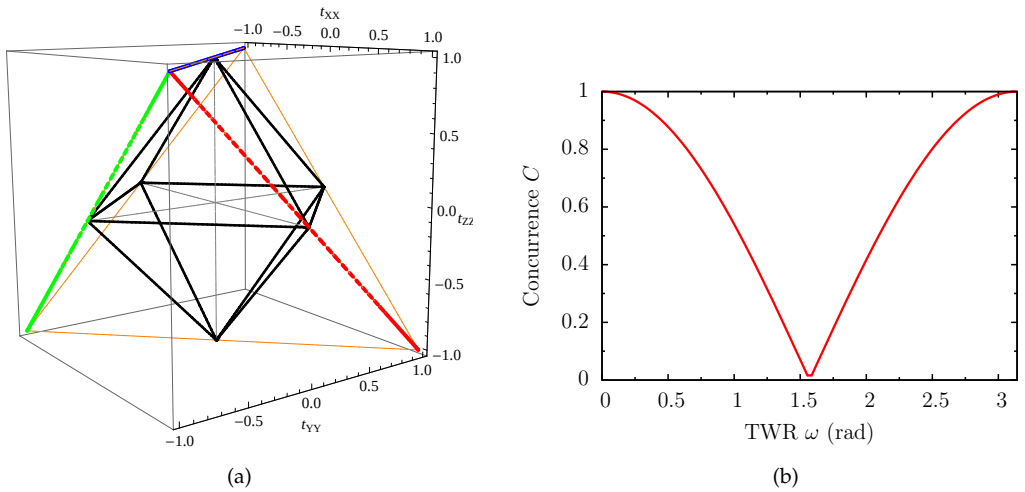

(a) (b)

Figure 4.2. Spin orbit and concurrence under $R_i \otimes \mathbf{1}$ with $\omega \in [0, \pi]$. (a) Initial state $\left|\Phi^+\right\rangle$ corresponds to vertex $(1, -1, 1)$, orbit for $R_X \otimes \mathbf{1}$ is shown red, $R_Y \otimes \mathbf{1}$ green and $R_Z \otimes \mathbf{1}$ blue. (b) Concurrence has the same shape for all $R_i \otimes \mathbf{1}$.

along the line towards the center of the face, reaching a separable state at $\omega = \pi/2$. Boosts with even higher speeds result again in entangled states. Finally, as the Thomas-Wigner rotation angle approaches π, the boosted observer sees the state $|\Psi^+\rangle$ instead of $|\Phi^+\rangle$.

Direct calculation shows that other rotations induce similar orbits. For $R_Y \otimes \mathbf{1}$ and $R_Z \otimes \mathbf{1}$ we obtain

$$\begin{aligned} t_{Y\otimes\mathbf{1}}(\omega) &= (\cos\omega, -1, \cos\omega) \ , \\ t_{Z\otimes\mathbf{1}}(\omega) &= (\cos\omega, -\cos\omega, 1) \ , \end{aligned} \tag{4.36}$$

with the concurrence given by the expression (4.35). The three orbits $t_{i\otimes 1}$ of $|\Phi^+\rangle$ are related by rotations of $2\pi n/3$, $n = 1, 2$, of the tetrahedron $\mathcal{T}$ where the axis of rotation is the line through $(0, 0, 0)$ and the vertex $(1, -1, 1)$ representing $|\Phi^+\rangle$.

Calculating rotations for other Bell states produce similar orbits, the only difference being the initial state. For a given state, orbits under different rotations $R_i \otimes \mathbf{1}$ are related again by rotations of $2\pi n/3$ of the tetrahedron around the axis through the origin and the vertex representing the respective state.

All in all, orbits of rotations of type $R_i \otimes \mathbf{1}$ generated by the product momenta $\left|M^\Sigma\right\rangle$ for all the Bell states belong to the same equivalence class which we denote by $[R_X \otimes \mathbf{1}, M^\Sigma_{Y0}, \Phi^+]$.

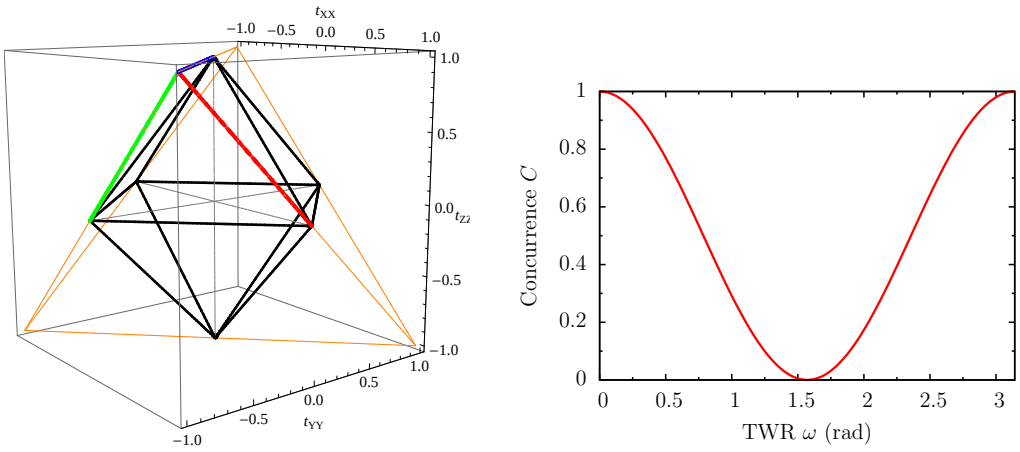

(a) (b)

Figure 4.3. Spin orbit and concurrence under $R_i \otimes R_i$ with $\omega \in [0, \pi]$. (a) Initial state $|\Phi^+\rangle$ corresponds to the vertex at $(1, -1, 1)$, $R_X \otimes R_X$ is shown red, $R_Y \otimes R_Y$ green and $R_Z \otimes R_Z$ blue. (b) Concurrence has the same shape for all $R_i \otimes R_i$.

4.5.2.2 Case $R_i \otimes R_i$

Rotations of the form $R_i(\omega) \otimes R_i(\omega)$ can be again implemented by various geometries. For example, when the boost is in the z-direction, then $R_X(\omega) \otimes R_X(\omega)$ is realised by the state $(|\mathbf{p}_y\rangle + |-\mathbf{p}_y\rangle)(|\mathbf{q}_y\rangle + |-\mathbf{q}_y\rangle)/2$ where momenta of both particles lie in the $y-z$-plane. A Lorentz boost sends the spin state $|\Phi^+\rangle$ to

$$\begin{aligned}\rho''_S(\omega) &= \frac{1}{4}\left(\mathbf{1}_4 + \sigma_x \otimes \sigma_x - \cos^2\omega\ \sigma_y \otimes \sigma_y + \cos^2\omega\ \sigma_z \otimes \sigma_z\right) \\ &= \rho^{\Phi+}\left(\frac{1+\cos^2\omega}{2}\right) + \rho^{\Psi+}\left(\frac{1-\cos^2\omega}{2}\right)\ ,\end{aligned} \tag{4.37}$$

which corresponds to the vector,

$$t_{X\otimes X}(\omega) = (1, -\cos^2\omega, \cos^2\omega)\ . \tag{4.38}$$

We calculate that the concurrence is given by

$$C(\omega) = \cos^2\omega\ . \tag{4.39}$$

Plots for the orbit of the state and concurrence are shown in Figure 4.3.

The effect of boosts on $|\Phi^+\rangle$ starts out qualitatively in a similar fashion to the previous case. Initially, as rotation increases, $|\Phi^+\rangle$ is again mapped into a mixture of itself and $|\Psi^+\rangle$, corresponding to a point on the line connecting the two states. When $\omega = \pi/2$, the moving observer sees a separable state. However, at boosts

that generate rotations larger than $\pi/2$ the orbit differs from the previous case since the boosted state moves back along the same path towards the rest frame state. At $\omega = \pi$, we obtain the original rest frame state $|\Phi^+\rangle$.

The concurrence is rather similar to the previous type in that it decreases monotonically from 1 to 0 between $[0, \pi/2]$ and increases monotonically from 0 to 1 between $[\pi/2, \pi]$, while the precise expression differs slightly from the previous case.

Analysis of other rotations and Bell states runs along similar lines. Rotations $R_Y \otimes R_Y$ and $R_Z \otimes R_Z$ produce orbits

$$\begin{aligned} t_{Y\otimes Y}(\omega) &= (\cos^2\omega, -1, \cos^2\omega)\ , \\ t_{Z\otimes Z}(\omega) &= (\cos^2\omega, -\cos^2\omega, 1)\ . \end{aligned} \tag{4.40}$$

These are related to $t_{X\otimes X}$ by a rotation of $2\pi n/3$, $n = 1, 2$, around the axis through origin and the vertex corresponding to $|\Phi^+\rangle$. By directly computing the trajectories for other Bell states we obtain orbits of similar form, where the only difference lies in the initial state. All these orbits are related by rotations of multiples $2\pi/3$ in the state space. In summary, orbits corresponding to rotations of type $R_i \otimes R_i$ generated by the product momenta $\left|M^\Sigma\right\rangle$ fall in the same equivalence class; we denote $[R_X \otimes R_X, M^\Sigma_{YY}, \Phi^+]$.

4.5.2.3 Case $R_i \otimes R_j$

Mixed rotations $R_i \otimes R_j$ can be implemented by momenta that lie in different boost planes. For instance, when boost is in the z-direction, then spins are rotated by $R_X \otimes R_Y$ given that momenta are of the form $(|\mathbf{p}_y\rangle + |-\mathbf{p}_y\rangle)(|\mathbf{q}_x\rangle + |-\mathbf{q}_x\rangle)/2$. In this case a boost maps $|\Phi^+\rangle$ to the state

$$\begin{aligned} \rho''_S(\omega) &= \frac{1}{4}\left(\mathbf{1}_4 + \cos\omega\ \sigma_x\otimes\sigma_x - \cos\omega\ \sigma_y\otimes\sigma_y + \cos^2\omega\ \sigma_z\otimes\sigma_z\right) \\ &= \rho^{\Phi+}\ \frac{(1+\cos\omega)^2}{4} + \rho^{\Phi-}\ \frac{(1-\cos\omega)^2}{4} \\ &\quad + \left(\rho^{\Psi+} + \rho^{\Psi-}\right)\left(\frac{1-\cos^2\omega}{4}\right)\ , \end{aligned} \tag{4.41}$$

This corresponds to the vector

$$t_{X\otimes Y}(\omega) = \left(\cos\omega, -\cos\omega, \cos^2\omega\right)\ . \tag{4.42}$$

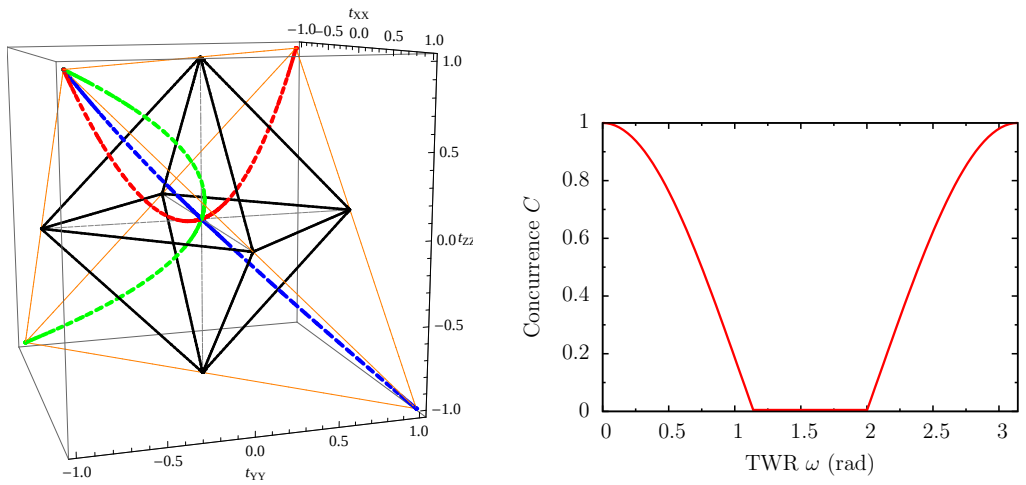

(a) (b)

Figure 4.4. Spin orbit and concurrence under $R_i \otimes R_j$, $i \neq j$ and $\omega \in [0, \pi]$. (a) Initial state $|\Phi^+\rangle$ corresponds to the vertex at $(1, -1, 1)$, $R_X \otimes R_Y$ is shown red, $R_X \otimes R_Z$ green and $R_Y \otimes R_Z$ blue. (b) Concurrence has the same shape for all $R_i \otimes R_j$.

The concurrence is given by

$$C(\omega) = \begin{cases} \frac{1}{4}\left(-1 + 4|\cos\omega| + \cos 2\omega\right) & \text{if} \quad 0 \leq \omega < \omega_-,\ \omega_+ < \omega < \pi \\ 0 & \text{if} \quad \omega_- \leq \omega \leq \omega_+ \end{cases} \tag{4.43}$$

where we find that $\omega_\mp = \arccos(\mp 1 \pm \sqrt{2})$ by solving the equation $C(\omega) = 0$ for ω.

Plots for spin orbit and concurrence are shown in Figure 4.4. The behaviour of spin under mixed rotations is quite different from the two previous cases. As is seen in Figure 4.4, the spin orbit has the shape of a curve that starts at the vertex $(1, -1, 1)$ representing the rest state $|\Phi^+\rangle$. It then evolves towards the origin, reaching it at $\omega = \pi/2$. The second half of the orbit for values $\omega \in [\pi/2, \pi]$ is symmetric to the first half. The state evolves towards the vertex $(-1, 1, 1)$ representing the Bell state $|\Phi^-\rangle$, reaching it when boosts approach the speed of light. The orbit lies in the plane that intersects the initial state $|\Phi^+\rangle$, the origin and the final state $|\Phi^-\rangle$.

It is interesting that spins become separable when the Thomas-Wigner angle lies between $[\omega_-, \omega_+]$, Figure 4.4b. While this might look puzzling if we only knew the behaviour of concurrence, the plot of the orbit clearly shows what is happening. The spin state evolves in the plane that intersects the octahedron of separable states, hitting the face of the octahedron when $\omega = \omega_-$, and then following a path towards the maximally mixed state $\frac{1}{4}\mathbf{1}_4$ represented by $(0, 0, 0)$. When $\omega = \pi/2$, the moving observer sees the maximally mixed state. The concurrence of the boosted state becomes non-zero again as ω becomes greater than ω_+, this corresponds to the point

where the spin state leaves the octahedron.

Other rotations $R_X \otimes R_Z$ and $R_Y \otimes R_Z$ produce similar orbits,

$$\begin{aligned} t_{X\otimes Z}(\omega) &= (\cos\omega, -\cos^2\omega, \cos\omega) \ , \\ t_{Y\otimes Z}(\omega) &= (\cos^2\omega, -\cos\omega, \cos\omega) \ . \end{aligned} \tag{4.44}$$

In analogy to the cases above, they are related to $t_{X\otimes Y}$ by rotations of $2\pi n/3$, $n = 1, 2$ around the axis through the origin and the vertex corresponding to $|\Phi^+\rangle$. In the same vein, we calculate that other Bell states produce similar orbits albeit with different initial states. In conclusion, orbits representing mixed rotations of type $R_i \otimes R_j$, $i \neq j$, for the product momenta $\left|M^{\Sigma}\right\rangle$ belong to the same class which we denote by $[R_X \otimes R_Y, M^{\Sigma}_{YX}, \Phi^+]$.

4.5.3 Product momenta $|M^{\times}\rangle$

The case of product momenta $|M^{\times}\rangle$ falls into two classes, the $R_i \otimes \mathbf{1}$ and the combination of $R_i \otimes R_i$ with $R_i \otimes R_j$. The latter is because $|M^{\times}\rangle$ consists of momentum terms that generate both types of rotation. For instance, if boost is in the z-direction and momenta are constrained to lie in the $x-z$- and $y-z$-planes, we get terms $|\pm\mathbf{p}_x, \pm\mathbf{p}_x\rangle$, $|\pm\mathbf{p}_y, \pm\mathbf{p}_y\rangle$, $|\pm\mathbf{p}_x, \pm\mathbf{p}_y\rangle$ and $|\pm\mathbf{p}_y, \pm\mathbf{p}_x\rangle$, which generate the respective rotations $R_X \otimes R_X$, $R_Y \otimes R_Y$, $R_Y \otimes R_X$ and $R_X \otimes R_Y$. It also follows that the maps and orbits of both classes can be calculated as convex combinations of transformations we have obtained above.

4.5.3.1 Case $R_i \otimes \mathbf{1}$

Let us consider the single particle rotation scenario where boost is in the z-direction and the first particle is in a superposition of momenta $|\pm\mathbf{p}_y\rangle$ and $|\pm\mathbf{p}_x\rangle$. The resulting orbit of $|\Phi^+\rangle$ is a convex sum of the orbits $t_{X\otimes\mathbf{1}}$ and $t_{Y\otimes\mathbf{1}}$ from section 4.5.2.1,

$$\begin{aligned} t_{XY\otimes\mathbf{1}}(\omega) &= \frac{1}{2}\left(t_{X\otimes\mathbf{1}}(\omega) + t_{Y\otimes\mathbf{1}}(\omega)\right) \ , \\ &= \left(\cos^2\frac{\omega}{2}, -\cos^2\frac{\omega}{2}, \cos\omega\right) \ . \end{aligned} \tag{4.45}$$

The corresponding concurrence is given by

$$C(\omega) = \begin{cases} \cos\omega & \text{if} \quad 0 \leq \omega < \pi/2 \ , \\ 0 & \text{if} \quad \pi/2 \leq \omega \leq \pi \ . \end{cases} \tag{4.46}$$

Plots of spin orbit and concurrence are shown in Figure 4.5. Since the orbit is a

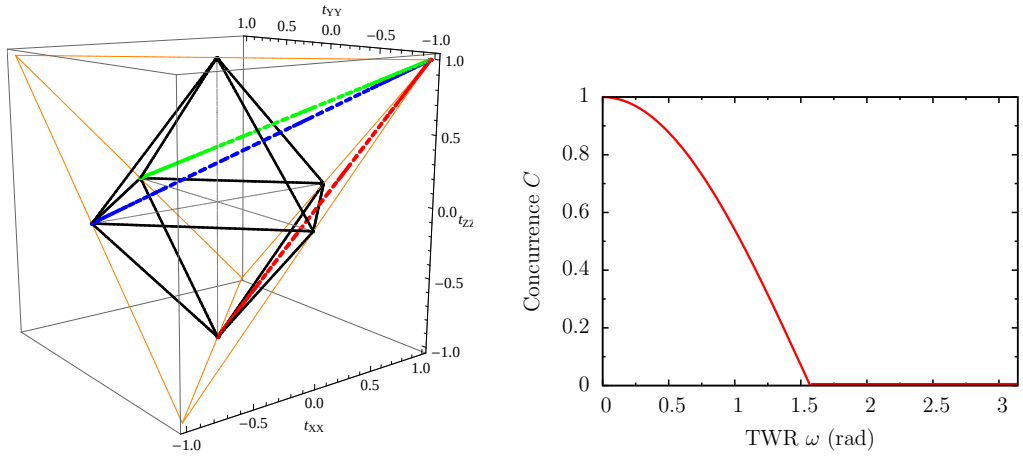

(a) (b)

Figure 4.5. Spin orbit and concurrence under $R_i \otimes \mathbf{1}$ generated by momenta $\left|M^{\times}\right\rangle$ with $\omega \in [0, \pi]$. (a) Initial state $\left|\Phi^{+}\right\rangle$ corresponds to the vertex at $(1, -1, 1)$, the orbit $t_{XY\otimes\mathbf{1}}$ is shown red, $t_{XZ\otimes\mathbf{1}}$ green and $t_{YZ\otimes\mathbf{1}}$ blue. (b) Spin concurrence has the same shape for all orbits.

convex sum of $t_{X\otimes\mathbf{1}}$ and $t_{Y\otimes\mathbf{1}}$, it is represented by a line connecting the initial state $(1, -1, 1)$ and the point that corresponds to the equal mixture of projectors onto $|\Psi^{+}\rangle$ and $|\Psi^{-}\rangle$. Accordingly, concurrence displays the same behaviour until $\omega = \pi/2$. In contrast to single particle rotations though it vanishes for all values of ω greater than $\pi/2$. This is because when boosts induce rotations larger than $\pi/2$, the state follows a path on the face of the octahedron until $\omega = \pi$.

The other rotations produce similar orbits,

$$t_{XZ\otimes\mathbf{1}}(\omega) = \left(\cos^2\frac{\omega}{2}, -\cos\omega, \cos^2\frac{\omega}{2}\right) ,$$
$$t_{YZ\otimes\mathbf{1}}(\omega) = \left(\cos\omega, -\cos^2\frac{\omega}{2}, \cos^2\frac{\omega}{2}\right) . \tag{4.47}$$

They are again related to each other by rotations in the state space analogously to the cases discussed above. Other Bell states have similar orbits, and all orbits belong to the same equivalence class which we denote $[R_{XY\otimes\mathbf{1}}, M^{\times}_{YX0}, \Phi^{+}]$.

4.5.3.2 Case $R_i \otimes R_i$ and $R_i \otimes R_j$

For two particle rotations let us consider the scenario where the boost is in the z-direction and momenta are constrained to lie in the $x-z$- and $y-z$-planes. The state $|M^{\times}\rangle$ then consist of momentum terms of the form $|\pm\mathbf{p}_x, \pm\mathbf{p}_x\rangle$, $|\pm\mathbf{p}_y, \pm\mathbf{p}_y\rangle$, $|\pm\mathbf{p}_x, \pm\mathbf{p}_y\rangle$ and $|\pm\mathbf{p}_y, \pm\mathbf{p}_x\rangle$, which generate respective rotation terms $R_Y \otimes R_Y$, $R_X \otimes R_X$, $R_X \otimes R_Y$ and $R_Y \otimes R_X$. The spin orbit can be calculated by combining

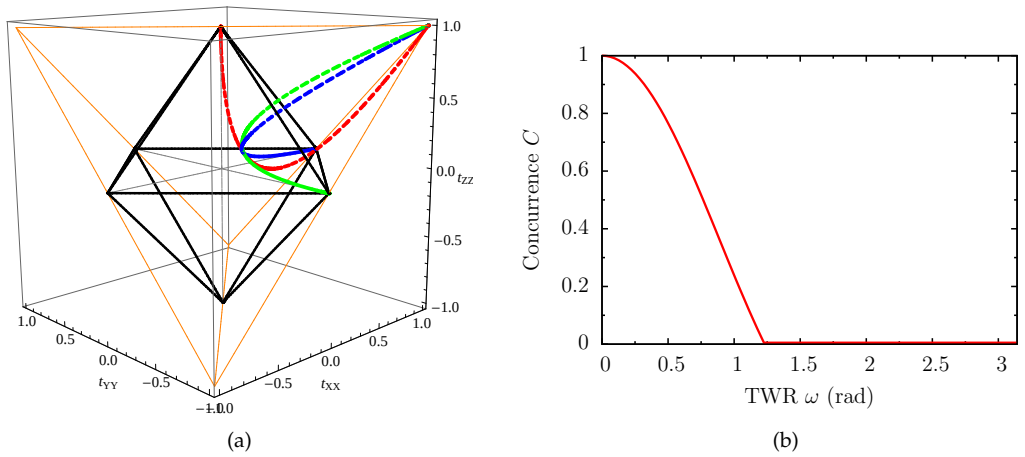

(a) (b)

Figure 4.6. Spin orbit and concurrence under $R_i \otimes R_i$ and $R_i \otimes R_j$ generated by momenta $\left|M^{\times}\right\rangle$ with $\omega \in [0, \pi]$. (a) Initial state $\left|\Phi^{+}\right\rangle$ corresponds to the vertex at $(1, -1, 1)$, the orbit $t_{X\otimes Y}$ is shown red, $t_{X\otimes Z}$ green and $t_{Y\otimes Z}$ blue. (b) Spin concurrence has the same shape for all orbits.

the respective orbits,

$$\begin{aligned} t^{M\times}_{X\otimes Y}(\omega) &= \frac{1}{4}\left(t^{M\Sigma}_{X\otimes X} + t^{M\Sigma}_{X\otimes Y} + t^{M\Sigma}_{Y\otimes X} + t^{M\Sigma}_{Y\otimes Y}\right) \\ &= \left(\cos^4\frac{\omega}{2}, -\cos^4\frac{\omega}{2}, \cos^2\omega\right) , \end{aligned} \tag{4.48}$$

where we have used superscripts to distinguish between the orbits generated by $\left|M^{\Sigma}\right\rangle$ and $|M^{\times}\rangle$. The concurrence is

$$C(\omega) = \begin{cases} \frac{1}{16}\left(-\left|4\cos\omega - \cos 2\omega - 3\right| + 4\cos\omega \right. & \\ \qquad\qquad \left. +7\cos 2\omega + 5\right) & \text{if} \quad 0 \le \omega < \omega_1 , \\ 0 & \text{if} \quad \omega_1 \le \omega \le \pi , \end{cases} \tag{4.49}$$

where we find that $\omega_1 = 1.23$ rad by solving the equation $C(\omega) = 0$ for ω. It is the angle at which the state enters the octahedron and becomes separable. Plots of spin orbit and concurrence are shown in Figure 4.6. The orbit exhibits interesting behaviour, starting out in a manner similar to $t_{X\otimes Y}$ generated by the symmetric momentum $\left|M^{\Sigma}\right\rangle$. After entering the octahedron, it changes course and evolves towards the tip of the top pyramid, ending at the state which corresponds to the equal mixture of projectors onto $|\Phi^{+}\rangle$ and $|\Phi^{-}\rangle$ when $\omega = \pi$. This explains why concurrence vanishes at all boosts that induce rotations larger than 1.23 rad.

Orbits induced by other rotations have similar form,

$$\begin{aligned} t_{X\otimes Z}(\omega) &= \left(\cos^4\frac{\omega}{2}, -\cos^2\omega, \cos^4\frac{\omega}{2}\right) , \\ t_{Y\otimes Z}(\omega) &= \left(\cos^2\omega, -\cos^4\frac{\omega}{2}, \cos^4\frac{\omega}{2}\right) , \end{aligned} \tag{4.50}$$

where we have omitted superscripts for brevity. Other Bell states produce orbits of similar structure. All belong to the same equivalence class, which we denote $[R_{X\otimes Y}, M^{\times}_{YX}, \Phi^{+}]$.

The significance of this momentum state lies in that it can be employed to model quite accurately the continuous momenta discussed in the seminal paper [15], see chapter 5 below.

4.5.4 Entangled momenta

In the following sections we will assume that momenta are entangled and take the form of Bell states $\left|M^{\Phi+}\right\rangle$, $\left|M^{\Psi+}\right\rangle$ or Bell-like states $\left|M^{[\Phi+]}\right\rangle$, $\left|M^{[\Psi+]}\right\rangle$. The former are instantiated by rotations of type $R_i \otimes R_i$ whereas the latter occur when rotations are around different axes, $R_i \otimes R_j$, $i \neq j$. As mentioned above, there is no need to consider momenta with other relative phases since they induce the same orbits for the spin state. Also, the case $R_i \otimes \mathbf{1}$ will be omitted since it is equivalent to the rotation generated by product momenta. This is because if only the first particle is rotated, the product momenta and the entangled momenta collapse into the same state. We will also leave out the implementations of concrete rotations since they are analogous to those of product momenta.

4.5.4.1 Case $R_i \otimes R_i$

The case of two-rotations $R_i \otimes R_i$ for entangled momenta is quite dissimilar from the behaviour generated by the product momenta. We begin by calculating the orbit of $|\Phi^{+}\rangle$ generated by $\left|M^{\Phi+}\right\rangle$. The three rotations fall into two cases. The $R_X \otimes R_X$ and $R_Z \otimes R_Z$ produce orbits

$$\begin{aligned} t_{X\otimes X}(\omega) &= (1, -\cos 2\omega, \cos 2\omega) \ , \\ t_{Z\otimes Z}(\omega) &= (\cos 2\omega, -\cos 2\omega, 1) \ , \end{aligned} \tag{4.51}$$

whereas $R_Y \otimes R_Y$ leaves the state invariant,

$$t_{Y\otimes Y}(\omega) = (1, -1, 1) \ . \tag{4.52}$$

This asymmetry arises from the fact that $\left|M^{\Phi+}\right\rangle$ consists of momentum terms which induce rotations in the positive direction, $R_i(\omega) \otimes R_i(\omega)$, and in the negative direction $R_i(-\omega) \otimes R_i(-\omega)$. $|\Phi^{+}\rangle$ is an eigenstate of such rotations around the y-axis, $R_Y(\pm\omega) \otimes R_Y(\pm\omega)$, but not around the other axes, $R_X(\pm\omega) \otimes R_X(\pm\omega)$ and

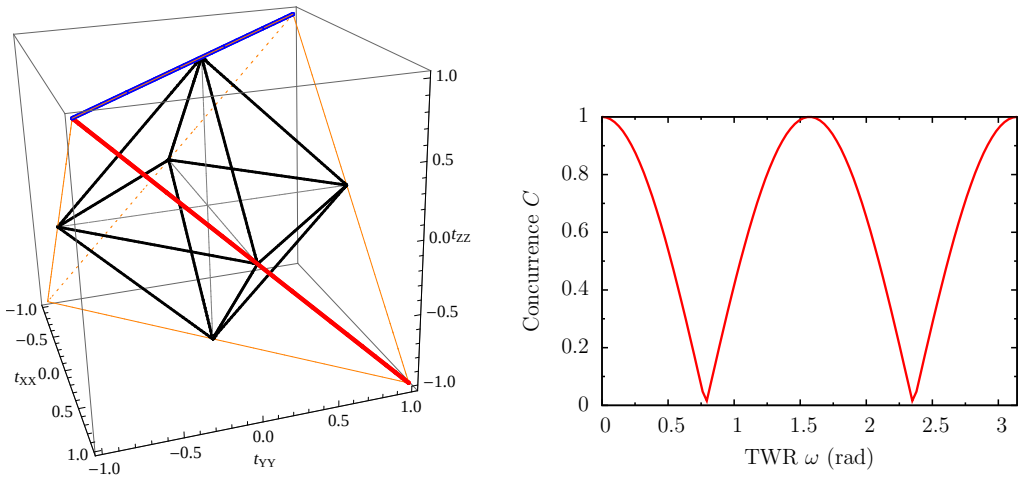

(a) (b)

Figure 4.7. Spin orbit and concurrence of $\left|\Phi^+\right\rangle$ under $R_i \otimes R_i$ with $i \in \{X, Z\}$ and $\omega \in [0, \pi]$. Entangled momenta are given by either $\left|M^{\Phi+}\right\rangle$ or $\left|M^{\Psi+}\right\rangle$. (a) Initial state $\left|\Phi^+\right\rangle$ corresponds to vertex $(1, -1, 1)$, orbit for $R_X \otimes R_X$ is shown red and $R_Z \otimes R_Z$ is blue. (b) Concurrence has the same shape for both orbits.

$R_Z(\pm\omega) \otimes R_Z(\pm\omega)$. The concurrence corresponding to the trivial orbit $t_{Y\otimes Y}$ is $C = 1$, whereas the nontrivial orbits $t_{X\otimes X}$ and $t_{Z\otimes Z}$ give

$$C(\omega) = |\cos 2\omega| \ , \tag{4.53}$$

Plots for non-trivial state evolution and concurrence are shown in Figure 4.7.

Other Bell states display similar systematic behaviour. Depending on whether or not they are eigenstates of the particular rotation, they do or do not show non-trivial behaviour. There are two equivalence classes, the non-trivial one which we denote $[R_X \otimes R_X, M^{\Phi+}_{YY}, \Phi^+]$ and the one with trivial orbit, $[R_Y \otimes R_Y, M^{\Phi+}_{XX}, \Phi^+]$.

The expression for spin concurrence in Equation (4.53) was first reported in [92]. The authors consider a geometry where momenta of both particles make an angle $\pi/2$ to the direction of boost, obtaining a change of entanglement shown between $[0, \pi/2]$ in Figure 4.7.

4.5.4.2 Case $R_i \otimes R_j$

Mixed rotations $R_i \otimes R_j$, $i \neq j$ realised by entangled momenta induce spin orbits that are not diagonal. For instance, the coefficient matrices $t_{i\otimes j}$ with $i, j \in \{X, Y, Z\}$, generated by the momentum state $\left|M^{[\Phi+]}\right\rangle$ for the rest frame spin $|\Phi^+\rangle$ are as fol-

lows,

$$t_{X\otimes Y}(\omega) = \begin{pmatrix} \cos\omega & 0 & 0 \\ -\sin^2\omega & -\cos\omega & 0 \\ 0 & 0 & \cos^2\omega \end{pmatrix}, \quad t_{X\otimes Z}(\omega) = \begin{pmatrix} \cos\omega & 0 & 0 \\ 0 & -\cos^2\omega & 0 \\ \sin^2\omega & 0 & \cos\omega \end{pmatrix},$$

$$t_{Y\otimes Z}(\omega) = \begin{pmatrix} \cos^2\omega & 0 & 0 \\ 0 & -\cos\omega & 0 \\ 0 & -\sin^2\omega & \cos\omega \end{pmatrix}. \tag{4.54}$$

We calculate that concurrence is the same for all three orbits,

$$C(\omega) = \cos^2\omega\ , \tag{4.55}$$

which we recognise as being identical to the concurrence of $R_i \otimes R_i$ generated by product momenta $\left|M^{\Sigma}\right\rangle$. The plot is shown in Figure 4.8

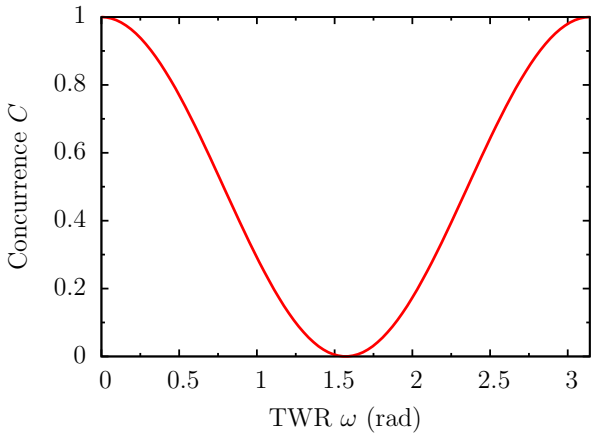

Figure 4.8. Spin concurrence for mixed rotations $R_i \otimes R_j$, $i \neq j$, generated by entangled momenta $\left|M^{[\Phi+]}\right\rangle$ and $\left|M^{[\Psi+]}\right\rangle$.

Although the states are not diagonal, the structure of $t_{i\otimes j}$ suggests that the orbits are isomorphic to each other. All three matrices contain the same diagonal terms as the orbit of $R_i \otimes R_j$ induced by product momenta. In addition, all matrices contain an off-diagonal term $\pm\sin^2\omega$, whose location varies systematically. This allows us to represent the matrices $t_{i\otimes j}$ by a four vector consisting of the diagonal and off-diagonal terms, $(t_{kk}, \pm\sin^2\omega)$. The three states can be thus seen to be related by a one-one map. They seem to share similar geometric structure as well. The first three components of the four vector represent the orbit of $R_i \otimes R_j$,

the fourth component varies in the same way (modulo sign) albeit in a different subspace for different rotations.

The expression for concurrence (4.55) is identical to that of $R_i \otimes R_i$ generated by product momenta. Could it be then that the orbit exhibits the same shape as well? This is not the case. Whereas the orbit of the product rotation is cyclic since it returns to the initial state at $\omega = \pi$, the orbit here starts at $|\Phi^+\rangle$ when $\omega = 0$ and ends at $|\Phi^-\rangle$ with $\omega = \pi$.

We conclude that more investigation is needed to to determine the geometric structure of the orbit but we will not pursue the issue further since it is not crucial at this point. By directly computing rotations for other Bell states we observe the same structure shared by all orbits and the concurrence is always given by (4.55). All in all there is one equivalence class whose orbits can be represented by four vectors and we denote $[R_X \otimes R_Y, M^{\Phi+}_{YX}, \Phi^+]$.

4.5.5 Intermediate summary

We summarise the results of the analysis of product and entangled momenta in Tables 4.1 and 4.2, excluding the simple product momenta $\left|M^1\right\rangle$ which leave entanglement invariant. We discern eight equivalence classes into which the behaviour

State	Orbit	Concurrence	Equivalence class
$\left\|M^\Sigma\right\rangle$	$(1, -\cos\omega, \cos\omega)$	$\max\{0, \lvert\cos\omega\rvert\}$	$[R_X \otimes \mathbf{1}, M^\Sigma_{Y0}, \Phi^+]$
	$(1, -\cos^2\omega, \cos^2\omega)$	$\max\left\{0, \cos^2\omega\right\}$	$[R_X \otimes R_X, M^\Sigma_{YY}, \Phi^+]$
	$(\cos\omega, -\cos\omega, \cos^2\omega)$	$\max\left\{0, \frac{1}{4}\left(-1 + 4\lvert\cos\omega\rvert + \cos 2\omega\right)\right\}$	$[R_X \otimes R_Y, M^\Sigma_{YX}, \Phi^+]$
$\left\|M^\times\right\rangle$	$\left(\cos^2\frac{\omega}{2}, -\cos^2\frac{\omega}{2}, \cos\omega\right)$	$\max\{0, \cos\omega\}$	$[R_{XY} \otimes \mathbf{1}, M^\times_{YX0}, \Phi^+]$
	$\left(\cos^4\frac{\omega}{2}, -\cos^4\frac{\omega}{2}, \cos^2\omega\right)$	$\max\left\{0, \frac{1}{16}\left(-\lvert 4\cos\omega - \cos 2\omega - 3\rvert + 4\cos\omega + 7\cos 2\omega + 5\right)\right\}$	$[R_X \otimes R_Y, M^\times_{YX}, \Phi^+]$

Table 4.1: Spin orbit and concurrence of the Bell states generated by product momenta $\left|M^\Sigma\right\rangle$ and $\left|M^\times\right\rangle$. The second column shows a typical orbit.

of spin and spin entanglement falls under Lorentz boosts generated by product and entangled momenta. Further investigation is needed to determine the shape of the orbit of $[R_X \otimes R_Y, M^{\Phi+}_{YX}, \Phi^+]$.

Rotation	Orbit	Concurrence	Equivalence class
$R_i \otimes R_i$	$(\cos 2\omega, -1, \cos 2\omega)$	$\max\{0, \lvert\cos 2\omega\rvert\}$	$[R_X \otimes R_X, M^{\Phi+}_{YY}, \Phi^+]$
	trivial	1	$[R_Y \otimes R_Y, M^{\Phi+}_{XX}, \Phi^+]$
$R_i \otimes R_j$	not diagonal	$\max\{0, \cos^2\omega\}$	$[R_X \otimes R_Y, M^{\Phi+}_{YX}, \Phi^+]$

Table 4.2: Spin orbit and concurrence of the Bell states generated by entangled momenta $\left|M^{\Phi+}\right\rangle$, $\left|M^{\Psi+}\right\rangle$, $\left|M^{[\Phi+]}\right\rangle$ and $\left|M^{[\Psi+]}\right\rangle$. The second column shows a typical orbit.

4.6 Mixed spins: Werner states

So far we have studied the behaviour of Bell states under Lorentz boosts; they are the pure states that span the set of Bell diagonal states. But the Bell diagonal states contain mixed states as well. We saw above that they have a rich structure, comprising both entangled and separable states. This raises the intriguing question of how the mixed spin states behave under Lorentz boosts, is the structure they display similar to that of the Bell states or is it quite different? We will tackle this question in the following sections by extending our treatment to mixed spin states.

As before the momentum space is assumed to be finite dimensional and spin–momentum degrees factorize, so the total state of the system is of the form,

$$\rho^{\psi} = \rho^{M} \otimes \rho^{\Psi} \,, \tag{4.56}$$

where ρ^{Ψ} is the spin state and ρ^{M} is momentum. As regards the spin state, we would like to cover many different cases and find the possibly widest range of behaviour. Orbits of different Bell states turned out to be isomorphic to each other, we expect to witness similar effect for mixed states. Another consideration is that we wish to study mixed states of different degrees of entanglement, possibly ranging from states with maximal entanglement to no entanglement at all. These considerations naturally lead to the so-called Werner states. The family of generalised Werner states are the states that interpolate between the maximally mixed and maximally entangled state $P_+ = |\Phi^+\rangle\langle\Phi^+|$,

$$\rho^{W}(\lambda) = \lambda \left|\Phi^+\right\rangle\left\langle\Phi^+\right| + (1-\lambda)\frac{1}{N}\mathbf{1} \quad \text{with} \;\; \lambda \in [0,1] \,, \tag{4.57}$$

where in the present case $N = 4$ for the bipartite two level systems. The Werner states lie on the line connecting the origin to the vertex $(1, -1, 1)$ that represents the maximally mixed Bell state $|\Phi^+\rangle$, see Figure 4.9. They contain both entangled and separable mixed states which have interesting properties. For certain values of the

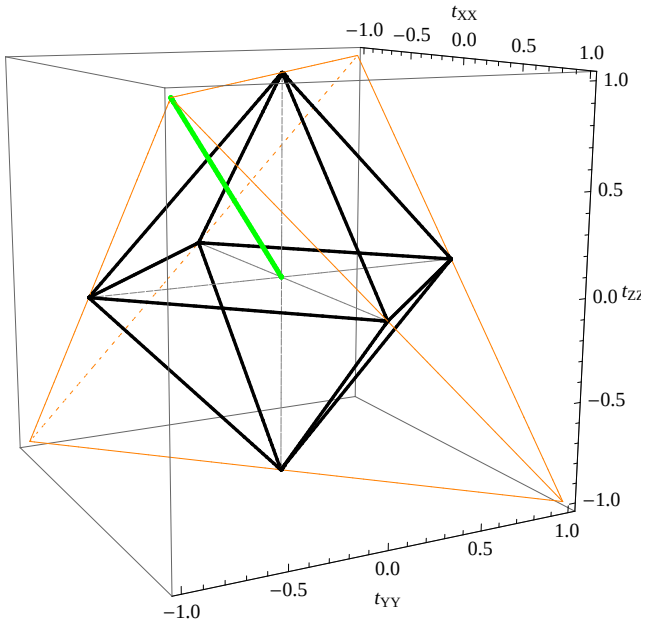

Figure 4.9. The geometry of Bell diagonal states. Werner states $\rho^W(\lambda)$ (green dashed) lie on the line connecting the origin and the vertex at $(1,-1,1)$.

parameter λ the Werner states are entangled but do not violate the Bell inequality [80]. As the mixture moves from the origin, which represents the maximally mixed state, towards the vertex corresponding to the Bell maximally entangled state, it becomes entangled when crossing the face of the octahedron. This corresponds to $\lambda_{\text{sep}} = 1/3$, or the distance $1/\sqrt{3}$ from the origin. However, as was shown in [95], the mixed state state violates the Bell inequality only when the distance is greater than $\sqrt{3}/\sqrt{2}$ from the origin, corresponding to $\lambda = 1/\sqrt{2}$. These features of Werner states make them particularly suitable for the purpose of probing the behaviour of a wide range of mixed states with different degrees of entanglement. We proceed in analogy to the Bell states and calculate the spin orbit as a function of the Thomas-Wigner angle ω and the parameter λ.

We would like to retain the same momenta used for the pure states, so we can take ρ^M in (4.56) to be projectors on the product, $\left|M^{\Sigma}\right\rangle\left\langle M^{\Sigma}\right| = P^{M\Sigma}$, or the entangled states, for instance, $\left|M^{\Phi+}\right\rangle\left\langle M^{\Phi+}\right| = P^{M\Phi+}$, and accordingly for the other entangled states. On the other hand, as long as we are only interested in the boosted spin state, we can also take momenta to be the mixed states that consist of the diagonal elements of the projector on the corresponding pure momenta,

$$\rho^M_{\text{d}} = \text{diag}\ |M\rangle\langle M| \ . \tag{4.58}$$

This is because if we assume that the momenta of the total rest frame state are given by mixed momenta that comprise the diagonal elements of the corresponding pure momenta,

$$\rho^{\psi} = \sum |\psi(\mathbf{p}_i, \mathbf{q}_j)|^2 \, |\mathbf{p}_i, \mathbf{q}_j\rangle \langle \mathbf{p}_i, \mathbf{q}_j| \otimes \rho^{\Psi} \ , \tag{4.59}$$

then a Lorentz boost Λ transforms this to

$$\rho^{\psi''} = \sum |\psi(\mathbf{p}_i, \mathbf{q}_j)|^2 \, |\Lambda\mathbf{p}_i, \Lambda\mathbf{q}_j\rangle \langle \Lambda\mathbf{p}_i, \Lambda\mathbf{q}_j| \otimes R(\Lambda, \mathbf{p}_i, \mathbf{q}_j) \rho^{\Psi} R^{\dagger}(\Lambda, \mathbf{p}_i, \mathbf{q}_j) \ . \tag{4.60}$$

By tracing out momenta we obtain the spin state

$$\rho_S^{\psi''} = \sum |\psi(\mathbf{p}_i, \mathbf{q}_j)|^2 R(\Lambda, \mathbf{p}_i, \mathbf{q}_j) \rho^{\Psi} R^{\dagger}(\Lambda, \mathbf{p}_i, \mathbf{q}_j) \ , \tag{4.61}$$

which is identical to the expression (4.8) that describes the boosted spin resulting from pure spin–momentum states [92]. In other words, only the diagonal elements of the momentum matrix contribute to the final spin state. This implies that we would have obtained the same results above if we had used mixed momenta (4.58) for the pure spin states. It also means we would arrive at the same spin state if we used the pure momentum state for the mixed spins. In the following calculations we will use mixed momenta (4.58) since we will be only interested in the spin state.[2]

4.6.1 Product momenta ρ^{M1}

We begin by discussing briefly the simplest product state $\rho^{M1} = \left|M^1\right\rangle \left\langle M^1\right|$. The analysis runs along the same lines as in the case of pure momentum. ρ^{M1} generates a unitary map of the form $U_1 \otimes U_2$ on the spin state, which takes the spin Werner state to

$$U_1 \otimes U_2 : \rho^W(\lambda) \longmapsto \rho'^W(\lambda) = \lambda \left|\Phi'\right\rangle \left\langle \Phi'\right| + (1-\lambda) \frac{1}{4} \mathbf{1}_4 \ , \tag{4.62}$$

where $|\Phi'\rangle = U_1 \otimes U_2 \, |\Phi^+\rangle$ is a maximally entangled pure state because the unitary does not change the degree of entanglement. The final spin state $\rho'^W(\lambda)$ again displays the form of a mixture of a maximally entangled and maximally mixed state parameterised by λ, thus containing the same amount of entanglement as the initial $\rho^W(\lambda)$. In summary, the degree of entanglement of spin Werner states

[2] However, if we were interested in the total state, then we would need to distinguish between pure and mixed momenta since they generate different total spin–momentum states.

remains invariant under maps generated by simple product momenta ρ^{M1}.

4.6.2 Product momenta $\rho_{\mathrm{d}}^{\Sigma}$

In the following sections 4.6.2.1–4.6.2.3 we will focus on the mixed momenta

$$\rho_{\mathrm{d}}^{M\Sigma} = \mathrm{diag}\left|M^{\Sigma}\right\rangle\left\langle M^{\Sigma}\right| \ , \tag{4.63}$$

which form the counterpart of pure product momenta $\left|M^{\Sigma}\right\rangle$ for the pure spin states.

4.6.2.1 Case $R_i \otimes \mathbf{1}$

We calculate that the orbit of the single particle rotation $R_X \otimes \mathbf{1}$ is given by

$$t_{X\otimes\mathbf{1}}(\omega,\lambda) = \lambda\,(1,-\cos\omega,\cos\omega) \ . \tag{4.64}$$

The concurrence has the form,

$$C(\omega,\lambda) = \begin{cases} \max\left\{0,\ \frac{1}{2}\left(-1+\lambda+2\lambda|\cos\omega|\right)\right\} & \text{if} \quad \lambda\in(\lambda_{\text{sep}},1] \\ 0 & \text{if} \quad \lambda\in[0,\lambda_{\text{sep}}] \end{cases} \tag{4.65}$$

where λ_{sep} corresponds to the point on the face of the octahedron where the initial state crosses the boundary of entangled and separable states. Figure 4.10 shows plots of state change and concurrence. We illustrate spin behaviour by plotting three orbits in Figure 4.10a for three different values of λ. This provides helpful insight into the behaviour of entanglement. For $\lambda = 1$ we recover the orbit of the Bell state $|\Phi^+\rangle$. As λ decreases, the initial state becomes mixed, moving closer to the center of the octahedron. At $\lambda = 3/5$, the initial state lies just outside the octahedron, still containing some entanglement at $C = 2/5$. Now, when the state is boosted, it moves along the orbit which is parallel to the orbit of the Bell state, becoming separable as it enters the octahedron. By setting concurrence zero in the first line of Equation (4.65), we find that the corresponding value of ω is

$$\omega_{\pm} = \arccos \pm\left(\frac{1-\lambda}{2\lambda}\right) \ , \tag{4.66}$$

which for $\lambda = 3/5$ evaluates to $\omega_+ = 1.23$ and $\omega_- = 1.91$. Thus in the range $\omega \in [1.23, 1.91]$ spins appear fully separable to the boosted observer. However, as boosts increase even further, entanglement becomes non-zero again when ω is

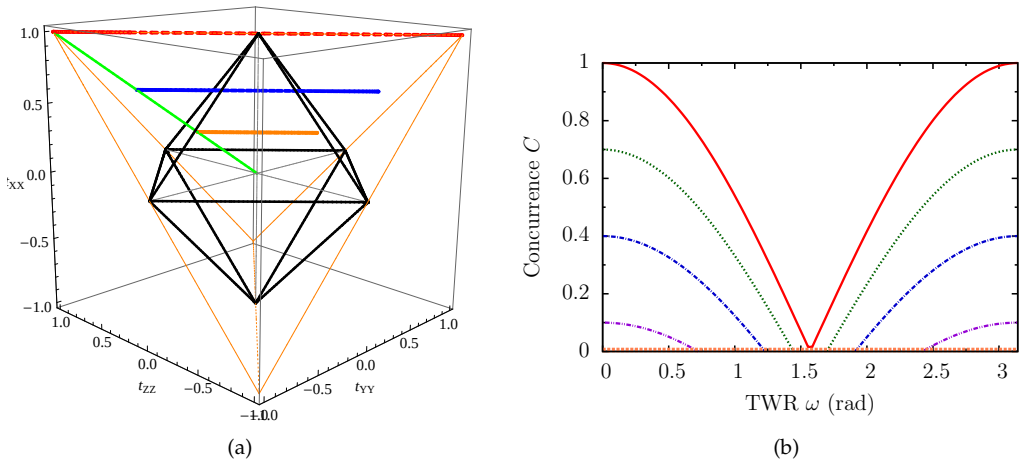

(a) (b)

Figure 4.10. Typical spin orbit and concurrence under $R_i \otimes \mathbf{1}$ with $\omega \in [0, \pi]$ generated by mixed momenta $\rho_{\mathrm{d}}^{M\Sigma}$. (a) Initial states $\rho^W(\lambda)$ lie on the line connecting the origin to the vertex $(1, -1, 1)$ and correspond to values $\lambda = 1, 3/5, 1/3$ with the respective colours red, blue and orange. Note that the figure has been rotated relative to the previous ones. (b) Concurrence is shown for $\lambda = 1, 4/5, 3/5, 2/5, 1/3$ with the respective colours red, green, blue, magenta, orange.

larger than 1.91. The orbit leaves the octahedron and enters the region of entangled states. As boosts near the speed of light, the Thomas-Wigner angle approaches π and the state is mapped to the point which is a mirror image of the initial state with respect to the plane $\mathcal{P}$ that intersects the origin and the vertices $(1, -1, -1)$ and $(1, 1, 1)$. This is a generalisation of the phenomenon we saw in the Bell states where boosts at the speed of light mapped $|\Phi^+\rangle$ to $|\Psi^+\rangle$. In the present case, maximal boosts map the Werner state $\rho^W(\lambda)$ to a another Werner state, which is written as a mixture of $|\Psi^+\rangle\langle\Psi^+|$ and the maximally mixed state,

$$\rho^{W\Psi+} = \lambda \left|\Psi^+\right\rangle \left\langle\Psi^+\right| + (1-\lambda)\frac{1}{4}\mathbf{1}_4 \quad \text{with} \quad \lambda \in [0, 1] \,. \tag{4.67}$$

When $\omega = \pi$, concurrence attains $2/5$, the same value it has in the rest frame.

States that lie initially in the octahedron, for instance when $\lambda = 1/3$, are separable. Boosts map the state to an orbit which is again parallel to that of the Bell state, with the total orbit being of symmetric shape with respect to the plane $\mathcal{P}$. However, because the whole orbit remains inside the octahedron of separable states, concurrence is zero at all boost values.

Other rotations display symmetric behaviour, there is only one equivalence class which we denote, in analogy to pure states, $[R_X \otimes \mathbf{1}, \rho_{\mathrm{d}}^{M\Sigma}, \rho^W]$.

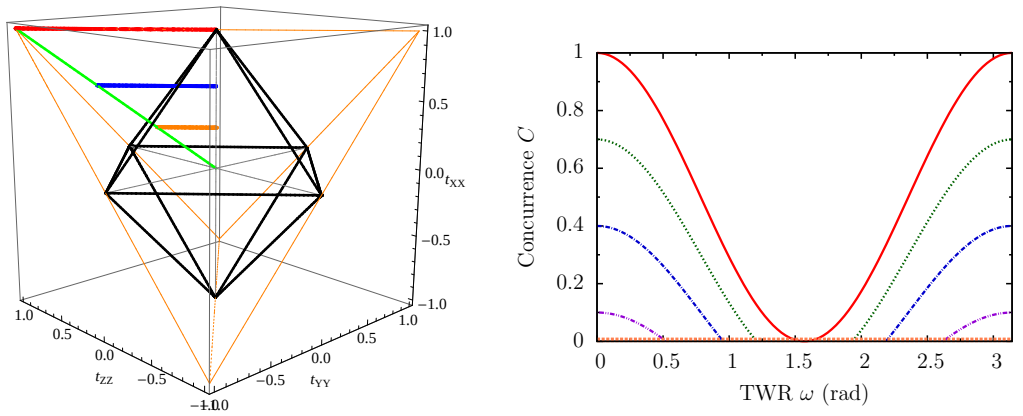

(a) (b)

Figure 4.11. Typical spin orbit and concurrence under $R_i \otimes R_i$ with $\omega \in [0, \pi]$ generated by mixed momenta $\rho_{\mathrm{d}}^{M\Sigma}$. (a) Initial states $\rho^W(\lambda)$ lie on the line connecting the origin to the vertex $(1, -1, 1)$ and correspond to values $\lambda = 1, 3/5, 1/3$ with the respective colours red, blue and orange. (b) Concurrence is shown for $\lambda = 1, 4/5, 3/5, 2/5, 1/3$ with the respective colours red, green, blue, magenta, orange.

4.6.2.2 Case $R_i \otimes R_i$

For boost scenarios involving rotations on two particles, we calculate the orbit of $R_X \otimes R_X$,

$$t_{X\otimes X}(\omega, \lambda) = \lambda \left(1, -\cos^2\omega, \cos^2\omega\right) \ , \tag{4.68}$$

which gives for concurrence

$$C(\omega, \lambda) = \begin{cases} \max\left\{0, \ -\frac{1}{2} + \lambda + \frac{1}{2}\lambda\cos 2\omega\right\} & \text{if} \quad \lambda \in (\lambda_{\text{sep}}, 1] \\ 0 & \text{if} \quad \lambda \in [0, \lambda_{\text{sep}}] \end{cases} \tag{4.69}$$

where as above λ_{sep} is the value where the rest frame state becomes separable. Plots of spin orbits and concurrence are shown in Figure 4.11.

Many characteristics are similar to the previous case. Orbits for initial states with less than maximal entanglement are parallel to the orbit of the Bell state $|\Phi^+\rangle$. As boost increases, an initially entangled state moves towards the octahedron and becomes separable when entering the octahedron. To find the corresponding values of ω, we set the concurrence to zero in Equation (4.69) and solve for ω, obtaining

$$\omega_{k,\pm} = \frac{1}{2}\left(2k\pi \pm \arccos\left(\frac{1-2\lambda}{\lambda}\right)\right) \ , \quad k \in \mathbb{N} \ . \tag{4.70}$$

The solutions relevant in the present case are $\omega_{0,+}$ and $\omega_{1,-}$. This means ρ_S'' is separable if $\omega \in [\omega_{0,+}, \omega_{1,-}]$. For instance, a state for which $\lambda = 3/5$, whose orbit

is shown blue in Figure 4.11, concurrence vanishes if $\omega \in [0.96, 2.19]$, corresponding to points at which the orbit enters and leaves the octahedron. In the similar vein, initial states that lie inside the octahedron and are separable follow an orbit for which entanglement remains zero. There is a difference from the previous case: when boosts approach the speed of light, the state is mapped back to the original state.

Other rotations again generate symmetric orbits and there is only one equivalence class which we denote $[R_X \otimes R_X, \rho_{\mathrm{d}}^{M\Sigma}, \rho^W]$.

4.6.2.3 Case $R_i \otimes R_j$

For boost scenarios that contain terms with different rotations for either particle we calculate that the orbit generated by $R_X \otimes R_Z$ is

$$t_{X\otimes Z}(\omega, \lambda) = \lambda \left(\cos\omega, -\cos^2\omega, \cos\omega\right) \ , \tag{4.71}$$

and concurrence is

$$C(\omega,\lambda) = \begin{cases} \max\left\{0,\ \frac{1}{8}\left(\big|\,|2+\lambda+4\lambda\cos\omega+\lambda\cos 2\omega| \right.\right. \\ \left.\left. -|2+\lambda-4\lambda\cos\omega+\lambda\cos 2\omega|\,\big| + 2\left(-2+\lambda+\lambda\cos 2\omega\right)\right)\right\} \\ \qquad\qquad\qquad\qquad\qquad\qquad\qquad\qquad \text{if} \quad \lambda \in (\lambda_{\text{sep}}, 1] \\ 0 \qquad\qquad\qquad\qquad\qquad\qquad\qquad\qquad\qquad\quad \text{if} \quad \lambda \in [0, \lambda_{\text{sep}}] \end{cases} \tag{4.72}$$

where at λ_{sep} the state becomes separable. Figure 4.12 shows plots of orbits and concurrence. We recognise a pattern of behaviour that is similar to the previous cases, albeit with a few differences. As before, the states follow an orbit that resides in the octahedron for a range of values around $\pi/2$. However, the region where concurrence vanishes is considerably larger than in the previous cases. Also, while above orbits of mixed states were parallel to the orbit of the Bell state, here all the orbits pass through the maximally mixed state $\frac{1}{4}\mathbf{1}_4$. To find the values of ω for which concurrence vanishes, we set concurrence to zero in the first line of Equation (4.72) and solve for ω,

$$\omega_{k,\pm} = k\pi \pm \arccos\left(\frac{\lambda - \sqrt{\lambda+\lambda^2}}{\lambda}\right) \ , \quad k = 0, 1 \ , \tag{4.73}$$

entailing that the state is separable if $\omega \in [\omega_{1,-},\, \omega_{0,+}]$. For example, when $\lambda = 3/5$, entanglement vanishes in the interval $\omega \in [0.89, 2.25]$. Orbits of other rotations

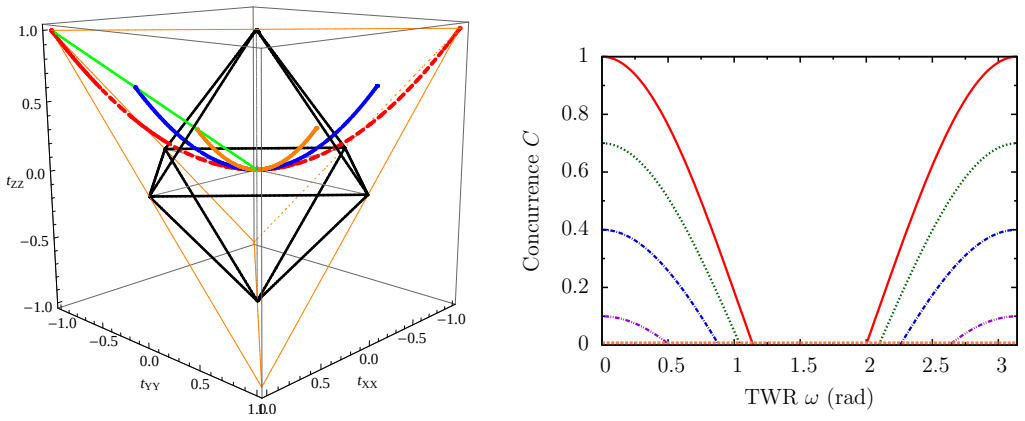

(a) (b)

Figure 4.12. Typical spin orbit and concurrence under $R_i \otimes R_j$, $i \neq j$ with $\omega \in [0, \pi]$ generated by mixed momenta $\rho_{\mathrm{d}}^{M\Sigma}$. (a) Initial states $\rho^W(\lambda)$ lie on the line connecting the origin to the vertex $(1, -1, 1)$ and correspond to values $\lambda = 1, 3/5, 1/3$ with the respective colours red, blue and orange. (b) Concurrence is shown for $\lambda = 1, 4/5, 3/5, 2/5, 1/3$ with the respective colours red, green, blue, magenta, orange.

belong to the same equivalence class which we denote $[R_X \otimes R_Z, \rho_{\mathrm{d}}^{M\Sigma}, \rho^W]$.

4.6.3 Product momenta $\rho_{\mathrm{d}}^{M\times}$

The analysis of product momenta $\rho_{\mathrm{d}}^{M\times}$ runs along the same lines as for the pure spins. It divides into two classes, the $R_i \otimes \mathbf{1}$ and the combination of $R_i \otimes R_i$ with $R_i \otimes R_j$, where the orbits of each can be found by taking convex combinations of the respective trajectories of maps found earlier.

4.6.3.1 Case $R_i \otimes \mathbf{1}$

Starting with the momentum where the first particle is a mixture of projectors on $|\pm\mathbf{p}_y\rangle$ and $|\pm\mathbf{p}_x\rangle$, we calculate the convex combination in analogy to the pure states, Equation (4.45),

$$t_{XY\otimes\mathbf{1}}(\omega, \lambda) = \lambda \left(\cos^2 \frac{\omega}{2}, -\cos^2 \frac{\omega}{2}, \cos\omega \right) . \tag{4.74}$$

Orbits of the other states can be obtained in the same fashion; they exhibit similar structure. The corresponding concurrence is

$$C(\omega, \lambda) = \begin{cases} \max\left\{0, \ \frac{1}{2}\left(-1 + \lambda + 2\lambda\cos\omega\right)\right\} & \text{if} \quad \lambda \in (\lambda_{\mathrm{sep}}, 1] \\ 0 & \text{if} \quad \lambda \in [0, \lambda_{\mathrm{sep}}] \end{cases} \tag{4.75}$$

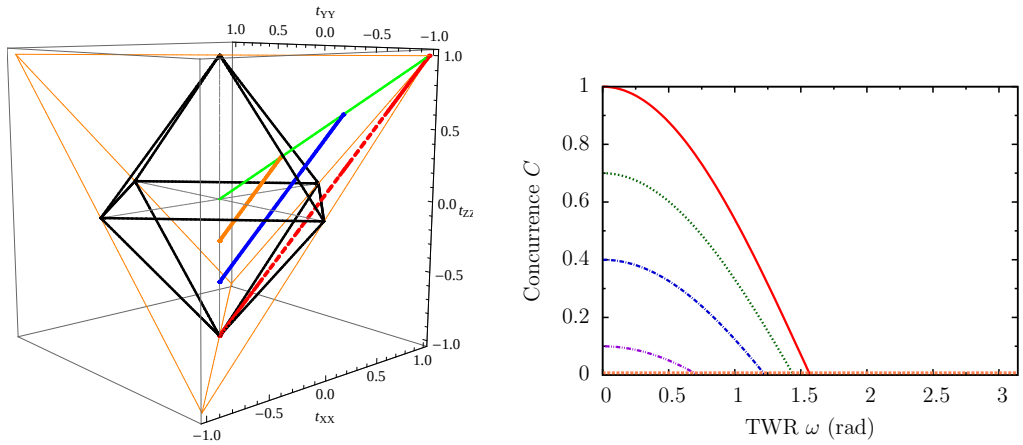

(a) (b)

Figure 4.13. Typical spin orbit and concurrence under $R_i \otimes \mathbf{1}$ generated by momenta $\rho_{\mathrm{d}}^{M\times}$ with $\omega \in [0, \pi]$. (a) Initial states $\rho^W(\lambda)$ lie on the line connecting the origin to the vertex $(1, -1, 1)$ and correspond to values $\lambda = 1, 3/5, 1/3$ with the respective colours red, blue and orange. (b) Concurrence is shown for $\lambda = 1, 4/5, 3/5, 2/5, 1/3$ with the respective colours red, green, blue, magenta, orange.

where λ_{sep} is the value at which the initial spin state becomes separable. Figure 4.13 shows plots of spin orbit and concurrence. For states with $\lambda < 1$, the states disentangle at lower values of ω. This is because the orbits remain parallel to the orbit of the Bell state and thus enter the octahedron sooner. Since they are also parallel to the face of the bottom pyramid, the state never escapes the region of separability. Other rotations generate similar orbits, there is one equivalence class which we denote $[R_{XY} \otimes \mathbf{1}, \rho_{\mathrm{d}}^{M\times}, \rho^W]$.

4.6.3.2 Case $R_i \otimes R_i$ and $R_i \otimes R_j$

In a scenario where boost is in the z-direction and momenta are constrained to the $x - z$- and $y - z$-planes, we calculate $t_{X\otimes Y}$ by taking a convex combination of respective orbits as in Equation (4.48),

$$t_{X\otimes Y}(\omega, \lambda) = \lambda \left(\cos^4 \frac{\omega}{2}, -\cos^4 \frac{\omega}{2}, \cos^2 \omega \right) . \tag{4.76}$$

Other orbits are similar and the concurrence is given by

$$C(\omega, \lambda) = \begin{cases} \max\left\{0,\ \frac{1}{16}\left(-|4\lambda\cos\omega - \lambda\cos 2\omega + \lambda - 4| \right.\right. & \\ \qquad \left.\left. + 4\lambda\cos\omega + 7\lambda\cos 2\omega + 9\lambda - 4)\right\} \right. & \text{if} \quad \lambda \in (\lambda_{\mathrm{sep}}, 1] \\ 0 & \text{if} \quad \lambda \in [0, \lambda_{\mathrm{sep}}] \, . \end{cases} \tag{4.77}$$

Plots of spin orbit and concurrence are shown in Figure 4.14. While on the face of it

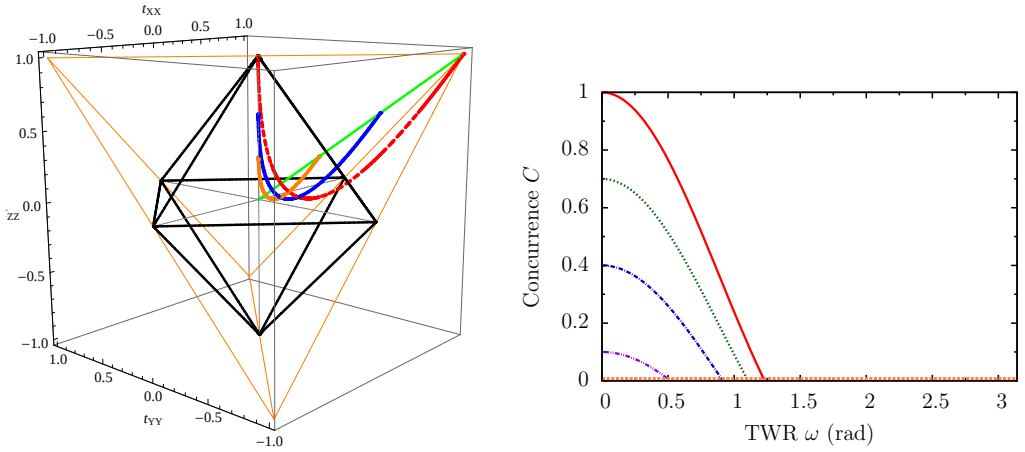

(a) (b)

Figure 4.14. Typical spin orbit and concurrence $R_i \otimes R_i$ and $R_i \otimes R_j$ generated by momenta $\rho_{\mathrm{d}}^{M\times}$ with $\omega \in [0, \pi]$. (a) Initial states $\rho^W(\lambda)$ lie on the line connecting the origin to the vertex $(1, -1, 1)$ and correspond to values $\lambda = 1, 3/5, 1/3$ with the respective colours red, blue and orange. (b) Concurrence is shown for $\lambda = 1, 4/5, 3/5, 2/5, 1/3$ with the respective colours red, green, blue, magenta, orange.

the concurrence is of almost analogous shape as the previous case, the reason why this occurs is quite different as the orbit follows a rather dissimilar path. The orbit initially moves downward as in the previous case, with the state disentangling slightly earlier; soon after entering the octahedron the orbit turns upward and ends at a point which lies at a point almost opposite to the point representing the final state under $R_{XY} \otimes \mathbf{1}$. Visualisation of the orbit clearly reveals the difference between the two cases. Other rotations produce similar orbits, we denote the only equivalence class by $[R_X \otimes R_Y, \rho_{\mathrm{d}}^{M\times}, \rho^W]$.

4.6.4 'Entangled' momenta

We will next focus on mixed momenta that correspond to the pure entangled states,

$$\begin{aligned}
\rho_{\mathrm{d}}^{M\Phi+} &= \mathrm{diag}\left|M^{\Phi+}\right\rangle\left\langle M^{\Phi+}\right|, \\
\rho_{\mathrm{d}}^{M\Psi+} &= \mathrm{diag}\left|M^{\Psi+}\right\rangle\left\langle M^{\Psi+}\right|, \\
\rho_{\mathrm{d}}^{M[\Phi+]} &= \mathrm{diag}\left|M^{[\Phi+]}\right\rangle\left\langle M^{[\Phi+]}\right|, \\
\rho_{\mathrm{d}}^{M[\Psi+]} &= \mathrm{diag}\left|M^{[\Psi+]}\right\rangle\left\langle M^{[\Psi+]}\right|.
\end{aligned} \tag{4.78}$$

They are clearly not entangled since they contain only the diagonal elements of the projectors on entangled states. We will, however, categorise the resulting spin states as if they had been generated by entangled momenta for the reason highlighted above, namely, that entangled momenta would lead to the same spin states.

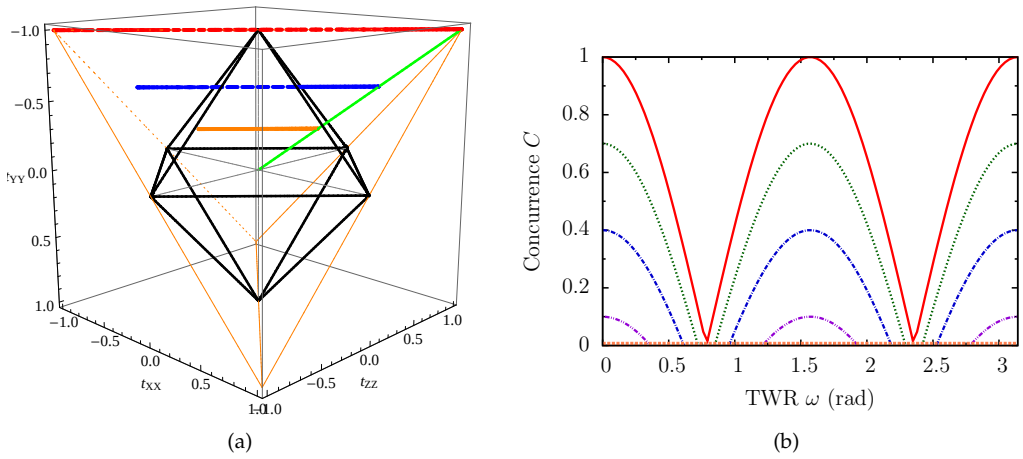

(a) (b)

Figure 4.15. Typical spin orbit and concurrence under $R_i \otimes R_i$ with $\omega \in [0, \pi]$ generated by mixed momenta $\rho_{\mathrm{d}}^{M\Phi+}$ or $\rho_{\mathrm{d}}^{M\Psi+}$. (a) Initial states $\rho^W(\lambda)$ lie on the line connecting the origin to the vertex $(1, -1, 1)$ and correspond to values $\lambda = 1, 3/5, 1/3$ with the respective colours red, blue and orange. (b) Concurrence is shown for $\lambda = 1, 4/5, 3/5, 2/5, 1/3$ with the respective colours red, green, blue, magenta, orange.

4.6.4.1 $R_i \otimes R_i$

In analogy to the pure momenta, the case of rotations around the same axis splits into two distinct classes. Taking cue from the pure momenta, we first calculate the non-trivial orbits generated by $\rho_{\mathrm{d}}^{M\Phi+}$ under $R_X \otimes R_X$ and $R_Z \otimes R_Z$,

$$\begin{aligned} t_{X\otimes X}(\omega, \lambda) &= \lambda\,(1, -\cos 2\omega, \cos 2\omega)\ , \\ t_{Z\otimes Z}(\omega, \lambda) &= \lambda\,(\cos 2\omega, -\cos 2\omega, 1)\ , \end{aligned} \tag{4.79}$$

which have the concurrence

$$C(\omega, \lambda) = \begin{cases} \max\left\{0,\ \frac{1}{2}\left(-1 + \lambda + 2\lambda|\cos 2\omega|\right)\right\} & \text{if} \quad \lambda \in (\lambda_{\mathrm{sep}}, 1] \\ 0 & \text{if} \quad \lambda \in [0, \lambda_{\mathrm{sep}}]\ . \end{cases} \tag{4.80}$$

The plots of orbits and concurrence are shown in Figure 4.15.

We also get the second equivalence class for $\rho_{\mathrm{d}}^{M\Phi+}$ which contains the trivial orbit generated by $R_Y \otimes R_Y$. The concurrence $C(\lambda) = (-1 + 3\lambda)/2$ of this class does not depend on ω.

The non-trivial orbits share the characteristics of the orbits induced by the pure momenta. The orbits of mixed spins are parallel to those of pure spins, and traverse the state space twice as fast as the single particle maps $R_i \otimes \mathbf{1}$ induced by product momenta, yielding an oscillating plot of concurrence in Figure 4.15b. In analogy to the single particle map, the state is sent to $\rho^{W\Psi+}$; but in contrast to the single particle map, this happens now already at $\omega = \pi/2$. When the rotation achieves the

maximal value π, the boosted observer sees again the original state $\rho^W(\lambda)$. Accordingly, and in contrast to the rotation $R_i \otimes \mathbf{1}$, there are now two separable regions because the state moves forward and backward through the octahedron. The lower the initial degree of entanglement, the larger the part of the orbit in the octahedron, and thus the larger the region of vanishing concurrence, see Figure 4.15b.

In summary, we get two equivalence classes, the non-trivial and the trivial, $[R_X \otimes R_X, \rho_{\mathrm{d}}^{M\Phi+}, \rho^W]$ and $[R_Y \otimes R_Y, \rho_{\mathrm{d}}^{M\Phi+}, \rho^W]$, depending on whether or not the spin state is an eigenstate of the rotation in question.

4.6.4.2 $R_i \otimes R_j$

In analogy to the pure states, the mixed rotations present a case where the orbits are not Bell diagonal. For instance, the momentum state $\rho_{\mathrm{d}}^{M[\Phi+]}$ generates the following orbits for $\rho^W(\lambda)$,

$$t_{X\otimes Y}(\omega,\lambda) = \lambda \begin{pmatrix} \cos\omega & 0 & 0 \\ -\sin^2\omega & -\cos\omega & 0 \\ 0 & 0 & \cos^2\omega \end{pmatrix},$$

$$t_{X\otimes Z}(\omega,\lambda) = \lambda \begin{pmatrix} \cos\omega & 0 & 0 \\ 0 & -\cos^2\omega & 0 \\ \sin^2\omega & 0 & \cos\omega \end{pmatrix}, \tag{4.81}$$

$$t_{Y\otimes Z}(\omega,\lambda) = \lambda \begin{pmatrix} \cos^2\omega & 0 & 0 \\ 0 & -\cos\omega & 0 \\ 0 & -\sin^2\omega & \cos\omega \end{pmatrix}.$$

The concurrence is given by

$$C(\omega,\lambda) = \begin{cases} \max\left\{0,\ -\frac{1}{2} + \lambda + \frac{1}{2}\lambda\cos 2\omega\right\} & \text{if} \quad \lambda \in (\lambda_{\text{sep}}, 1] \\ 0 & \text{if} \quad \lambda \in [0, \lambda_{\text{sep}}]\,. \end{cases} \tag{4.82}$$

Plots of concurrence for different values of λ are shown in Figure 4.16. We discern the same structure as in the case of product momenta under $R_i \otimes R_i$. The same considerations apply about the geometric structure of the orbits as in the case of Bell states. We denote the equivalence class $[R_X \otimes R_Y, \rho_{\mathrm{d}}^{M[\Phi+]}, \rho^W]$.

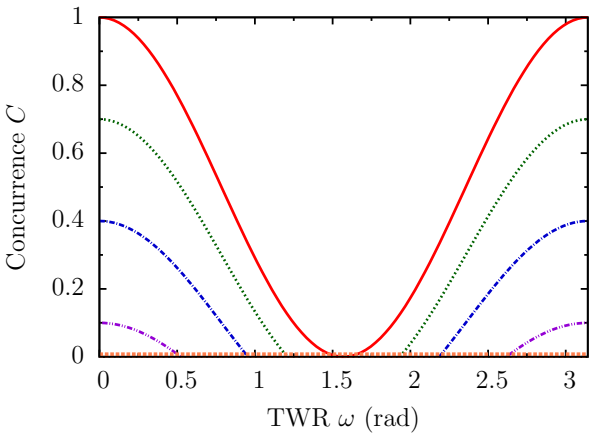

Figure 4.16. Spin concurrence under $R_i \otimes R_j$, $i \neq j$ with $\omega \in [0, \pi]$ generated by mixed momenta $\rho_{\rm d}^{M[\Phi+]}$ and $\rho_{\rm d}^{M[\Psi+]}$. Concurrence is shown for $\lambda = 1, 4/5, 3/5, 2/5, 1/3$ with the respective colours red, green, blue, magenta, orange.

4.7 Summary and discussion

In this chapter we examined entanglement in the spin degree of freedom of a two particle system. We systematically studied various boost scenarios involving both product and entangled momenta with the aim of surveying and classifying the structure of maps that momenta induce on spins. Momenta were assumed to be discrete and spins in the Werner state. The latter subsume the Bell states when $\lambda = 1$. Because the Bell states play such a fundamental role in quantum information theory they were discussed separately. The results are summarised in Tables 4.3 and 4.4.

State	Orbit	Concurrence	Equivalence class
$\rho^{M\Sigma}$	$\lambda(1, -\cos\omega, \cos\omega)$	$\max\left\{0,\ \frac{1}{2}\left(-1+\lambda+2\lambda\lvert\cos\omega\rvert\right)\right\}$	$[R_X \otimes \mathbf{1}, \rho_{\rm d}^{M\Sigma}, \rho^W]$
	$\lambda(1, -\cos^2\omega, \cos^2\omega)$	$\max\left\{0,\ -\frac{1}{2}+\lambda+\frac{1}{2}\lambda\cos 2\omega\right\}$	$[R_X \otimes R_X, \rho_{\rm d}^{M\Sigma}, \rho^W]$
	$\lambda(\cos\omega, -\cos^2\omega, \cos\omega)$	$\max\left\{0,\ \frac{1}{8}\left(\lvert\, \lvert 2+\lambda+4\lambda\cos\omega +\lambda\cos 2\omega\rvert - \lvert 2+\lambda -4\lambda\cos\omega+\lambda\cos 2\omega\rvert\,\right.\right.$ $\left.\left.+2\left(-2+\lambda+\lambda\cos 2\omega\right)\right)\right\}$	$[R_X \otimes R_Z, \rho_{\rm d}^{M\Sigma}, \rho^W]$
$\rho^{M\times}$	$\lambda(\cos^2\frac{\omega}{2}, -\cos^2\frac{\omega}{2}, \cos\omega)$	$\max\left\{0,\ \frac{1}{2}\left(-1+\lambda+2\lambda\cos\omega\right)\right\}$	$[R_{XY} \otimes \mathbf{1}, \rho_{\rm d}^{M\times}, \rho^W]$
	$\lambda(\cos^4\frac{\omega}{2}, -\cos^4\frac{\omega}{2}, \cos^2\omega)$	$\max\left\{0,\ \frac{1}{16}\left(-\lvert 4\lambda\cos\omega-\lambda\cos 2\omega +\lambda-4\rvert+4\lambda\cos\omega+7\lambda\cos 2\omega +9\lambda-4\right)\right\}$	$[R_X \otimes R_Y, \rho_{\rm d}^{M\times}, \rho^W]$

Table 4.3: Spin orbit and concurrence for $\rho^W(\lambda)$ generated by product momenta $\rho_{\rm d}^{M\Sigma}$ and $\rho^{M\times}$. The second column shows typical orbit.

The overall lesson we draw is that Lorentz boosts generally cause non-trivial be-

Rotation	Orbit	Concurrence	Equivalence class
$R_i \otimes R_i$	$\lambda(\cos 2\omega, -1, \cos 2\omega)$	$\max\left\{0,\ \frac{1}{2}\left(-1+\lambda+2\lambda\lvert\cos 2\omega\rvert\right)\right\}$	$[R_X \otimes R_X, \rho_{\mathrm{d}}^{M\Phi+}, \rho^W]$
	trivial	$(-1+3\lambda)/2$	$[R_Y \otimes R_Y, \rho_{\mathrm{d}}^{M\Phi+}, \rho^W]$
$R_i \otimes R_j$	not diagonal	$\max\left\{0,\ -\frac{1}{2}+\lambda+\frac{1}{2}\lambda\cos 2\omega\right\}$	$[R_X \otimes R_Y, \rho_{\mathrm{d}}^{M[\Phi+]}, \rho^W]$

Table 4.4: Spin orbit and concurrence for $\rho^W(\lambda)$ generated by momenta $\rho_{\mathrm{d}}^{M\Phi+}$, $\rho_{\mathrm{d}}^{M\Psi+}$, $\rho_{\mathrm{d}}^{M[\Phi+]}$ and $\rho_{\mathrm{d}}^{M[\Psi+]}$. The second column shows typical orbit.

haviour in the spin degree of freedom of two particle systems. However, whether or not, and to what extent, the state and entanglement of spins changes depends substantially on the spin and momentum states involved, as well as on the geometry of the boost scenario. Whereas some states and geometries leave entanglement invariant, others give rise to rapid changes of concurrence. Examples of the former comprise Bell states with product momenta of the form $|\mathbf{p}, \mathbf{q}\rangle$, as well as the interesting special case of type $R_i \otimes R_i$ for entangled momenta where spin is an eigenstate of rotation, represented by the equivalence class $[R_Y \otimes R_Y, \rho_{\mathrm{d}}^{M\Phi+}, \rho^W]$. All other types of rotations and momenta were found to bring about entanglement change that ranges from maximal to zero, with the class $[R_X \otimes R_X, M^{\Phi+}, \Phi^+]$ for the entangled momenta causing the fastest decay and rebirth of entanglement.

While the literature on relativistic entanglement commonly analyses pure entangled states, it is important to consider mixed states as well in order to gain full understanding. The present work makes a step in this direction by classifying the behaviour of the Werner states, whose entanglement ranges between maximal and no entanglement at all. Compared to pure states, they display less change as the maximal degree of entanglement is bounded by the parameter λ. The latter highlights an important conclusion, which applies to both pure and entangled spin states: spin entanglement cannot be increased under Lorentz boosts if there is no spin-momentum entanglement present in the first place. This was first proved for pure states in [15]. Our investigation shows that this result holds true for mixed spin states as well if spin and momentum initially factorise. It should be stressed though that the result is valid only for initial states whose spin-momentum factorise [15]. If spin and momentum degrees are initially entangled, the boosted state might be more entangled than the initial one. Although proper study of this very interesting case is beyond the scope of the current thesis, as noted in section 4.2, it has been implicit to some extent in the scenarios we examined.

Perhaps even more valuable are the qualitative insights. The basic geometric

framework introduced in the chapter on single particle systems remains in place. The geometric approach unifies the various results reported in the literature, i.e. that spin entanglement did or did not change in a particular boost scenario, by explaining them in a convenient, simplified framework which involves discrete momenta and spins. For example, while the authors of [17] report no change of entanglement, the study in [15] reports up to maximal decay of entanglement for the moving observer. These results are consistent since they employ different momentum states. The model considered in [17] consists of product momenta $|\mathbf{p}, \mathbf{q}\rangle$, whose action leaves Bell states invariant as discussed above. The authors of [15], however, assume continuous origin centred momenta. As we will see in more detail in the next chapter, these continuous momentum states can modelled in many situations quite accurately in terms of the state $|M^{\times}\rangle$, which decay the entanglement of spins as documented above.

Finally, in the context of possible implementations of quantum computation, or quantum communication protocols, in the relativistic setting, the import of our results is twofold. On the one hand relativity might appear as a phenomenon that causes disturbance in the given problem setting, for instance, by reducing fidelities or channel capacities when implementing a quantum communication protocol. Then the results obtained in this chapter might be used to engineer states so that the negative relativistic effects are diminished. On the other hand, relativity may appear as a resource that could be used to generate entangled states or realise, or enhance quantum communication or computation, see e.g. [54, 61]. The results here could be helpful in finding states and scenarios that help achieve the desired goal. As part of the future work, we envisage working out the implications of foregoing results to quantum information theory in more detail.

Chapter 5

Two particles II: continuous momenta

5.1 Introduction

In this chapter we will complete the study of two particle systems by focussing on states involving continuous momenta. In many ways, the discussion will be parallel to that of systems with discrete momenta, with the difference that the spin subsystem will be restricted to the Bell states.

The chapter is organised as follows. We begin by deriving the generic transformation of the two particle's state under Lorentz transformations. We then construct a two particle model involving Gaussian momenta of different kinds, which we thereafter systematically study in various boost scenarios involving both product and entangled momenta.

5.2 Two particle state under Lorentz boosts

We begin by computing the generic transformation of a two particle state under Lorentz boosts. Proceeding along the same lines as for the single particle system and using basis vectors of the form $|\mathbf{p}, \lambda\rangle$, where $\mathbf{p}$ is the label for the single particle momentum and $\lambda = \pm\frac{1}{2}$ is spin, we write a generic pure state of two particles as

$$|\psi\rangle = \sum_{\lambda\eta} \int \mathrm{d}\mu(p,q)\, \psi_{\lambda\eta}(\mathbf{p},\mathbf{q})\, |\mathbf{p},\lambda\rangle\, |\mathbf{q},\eta\rangle \ , \tag{5.1}$$

where $\mathrm{d}\mu(p) = (2E(\mathbf{p}))^{-1}\mathrm{d}\mathbf{p}$ is the Lorentz invariant integration measure and we have abbreviated $\mathrm{d}\mu(p,q) = \mathrm{d}\mu(p)\mathrm{d}\mu(q)$. The wave function satisfies the normalisation condition

$$\sum_{\lambda\eta}\int \mathrm{d}\mu(p,q)|\psi_{\lambda\eta}(\mathbf{p},\mathbf{q})|^2 = 1 \ , \tag{5.2}$$

and the (improper) spin and momentum eigenstates satisfy the orthogonality condition

$$\langle \mathbf{p}', \lambda'|\mathbf{p},\lambda\rangle = 2E(\mathbf{p})\delta^3(\mathbf{p}-\mathbf{p}')\delta_{\lambda\lambda'} \ . \tag{5.3}$$

An observer O'' who is Lorentz boosted relative to O by Λ^{-1} sees the state of the particle $|\psi\rangle$ as transformed by the product $U(\Lambda)\otimes U(\Lambda)$,

$$\left|\psi''\right\rangle = U(\Lambda)\otimes U(\Lambda)\left|\psi\right\rangle \ . \tag{5.4}$$

In order to calculate the transformation on the wave function, we note the action of $U(\Lambda)$ on a basis vector of the single particle, given by Equation (3.5), and substitute (5.1) into (5.4), obtaining

$$\begin{aligned}
\left|\psi''\right\rangle &= \sum_{\lambda\eta}\int \mathrm{d}\mu(p,q)\,\psi_{\lambda\eta}(\mathbf{p},\mathbf{q})\,|\Lambda\mathbf{p}\rangle\otimes\left(\sum_{\kappa}U_{\kappa\lambda}(R(\Lambda,\mathbf{p}))\,|\kappa\rangle\right) \\
&\qquad\qquad \otimes|\Lambda\mathbf{q}\rangle\otimes\left(\sum_{\nu}U_{\nu\eta}(R(\Lambda,\mathbf{q}))\,|\nu\rangle\right) \\
&= \sum_{\lambda\eta}\int \mathrm{d}\mu(\Lambda^{-1}p'',\Lambda^{-1}q'')\,\psi_{\lambda\eta}(\Lambda^{-1}\mathbf{p}'',\Lambda^{-1}\mathbf{q}'')\left|\mathbf{p}''\right\rangle \\
&\quad\otimes\left(\sum_{\kappa}U_{\kappa\lambda}(R(\Lambda,\Lambda^{-1}\mathbf{p}''))\,|\kappa\rangle\right)\otimes\left|\mathbf{q}''\right\rangle\otimes\left(\sum_{\nu}U_{\nu\eta}(R(\Lambda,\Lambda^{-1}\mathbf{q}''))\,|\nu\rangle\right) \\
&= \sum_{\kappa\nu}\int \mathrm{d}\mu(p,q)\,\psi''_{\kappa\nu}(\mathbf{p},\mathbf{q})\,|\mathbf{p},\kappa\rangle\,|\mathbf{q},\nu\rangle \ ,
\end{aligned} \tag{5.5}$$

where in the last line we have replaced the dummy variables with $\mathbf{p}$ and $\mathbf{q}$, and denoted

$$\psi''_{\kappa\nu}(\mathbf{p},\mathbf{q}) = \sum_{\lambda\eta}U_{\kappa\lambda}(R(\Lambda,\Lambda^{-1}\mathbf{p}))U_{\nu\eta}(R(\Lambda,\Lambda^{-1}\mathbf{q}))\psi_{\lambda\eta}(\Lambda^{-1}\mathbf{p},\Lambda^{-1}\mathbf{q}) \ . \tag{5.6}$$

In the following we will be interested in how the entanglement of the spin state changes in various boost scenarios. To obtain the boosted spin state ρ''_S, we trace

out the momentum degrees of freedom,

$$\begin{aligned}\rho''_S &= \mathsf{Tr}_{P,Q}\left(|\psi''\rangle\langle\psi''|\right) = \int \mathrm{d}\mu(p,q)\ \langle \mathbf{p},\mathbf{q}|\psi''\rangle\langle\psi''|\mathbf{p},\mathbf{q}\rangle \\ &= \sum_{\kappa\nu\lambda\eta}\int \mathrm{d}\mu(p,q)\ \int \mathrm{d}\mu(k,t)\,\mathrm{d}\mu(v,w)\,\delta^3(\mathbf{p}-\mathbf{k})\delta^3(\mathbf{q}-\mathbf{t})\delta^3(\mathbf{v}-\mathbf{p}) \\ &\qquad \times \delta^3(\mathbf{w}-\mathbf{q})\psi''_{\kappa\nu}(\mathbf{k},\mathbf{t})\psi''^{*}_{\lambda\eta}(\mathbf{v},\mathbf{w})\,|\kappa\rangle\langle\lambda|\otimes|\nu\rangle\langle\eta| \\ &= \sum_{\kappa\nu\lambda\eta}\int \mathrm{d}\mu(p,q)\psi''_{\kappa\nu}(\mathbf{p},\mathbf{q})\psi''^{*}_{\lambda\eta}(\mathbf{p},\mathbf{q})\,|\kappa\rangle\langle\lambda|\otimes|\nu\rangle\langle\eta|\ , \end{aligned} \tag{5.7}$$

where we used (5.3). In analogy to the discrete case, we will use concurrence to quantify how much entanglement has changed in the course of the transformation $\rho_S \mapsto \rho''_S$ from frame O to O''.

5.3 Entangled spins: Bell states

We proceed in analogy to the discussion of discrete systems and assume that spin and momentum initially factorise,

$$|\psi\rangle = \int \mathrm{d}\mu(p,q)\psi(\mathbf{p},\mathbf{q})\,|\mathbf{p},\mathbf{q}\rangle\otimes|\Psi\rangle\ , \tag{5.8}$$

where the spin state is a Bell state, $|\Psi\rangle = |\Phi^+\rangle$. Momenta are taken to be combinations of Gaussian wave packets in product and entangled forms which correspond to the discrete product and entangled states, $\left|M^{\Sigma}\right\rangle$, $|M^{\times}\rangle$ and $\left|M^{\Phi+}\right\rangle$, examined in the previous chapter. For the former we have,

$$f^{\Sigma}(\mathbf{p},\mathbf{q},\mathbf{p}_0,\mathbf{q}_0) = [N(\sigma)]^{-\frac{1}{2}}\left(g(\mathbf{p},\mathbf{p}_0)+g(\mathbf{p},-\mathbf{p}_0)\right)\left(g(\mathbf{q},\mathbf{q}_0)+g(\mathbf{q},-\mathbf{q}_0)\right) \tag{5.9}$$

and

$$\begin{aligned} f^{\times}(\mathbf{p},\mathbf{q},\mathbf{p}_0,\mathbf{q}_0) = [N(\sigma)]^{-\frac{1}{2}} &\Big(g(\mathbf{p},\mathbf{p}_0)+g(\mathbf{p},-\mathbf{p}_0)+g(\mathbf{p},\mathbf{p}_0^{\perp})+g(\mathbf{p},-\mathbf{p}_0^{\perp})\Big) \\ &\times\Big(g(\mathbf{q},\mathbf{q}_0)+g(\mathbf{q},-\mathbf{q}_0)+g(\mathbf{q},\mathbf{q}_0^{\perp})+g(\mathbf{q},-\mathbf{q}_0^{\perp})\Big)\ , \end{aligned} \tag{5.10}$$

and the entangled state is described by

$$f^{\Phi+}(\mathbf{p},\mathbf{q},\mathbf{p}_0,\mathbf{q}_0) = [N(\sigma)]^{-\frac{1}{2}}\left(g(\mathbf{p},\mathbf{p}_0)\,g(\mathbf{q},\mathbf{q}_0)+g(\mathbf{p},-\mathbf{p}_0)\,g(\mathbf{q},-\mathbf{q}_0)\right)\ , \tag{5.11}$$

where $N(\sigma)$ is the normalisation and $g(\mathbf{p}, \mathbf{p}_0)$ a Gaussian of width σ

$$g(\mathbf{p}, \mathbf{p}_0) = \left[\exp\left(\frac{(p_x - p_{x0})^2}{2\sigma^2} \right) \exp\left(\frac{(p_y - p_{y0})^2}{2\sigma^2} \right) \exp\left(\frac{(p_z - p_{z0})^2}{2\sigma^2} \right) \right]^{\frac{1}{2}} . \quad (5.12)$$

Throughout boosts are assumed to be in the z-direction, $\Lambda \equiv \Lambda_z(\xi)$,

$$\Lambda = \begin{pmatrix} \cosh\xi & 0 & 0 & \sinh\xi \\ 0 & 1 & 0 & 0 \\ 0 & 0 & 1 & 0 \\ \sinh\xi & 0 & 0 & \cosh\xi \end{pmatrix} . \quad (5.13)$$

This implies that the unitary representation of the Thomas-Wigner rotation $U(\Lambda, \mathbf{p})$ acting on the one particle subsystem takes the same form as in the discussion of the single particle,

$$U(\Lambda_z, \mathbf{p}) = \begin{pmatrix} \alpha & \beta(p_x - \mathrm{i}p_y) \\ -\beta(p_x + \mathrm{i}p_y) & \alpha \end{pmatrix} , \quad (5.14)$$

where as before we have denoted

$$\alpha = \sqrt{\frac{E+m}{E''+m}} \left(\cosh\frac{\xi}{2} + \frac{p_z}{E+m} \sinh\frac{\xi}{2} \right) ,$$

$$\beta = \frac{1}{\sqrt{(E+m)(E''+m)}} \sinh\frac{\xi}{2} , \quad (5.15)$$

with ξ being the rapidity of the boost in the z-direction, and

$$E'' = E\cosh\xi + p_z \sinh\xi . \quad (5.16)$$

Because the expression of the boosted spin state in Equation (5.7) is too complex to be tackled by analytic methods, we will resort to numerical treatment in determining the concurrence and the orbits of states. The computer code that has been used to obtain the numerical results in the following sections is described in appendix B. As in the case of single particle, no numerical approximations are involved except for the discretisation of the momentum space.

5.3.1 Product momenta f^{Σ}

In the following sections 5.3.1.1-5.3.1.3 we focus on spin rotations generated by the product momenta of the form $f^{\Sigma}(\mathbf{p}, \mathbf{q}, \mathbf{p}_0, \mathbf{q}_0)$. In order to compare the continuous and discrete systems, the boost scenarios will be chosen so that spins undergo almost maximum Thomas-Wigner rotation. In realising these we will oftentimes make use of the same geometric vectors as in chapter 3, section 3.4.2, $\pm\mathbf{p}_{X0} = (\pm 17.13, 0, -98.5)$ and $\pm\mathbf{p}_{Y0} = (0, \pm 17.13, -98.5)$, to be specified in detail below.

5.3.1.1 $R_i \otimes \mathbf{1}$

It is not easy to implement rotations of type $R_i \otimes \mathbf{1}$ in the continuous regime as long as we are concerned with the physical situation where the observer moves relative to both particles. The problem lies in realising the identity map. If the particle is not in the rest frame, the spin state undergoes non-trivial transformation as we learned in studying the continuous momentum models in the single particle case in section 3.4 above. A wave packet of non-zero width induces non-trivial changes of spin entropy, with the effect becoming more noticeable as the width increases. We will thus adopt the strategy of constructing a model that approximates the identity map to as high a degree as possible.

Above we fixed the boost to be always in the z-direction. In order to realise $R_i \otimes \mathbf{1}$ rotations, we follow the discrete case and take the momentum of the first particle to lie in the $z - x$-plane with $\pm\mathbf{p}_0 = \pm\mathbf{p}_{X0}$, while the momentum of the second particle is located at the origin of the $x - y$-plane with the z-component equal to that of the first particle, $\mathbf{q}_0 = (0, 0, -98.5)$. Since the momentum of the second particle is aligned with the direction of the boost, the resulting rotation of the spin field approximates the identity map.

Plots of the orbit and concurrence are shown in Figure 5.1. While the behaviour agrees quite well with the discrete system in the first part until concurrence becomes zero, the approximate character of the model becomes evident in the second part when boosts become larger than 2.7. Even for $\sigma/m = 1$ the fit with the discrete model is relatively bad. Although the concurrence initially begins to increase for rapidities larger than 2.7, thereby resembling the discrete model, it only reaches the value 0.6 and declines thereafter for $\xi > 4.16$. Such deviation from the discrete model is still more dramatic for $\sigma/m = 2$, with the $\sigma/m = 4$ bearing little resemblance to the discrete case at all. Since the disagreement correlates with the growth of the Gaussian width, it is most likely caused by the deteriorating approximation

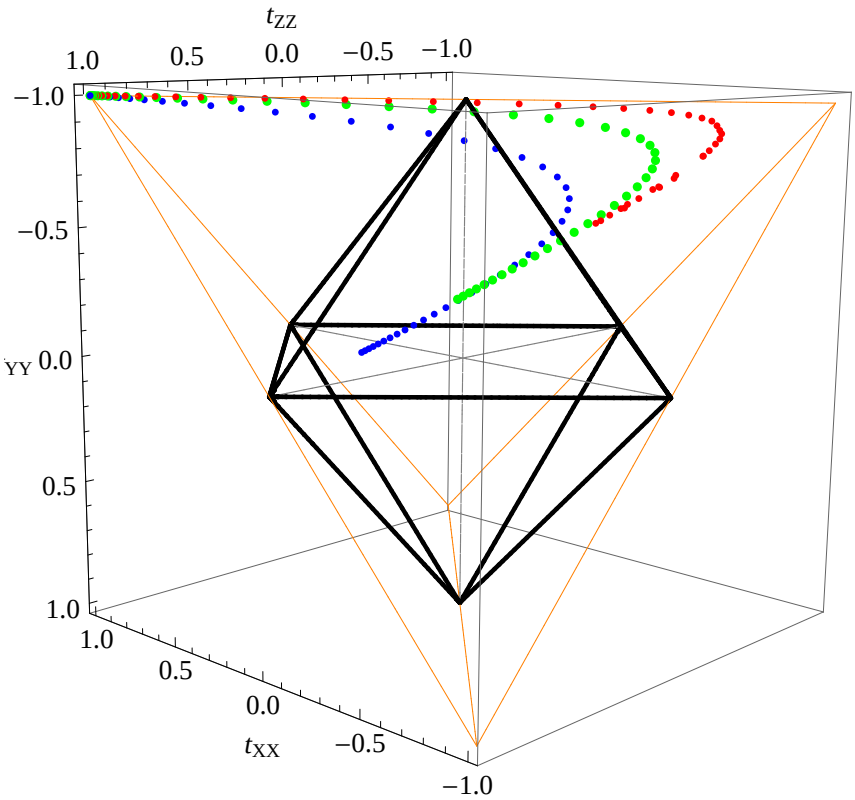

(a)

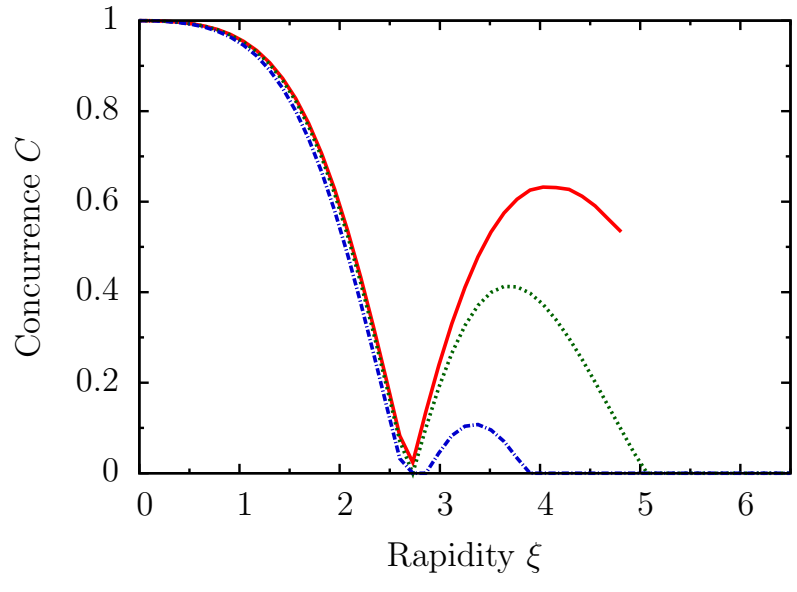

(b)

Figure 5.1. Spin orbit and concurrence under $R_i \otimes \mathbf{1}$ for Gaussian momenta with $\sigma/m = 1, 2, 4$. Product momenta are given by f^{Σ}. Data for $\sigma/m = 1$ is shown red, $\sigma/m = 2$ green and $\sigma/m = 4$ blue. (a) Initial state $|\Phi^+\rangle$ corresponds to vertex $(1, -1, 1)$. (b) Concurrence. Due to difficulties in numerical integration concurrence could not be obtained for $\xi > 4.8$.

of the identity map. This demonstrates that the features of realistic wave packets may be quite distinct from those of idealised models. We will gain more insight into origin centred momenta in section 5.3.2 below.

5.3.1.2 $R_i \otimes R_i$

To implement the type of rotation where both particles undergo the same rotation, the momenta $\mathbf{p}_0$ and $\mathbf{q}_0$ need to lie in the same boost plane. Since the boost is in the z-direction, we will assume that the Gaussians are centered at the geometric vectors $\pm\mathbf{q}_0 = \pm\mathbf{p}_0 = \pm\mathbf{p}_{X0}$, realising the rotation $R_Y \otimes R_Y$. Plots of the orbit and concurrence are shown in Figure 5.2.

Comparing with the plots of the discrete model in Figure 4.3, we see that for $\sigma/m = 1$ the behaviour of the continuous model and of the discrete model coincide to quite a high degree of accuracy. The orbit of the continuous model follows the same path as the discrete model, almost reaching the rest frame state $|\Phi^+\rangle$. The reason it stops short of $|\Phi^+\rangle$ is that while in the discrete model we assume that the system reaches the maximum Thomas-Wigner rotation of $180°$, the maximum rotation implemented by the continuous model at $\xi = 6.5$ is $\omega_m \approx 163°$ or 2.81 rad. Substituting ω_m into the expression (4.40) that describes the discrete orbit yields $t_{Y\otimes Y}(\omega_m) = (0.9, -1, 0.9)$, which is in good agreement with the numerically calculated value $(0.89, -0.99, 0.90)$ representing the final state for $\sigma/m = 1$ in Figure 4.3. Likewise, Equation (4.39), which describes the concurrence of the discrete model, evaluates to $C(\omega_m) = 0.89$, showing again good fit with the continuous model. The orbits for $\sigma/m = 2$ and $\sigma/m = 4$ diverge from the behaviour of the discrete model, with the disagreement growing larger as the width increases. This is to be expected since larger Gaussians contain spins, some of which undergo less and others more rotation than spins at the centre of the wave packet, thereby causing the traced out spin state to be in general a mixed state. Larger values of σ/m lead in general to a higher degree of mixedness of the boosted state, and the effect becomes more pronounced at extremely large boosts: at $\xi = 6.5$, the boosted state with $\sigma/m = 4$ is closer to the centre of the octahedron than the states with lower σ/m.

5.3.1.3 $R_i \otimes R_j$

In order to realise mixed rotations the centres of Gaussians need to lie in different boost planes. With the boost in the z-direction, we will choose $\pm\mathbf{p}_0 = \pm\mathbf{p}_{Y0}$ and $\pm\mathbf{q}_0 = \pm\mathbf{p}_{X0}$, which means that the spin state is rotated by $R_X \otimes R_Y$. The orbit and concurrence are given in Figure 5.3.

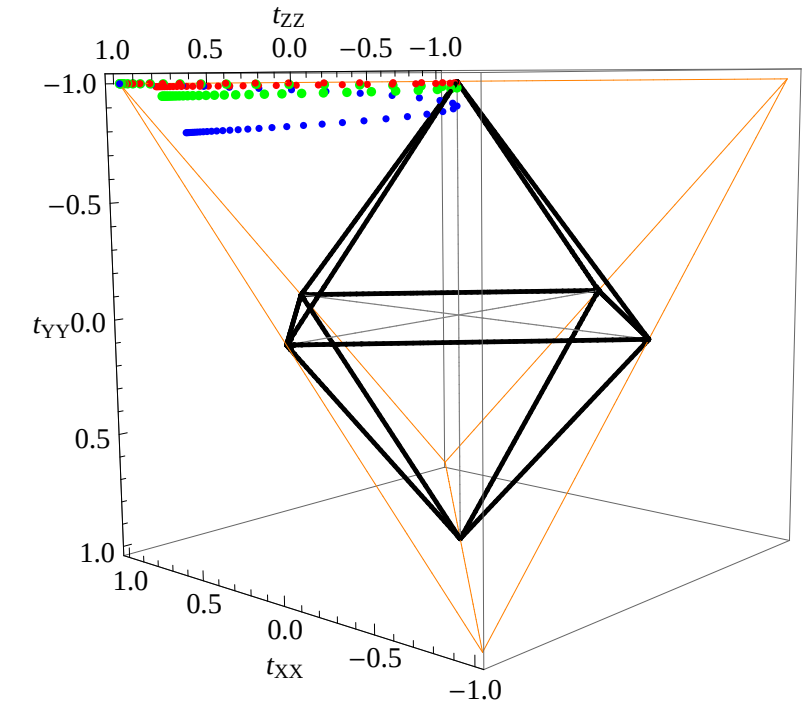

(a)

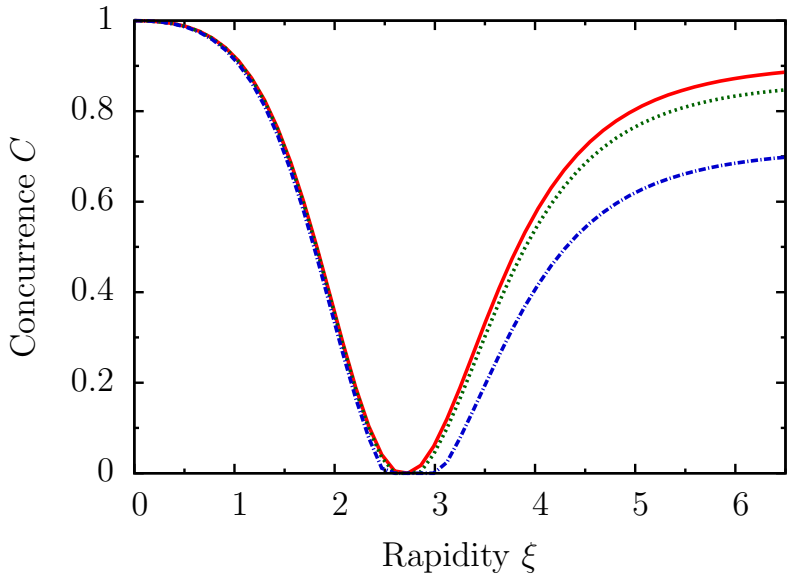

(b)

Figure 5.2. Spin orbit and concurrence under $R_i \otimes R_i$ for Gaussian momenta with $\sigma/m = 1, 2, 4$. Product momenta are given by f^{Σ}. Data for $\sigma/m = 1$ is shown red, $\sigma/m = 2$ green and $\sigma/m = 4$ blue. (a) Initial state $|\Phi^+\rangle$ corresponds to vertex $(1, -1, 1)$. (b) Concurrence.

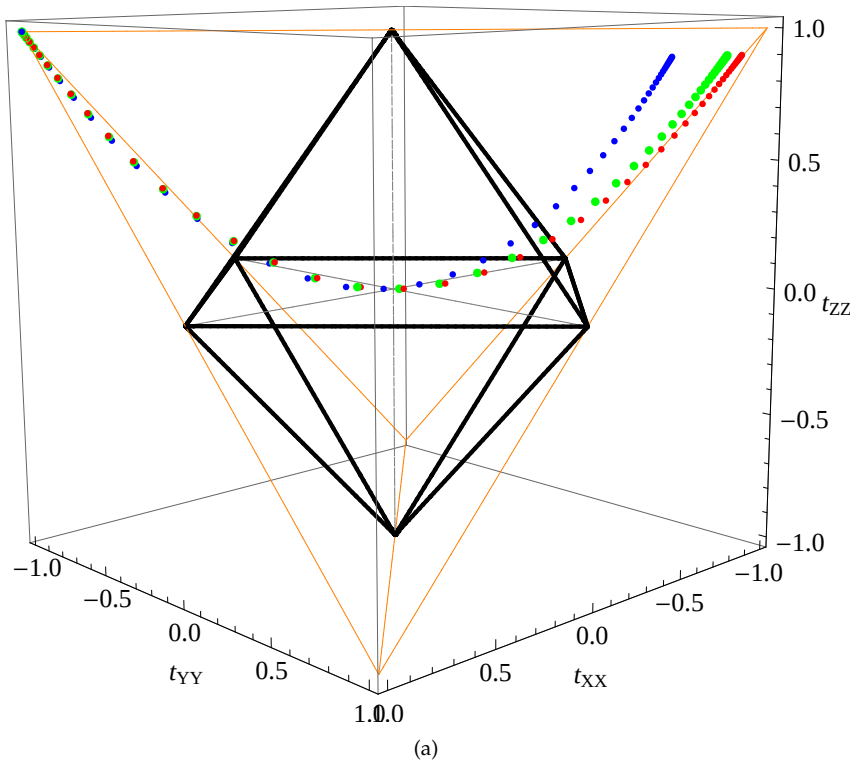

(a)

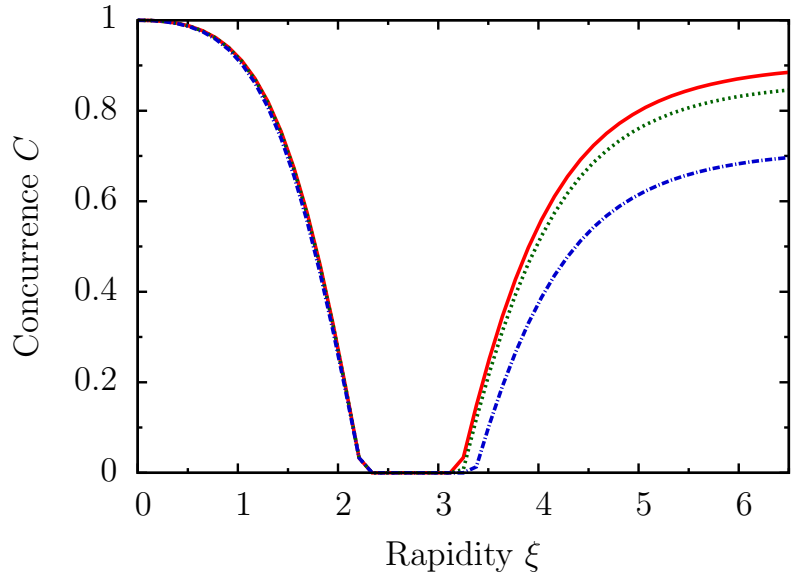

(b)

Figure 5.3. Spin orbit and concurrence under $R_i \otimes R_j$, $i \neq j$ for Gaussian momenta with $\sigma/m = 1, 2, 4$. Product momenta are given by f^{Σ}. Data for $\sigma/m = 1$ is shown red, $\sigma/m = 2$ green and $\sigma/m = 4$ blue. (a) Initial state $\left|\Phi^{+}\right\rangle$ corresponds to vertex $(1, -1, 1)$. (b) Concurrence.

We observe a good fit with the discrete model for the narrower Gaussian with $\sigma/m = 1$. In analogy to Figure 4.4 of the discrete model, the orbit follows a path through the centre of the octahedron, evolving towards the vertex $(-1, 1, 1)$, which represents the Bell state $|\Phi^-\rangle$. As in the previous case, at $\xi = 6.5$ the system achieves maximum Thomas-Wigner rotation $\omega_m \approx 163°$, with the spin state represented by $(-0.94, 0.94, 0.90)$. This is quite well approximated by the discrete orbit given by Equation (4.42), from which we calculate $t_{X\otimes Y}(\omega_m) = (-0.96, 0.96, 0.92)$. The discrete concurrence, given by Equation (4.43), and yielding $C(\omega_m) = 0.92$, shows relatively good agreement with the value 0.89 of the continuous model too. Gaussians with larger $\sigma/m = 2$ and $\sigma/m = 4$ diverge from the idealised, discrete model for the reasons highlighted above, and tend to be more mixed at extremely large boosts.

5.3.2 Origin centred Gaussians

We will next examine Gaussians centred at the origin, and more generally at any $(0, 0, p_z)$, extending to two particles what we did for the single particle system above in section 3.4.1. Note that such momenta were not studied in the previous chapter since they show non-trivial behaviour only for systems whose momentum wave packets have non-zero width.

The same scenarios will be considered as for the single particle, with momenta centred at $(0, 0, -4)$, $(0, 0, 0)$ and $(0, 0, 4)$. Plots for $\sigma/m = 1$ and $\sigma/m = 4$ are shown in Figure 5.4 and 5.5. We note that for $\sigma/m = 1$ and $\sigma/m = 4$ with the momentum at $(0, 0, 0)$ we recover the results for concurrence which were first reported in the seminal paper [15].

The results for single and two particle systems are not directly comparable because the entanglement in question is between different degrees of freedom and it has been generated by maps whose structure is dissimilar. Also, the initial states for the two kinds of systems are not the same. Despite this a number of analogies are manifest. For instance, the scenario with $(0, 0, 4)$ which contains momenta in the direction of boost displays less pronounced changes of entanglement than the one with momenta $(0, 0, -4)$ which are opposite to the direction of boost. As we have learned above, this originates in the sensitivity of Thomas-Wigner's rotation to the angle between boosts. Secondly, as for the single particle, Gaussians with larger widths show in general more rapid changes of concurrence, which can be traced back to the dependance of Thomas-Wigner's rotation on the magnitude of boost. Third, both single and two particle systems exhibit saturation, which comes

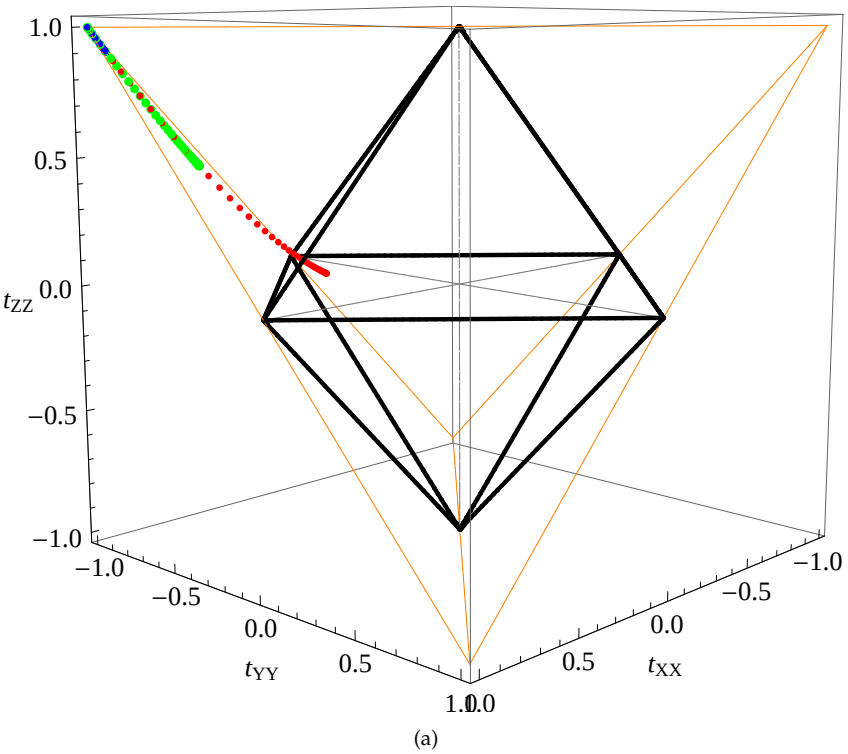

(a)

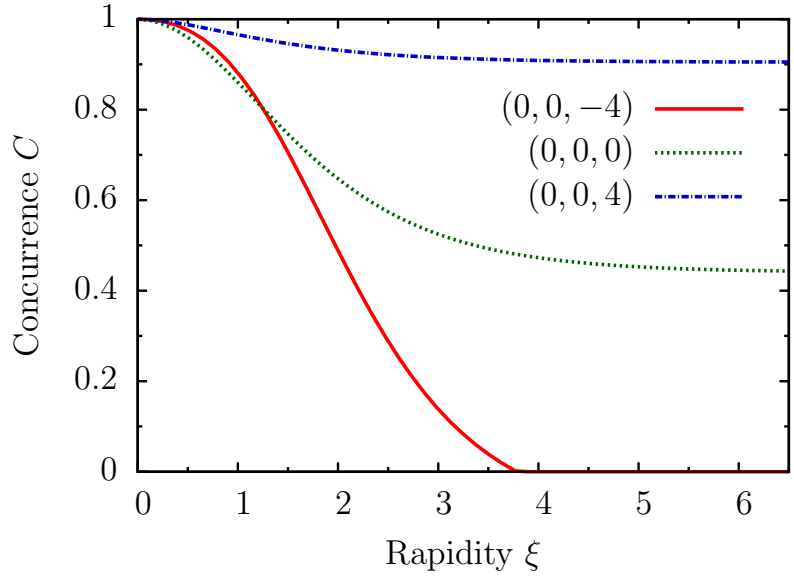

(b)

Figure 5.4. Spin orbit and concurrence for origin centred Gaussian momenta with $\sigma/m = 1$. Data for $(0, 0, -4)$ is shown red, $(0, 0, 0)$ green and $(0, 0, 4)$ blue. (a) Initial state $\left|\Phi^+\right\rangle$ corresponds to vertex $(1, -1, 1)$. (b) Concurrence.

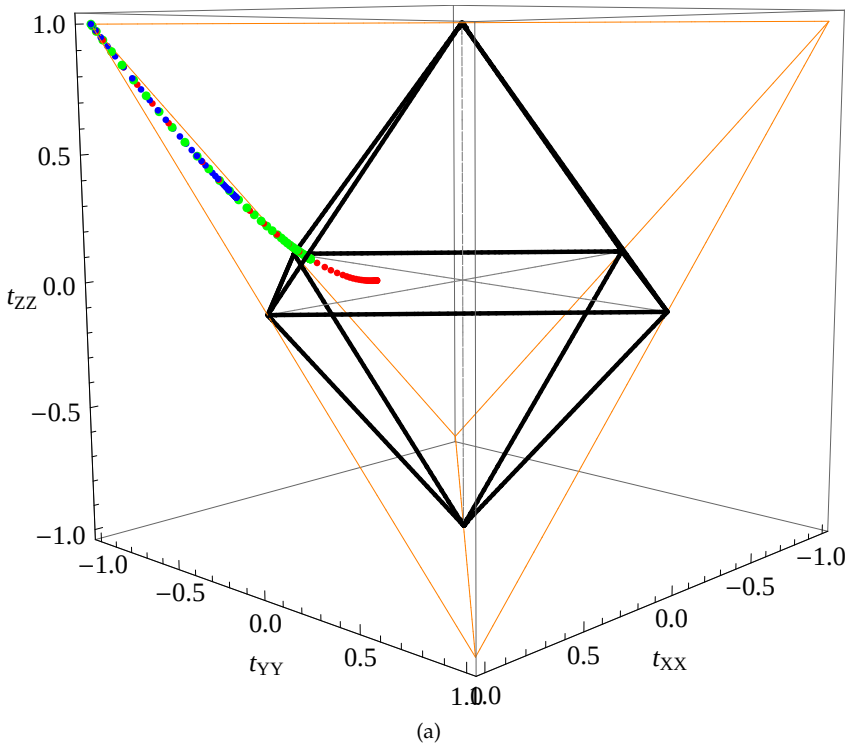

(a)

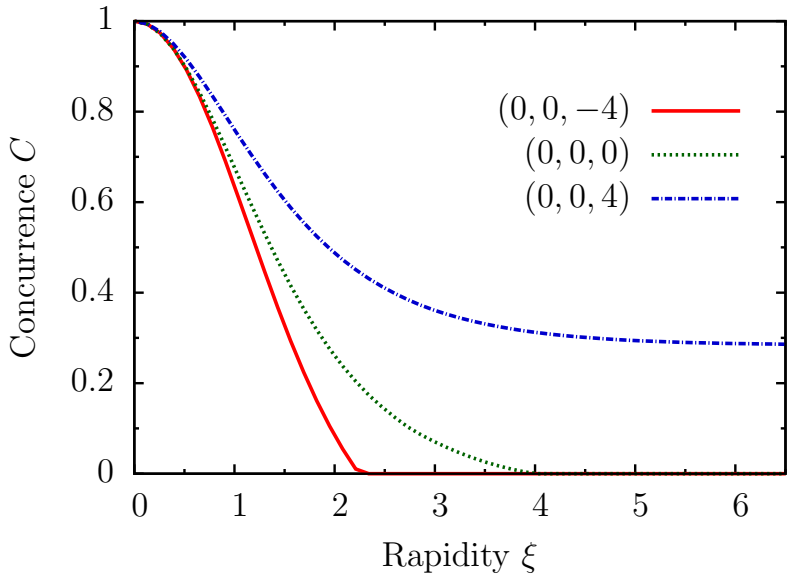

(b)

Figure 5.5. Spin orbit and concurrence for origin centred Gaussian momenta with $\sigma/m = 4$. Data for $(0, 0, -4)$ is shown red, $(0, 0, 0)$ green and $(0, 0, 4)$ blue. (a) Initial state $\left|\Phi^+\right\rangle$ corresponds to vertex $(1, -1, 1)$. (b) Concurrence.

from the fact that the Thomas-Wigner rotation achieves a maximum value which, for a given boost angle, is determined by the smaller boost.

Let us next turn to the case of extreme rotations. Plots for $\sigma/m = 1, 2, 4, 8$ with $\mathbf{p}_0 = (0, 0, -98.5)$ are shown in Figure 5.6. Interestingly, contrary to what one might have expected based on the findings so far, entanglement declines slower than in the previous scenarios. For instance, states with $\sigma/m = 1$ remain nearly maximally entangled for rapidities up to about 2 and decohere thereafter, but this occurs later than with the momenta $(0, 0, -4)$, which on the face of it generate less rotation than the extreme momenta $(0, 0, -98.5)$. However, such puzzling behaviour can be explained using the properties of Thomas-Wigner's rotation. Instead of a Gaussian, let us think of a rough, simple model consisting of discrete momenta as depicted in Figure 5.7. We know that larger momenta generate more rotation, but their amplitude is smaller, so for the sake of argument, let us assume the Gaussian is represented by two momenta at the distance of 0.75 its width. We will next argue that concurrence changes more rapidly for the Gaussian centred at or close to the origin than for the one centred at the very large momentum $(0, 0, -98.5)$. The key is to realise that the boost angle θ is $\pi/2$ for the origin centred Gaussian, while it is larger, about 170° or 2.97 rad, for the Gaussian at $(0, 0, -98.5)$. In Figure 2.2, which describes the dependence of Thomas-Wigner's angle on boost angle and rapidity, these states lie, respectively, in the middle and almost at the right end of the horizontal axis. Boosting the system means we keep θ fixed and move towards the back of the surface representing the Thomas-Wigner angle for given θ and ξ. Now for $\theta = \pi/2$, the rotation grows initially faster than for $\theta = 2.85$, meaning that the concurrence of the origin centred Gaussian changes sooner than the one at the extremely large momentum. However, as rapidity grows even larger, the rotation increases rapidly for $\theta = 2.85$, leading to the decrease of concurrence as seen in Figure 5.6. The decrease becomes steeper as width increases, as is to be expected since larger width means we move towards slightly lower values of θ which cause faster rotations and hence quicker drop of concurrence. Along the same lines, for Gaussians at $(0, 0, -4)$ which are relatively close to the origin in comparison to $(0, 0, -98.5)$, θ is slightly but not significantly larger than $\pi/2$, still leading to faster initial increase than for the extremely large momenta.

To substantiate these qualitative considerations with a rough numerical model, we plot the dependence of Thomas-Wigner's rotation on rapidity for four momenta in Figure 5.8. The first one at $(3, 0, 0)$ corresponds to the origin centred Gaussian and the second $(3, 0, -4)$ to the one close to the origin. The third $(3, 0, -98)$ repre-

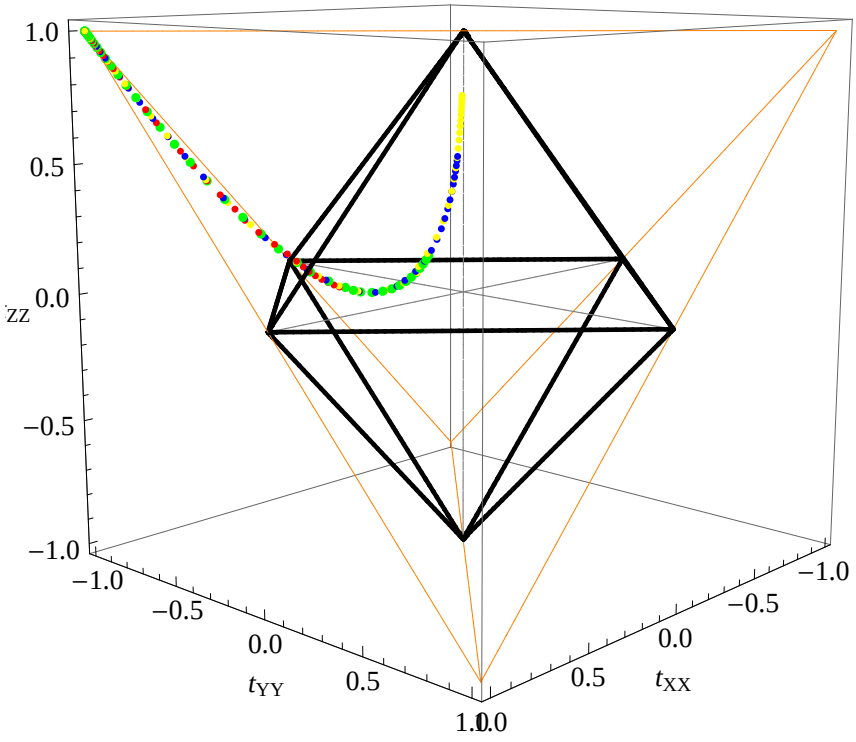

(a)

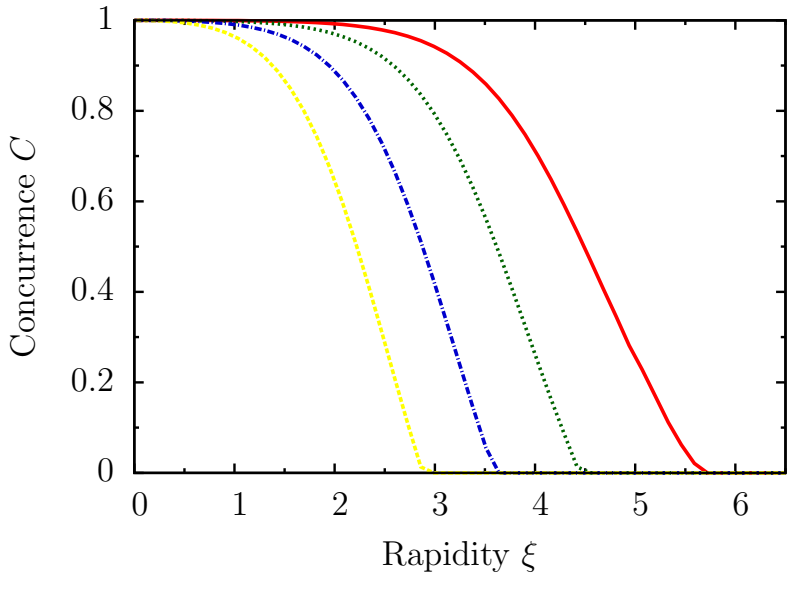

(b)

Figure 5.6. Spin orbit and concurrence for origin centred Gaussian momenta with $\sigma/m = 1, 2, 4, 8$ and $\mathbf{p}_0 = (0, 0, -98.5)$. Data for $\sigma/m = 1$ is shown red, $\sigma/m = 2$ green, $\sigma/m = 4$ blue and $\sigma/m = 8$ yellow. (a) Initial state $\left|\Phi^+\right\rangle$ corresponds to vertex $(1, -1, 1)$. (b) Concurrence.

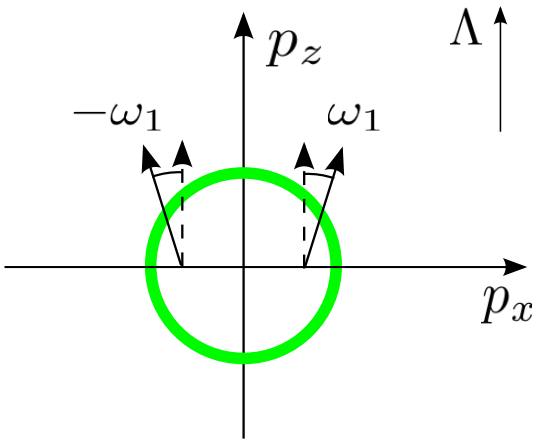

Figure 5.7. Schematic representation of an origin centred Gaussian spin field.

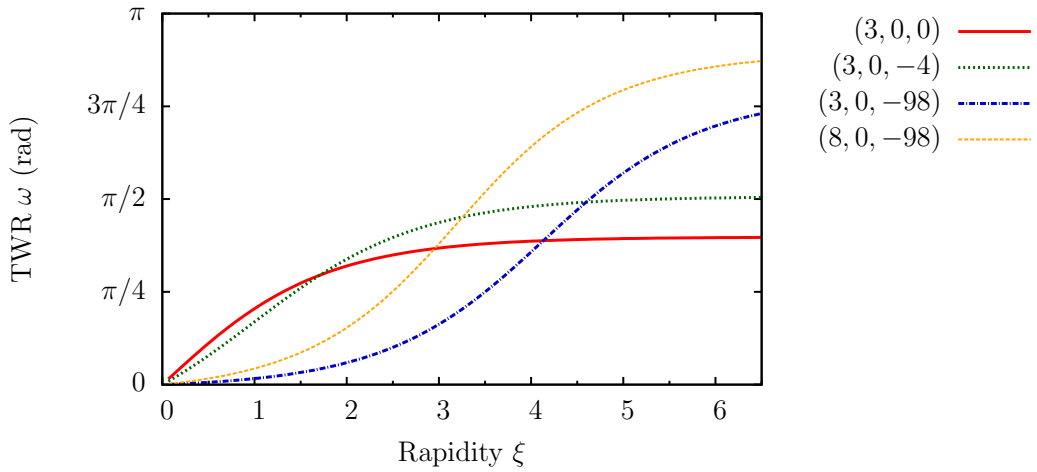

Figure 5.8. Thomas-Wigner rotation for origin centred Gaussians in different geometries.

sents a distribution with the same width at the extreme momentum and the fourth $(8, 0, -98)$ corresponds to a Gaussian with larger width at the extreme momentum. The qualitative behaviour of Thomas-Wigner's rotation and hence of concurrence follows the pattern we have just outlined. Quantitatively, however, our discrete considerations in the 2D setting cannot accurately represent the more complex workings of realistic 3D Gaussian wave packets. The model in Figure 5.8 does not reproduce the precise numerical values for concurrence in Figures 5.4, 5.5 or 5.6. All in all, the claim we make is that for a Gaussian of given width, reasons of the sorts given do cause the differences of behaviour observed above.

Another intriguing aspect of Figure 5.6 is that the orbits resemble closely the orbits generated by $|M^{\times}\rangle$ in the previous chapter. We will explore this in more detail shortly.

5.3.3 Product momenta $f^{\times}$

While in the previous chapter the states $|M^{\times}\rangle$ entered the discussion more as a logical followup of $|M^{\Sigma}\rangle$, we can now appreciate their true significance. The similarity between the orbits of $|M^{\times}\rangle$ in Figure 4.6 and those of Gaussians centred at $(0, 0, p_z)$ in the previous section suggests that the latter can be modelled in terms of the former. Indeed this is the claim we will explore below. We will first verify the correspondence between the discrete and the Gaussian states and then focus on the modelling aspect.

We will consider the scenario where the geometric vectors in the state $f^{\times}$ are described by

$$\pm\mathbf{p}_0 = \pm\mathbf{q}_0 = \pm\mathbf{p}_{Y0} \ , \quad \pm\mathbf{p}_0^{\perp} = \pm\mathbf{q}_0^{\perp} = \pm\mathbf{p}_{X0} \ ,$$

which generate maximum spin rotations. Figure 5.9 shows plots of orbits and concurrence for $\sigma/m = 1, 2, 4$. In previous chapter we calculated from Equation (4.49) that the concurrence of the discrete system becomes zero at $\omega = 1.23$ rad. This corresponds to about $\xi = 2.3$ in the continuous model, showing good fit between the two. Likewise, the discrete orbit in Equation (4.48) evaluates to $t(\omega_m) = (0, 0, 0.92)$ at the maximum Thomas-Wigner angle $\omega_m \approx 163^{\circ}$, while the numerical model gives $(0, 0, 0.90)$ for $\sigma/m = 1$ and $(0, 0, 0.89)$ for $\sigma/m = 4$. In contrast to the other types of product momenta, there is somewhat less dependence on width. We hypothesise that this might be caused by the symmetry of the state, but will not pursue it further at this point.

We will next turn to the correspondence between the z-axis centred momenta and the $f^{\times}$ model. When analysing the curious behaviour of the z-axis Gaussians in the previous section, we resorted to a naive 2D model. Realistic Gaussians however involve a third dimension as well, and generalising the 2D model to three dimensions naturally leads to the state which in the discrete case is given by $|M^{\times}\rangle$ and in the continuous case by $f^{\times}$. The latter explains why there is a close match between the orbits of the z-axis centred states containing extreme momenta $(0, 0, -98.5)$ and those of $|M^{\times}\rangle$ and $f^{\times}$ above. This raises the question of whether the z-axis centred states shown in Figure 5.5 can be modelled using the $f^{\times}$ states with suitably chosen momenta. Proceeding in the same naive way as above for the 2D model, let us approximate the states in Figure 5.5 with $f^{\times}$ by assuming that momenta are given by

$$\pm\mathbf{p}_0 = \pm\mathbf{q}_0 = (0, \pm 3, p_z) \ , \quad \pm\mathbf{p}_0^{\perp} = \pm\mathbf{q}_0^{\perp} = (\pm 3, 0, p_z) \ ,$$

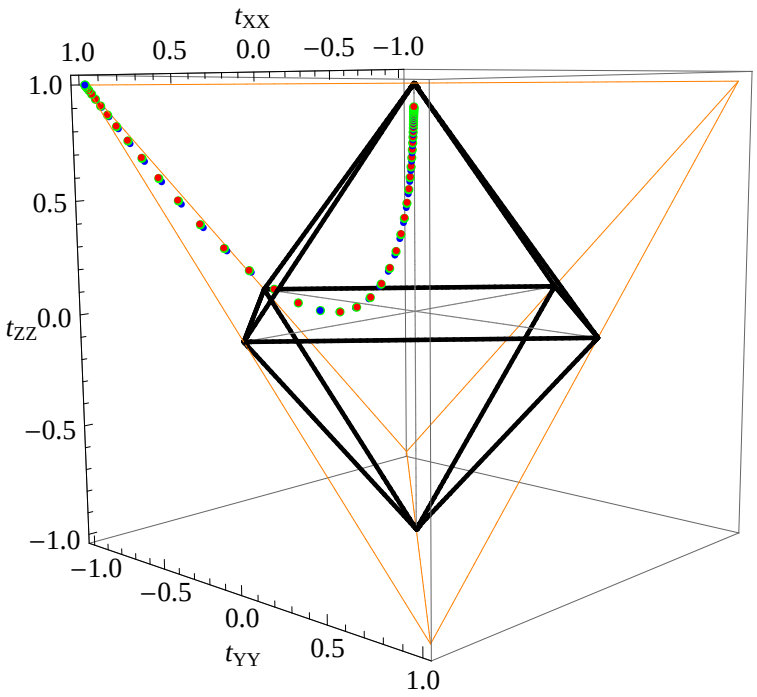

(a)

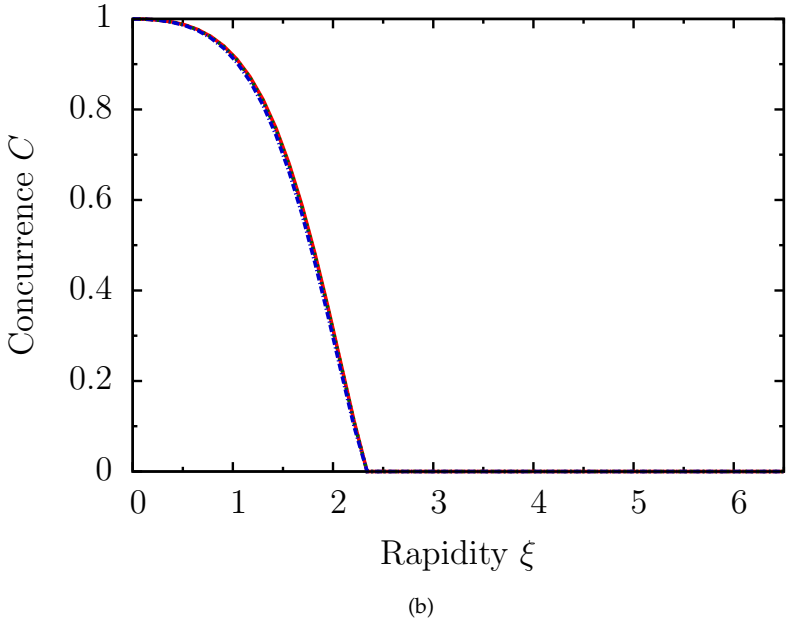

(b)

Figure 5.9. Spin orbit and concurrence for Gaussian momenta with $\sigma/m = 1, 2, 4$. Product momenta are given by $f^{\times}$ with $\pm\mathbf{p}_0 = \pm\mathbf{p}_{X0}$ and $\pm\mathbf{p}_0^{\perp} = \pm\mathbf{p}_{Y0}$. Data for $\sigma/m = 1$ is shown red, $\sigma/m = 2$ green and $\sigma/m = 4$ blue. (a) Initial state $|\Phi^+\rangle$ corresponds to vertex $(1, -1, 1)$. (b) Concurrence.

where $p_z = -4, 0, 4$. Figure 5.10 shows plots for $\sigma/m = 0.25$, which we have chosen smaller than in the models above to minimise width related effects.

While the agreement with Figure 5.5 is not perfect, we can easily recognise the features present in the original z-axis case. The concurrence of the $f^{\times}$ model exhibits, roughly, the same kind of dependence to the boost angle as the z-axis centred states. While the momenta with $p_z = 4$ diverge considerably from those with $(0, 0, 4)$ in Figure 5.5, the fit is relatively good for $p_z = -4$ and $p_z = 0$ considering this is a simple model. The orbits follow the same pattern, with the one for $p_z = 4$ deviating more, and those for $p_z = 0$ and $p_z = -4$ relatively little from the z-axis centred states.

To recap, we have been arguing all along that systems involving continuous momenta, and specifically those of Gaussian form, can be understood in terms of discrete models, possibly containing many momentum eigenstates. The foregoing discussion demonstrates that in some cases Gaussian momenta admit very simple models, in particular the momenta centred at the axis parallel to the direction of boost can be modelled in terms of four narrow Gaussians, which approximate discrete momenta.

5.3.4 Entangled momenta

In the following two sections we will examine spin transformations generated by entangled Gaussians of the form $f^{\Phi+}$. We will leave out concrete realisations since they are analogous to the scenarios for the product momenta. As before maximum rotation angles generated by $\mathbf{p}_{X0}$ and $\mathbf{p}_{Y0}$ will be used.

5.3.4.1 $R_i \otimes R_i$

The case of $R_i \otimes R_i$ realised with entangled momenta falls into two equivalence classes as we learned above in section 4.5.4.1 in the discussion of discrete systems. We will consider only the interesting, non-trivial case, which will be implemented by $R_X \otimes R_X$. Plots of orbits and concurrence are shown in Figure 5.11.

The idiosyncratic double dip behaviour found in the discrete case is clearly recognisable for $\sigma/m = 1$, compare Figure 4.7. The orbit of $\sigma/m = 1$ follows the path of the discrete state to quite a high degree of precision. We calculate that, for the maximum Thomas-Wigner rotation $\omega_m \approx 163^\circ$ in the continuous model, the discrete state yields $t_{X\otimes X}(\omega_m) = (1, -0.84, 0.84)$, which agrees relatively well with the numerically calculated values $(0.99, -0.80, 0.80)$ for the continuous state. The discrete concurrence in Equation (4.53) gives $C(\omega_m) = 0.84$, showing relatively

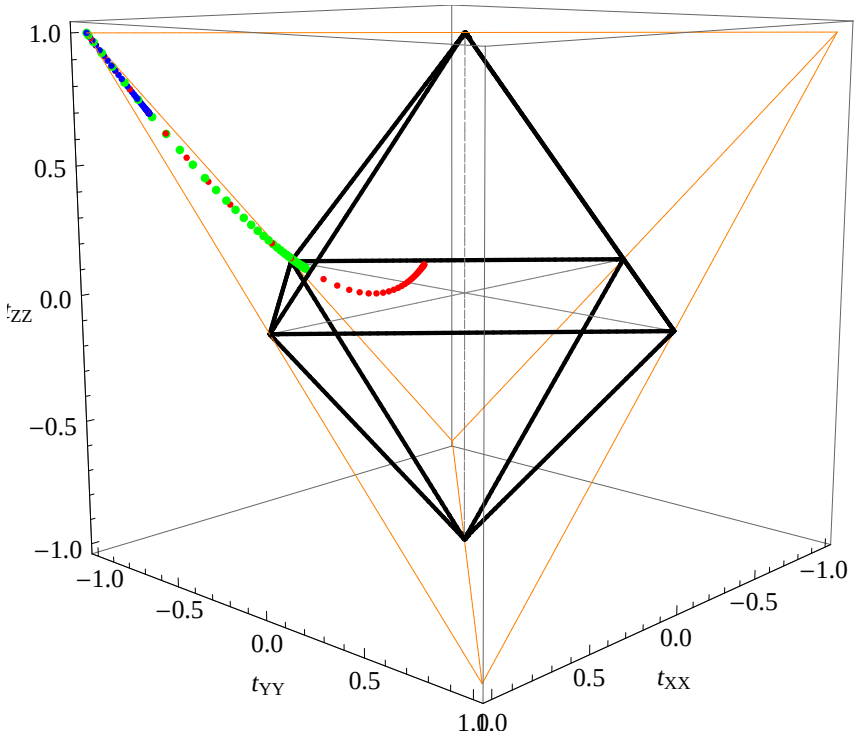

(a)

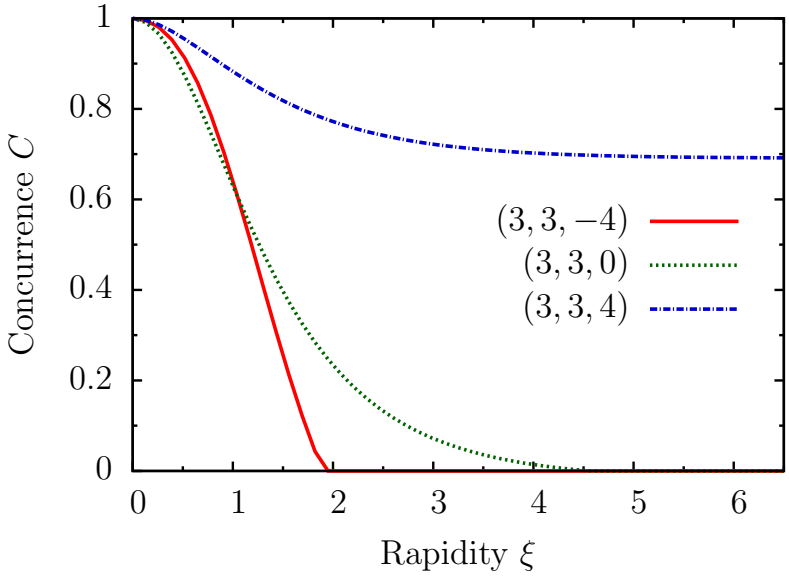

(b)

Figure 5.10. Spin orbit and concurrence for Gaussian momenta with $\sigma/m = 0.25$. Product momenta are given by $f^{\times}$. Data for $(3, 3, -4)$ is shown red, $(3, 3, 0)$ green and $(3, 3, 4)$ blue. (a) Initial state $\left|\Phi^{+}\right\rangle$ corresponds to vertex $(1, -1, 1)$. (b) Concurrence.

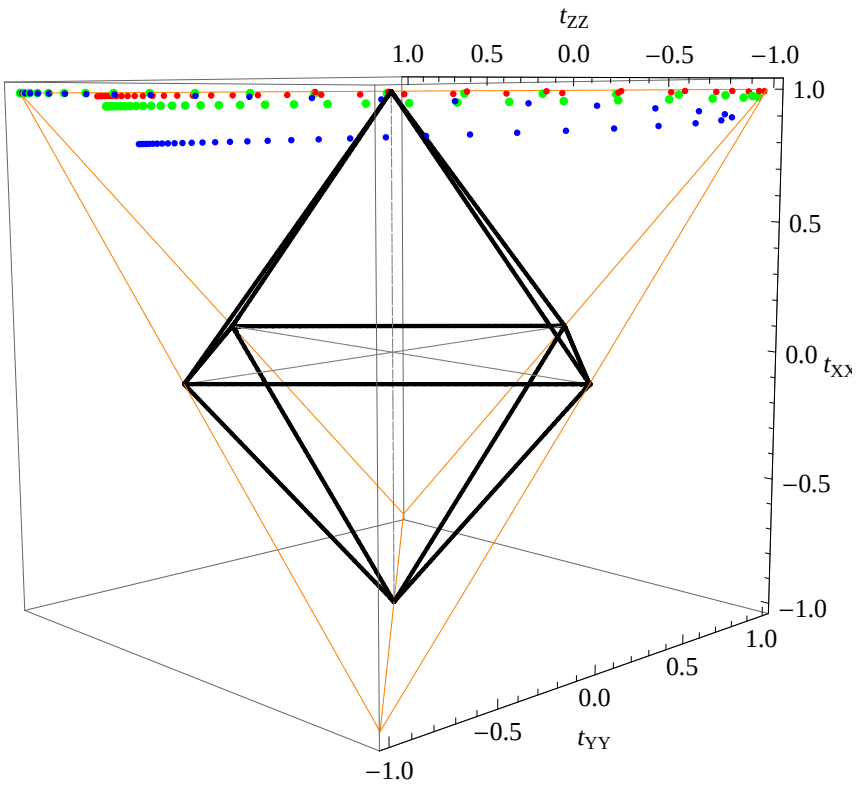

(a)

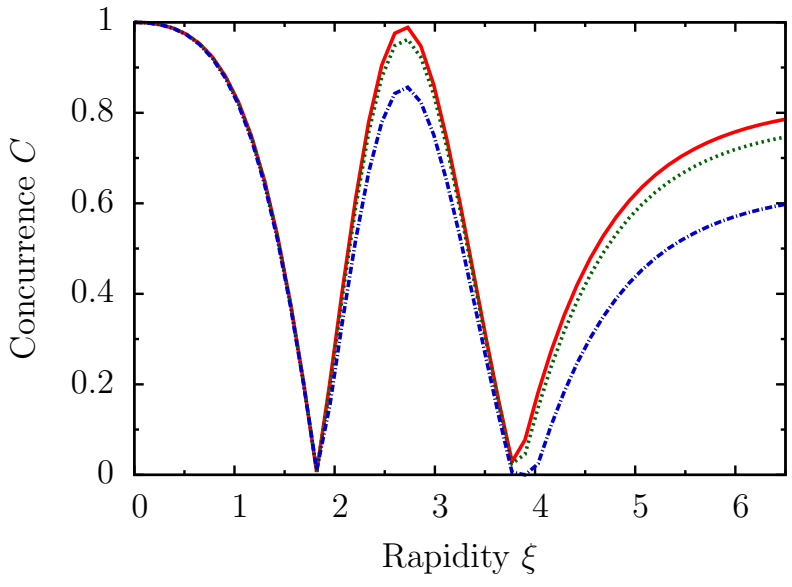

(b)

Figure 5.11. Spin orbit and concurrence under $R_i \otimes R_i$ for entangled Gaussian momenta with $\sigma/m = 1, 2, 4$. Momenta are given by $f^{\Phi+}$. Data for $\sigma/m = 1$ is shown red, $\sigma/m = 2$ green and $\sigma/m = 4$ blue. (a) Initial state $\left|\Phi^+\right\rangle$ corresponds to vertex $(1, -1, 1)$. (b) Concurrence.

good fit with the numerically determined value 0.79. In analogy to the previous cases, Gaussians with larger widths $\sigma/m = 2$ and $\sigma/m = 4$ diverge from the idealised behaviour and end up in increasingly more mixed states for extremely large boosts $\xi = 6.5$ as the width grows. Also, larger widths lead to degradation of the double dip pattern as the state does not quite reach $|\Psi^+\rangle$, represented by $(1, 1, -1)$, when $\omega = 90°$, and traverse the top part of the octahedron on their way back to $|\Phi^+\rangle$.

5.3.4.2 $R_i \otimes R_j$

We will focus on the implementation $R_X \otimes R_Y$ whose concurrence is plotted in Figure 5.12. Unfortunately, the orbit cannot be visualised since it is not Bell diagonal.

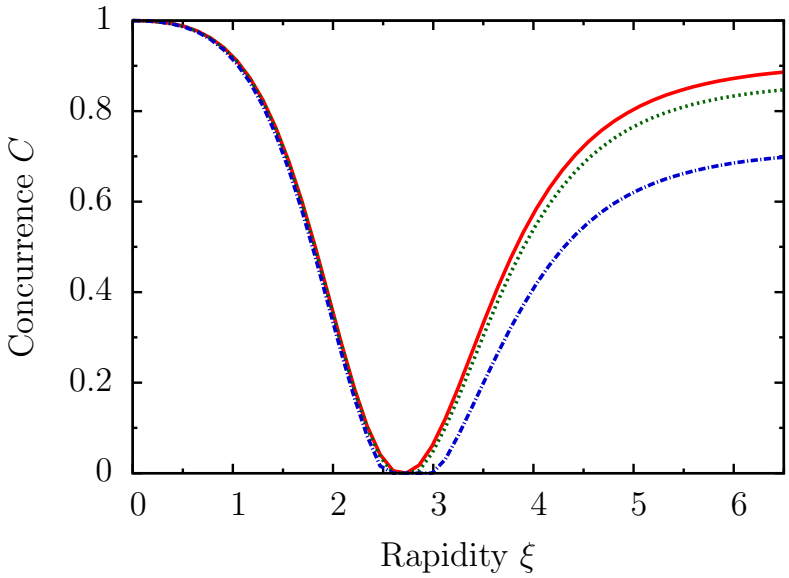

Figure 5.12. Spin concurrence under $R_i \otimes R_j$, $i \neq j$ for entangled Gaussian momenta with $\sigma/m = 1, 2, 4$. Momenta are given by $f^{\Phi+}$. Data for $\sigma/m = 1$ is shown red, $\sigma/m = 2$ green and $\sigma/m = 4$ blue.

The generic pattern observed in previous cases is present here as well. From Equation (4.55) characterising the concurrence of the discrete model, we calculate $C(\omega_m) = 0.92$, which is in relatively good agreement with the numerically obtained value 0.89. Gaussians of larger widths show almost the same behaviour until $\omega = 90°$ but diverge increasingly thereafter as width and rapidity become larger. The larger the width, the lower the concurrence at extremely large boosts $\xi = 6.5$.

5.4 Summary and discussion

In this chapter we studied spin entanglement of two particles with continuous momenta. The treatment has been parallel to the one of discrete momenta in the previous chapter in that we systematically surveyed a number of boost scenarios with momenta both in product and entangled states. We have confined attention to pure spins only, which were assumed to be in the Bell state $|\Phi^+\rangle$.

As expected, we observe relatively good agreement between discrete systems and Gaussians of narrower widths with $\sigma/m = 1$. Wave packets of larger widths lead to deviation from the idealised discrete models. In analogy to the the single particle system, the analysis has been numerical throughout as the two particle system is too complex to be tackled by analytic methods. However, the lack of analytic models is to some extent compensated by the discrete model, which was introduced in the discussion of the single particle. In this picture, systems involving three dimensional Gaussians can be thought of as fields comprising spins at a large number of discrete momenta, where boosting means that each spin undergoes a different, momentum dependent rotation for a given value of rapidity. It is remarkable that such a complex behaviour can be reduced to simple models. In particular, we note two successful cases which further justify its use. In section 5.3.2 we were able to understand the somewhat counterintuitive behaviour of z-axis centred Gaussians in terms of a simple discrete 2D model involving two spins. And in section 5.3.3 we employed the $|M^\times\rangle$ and $f^\times$ states to obtain another simple model involving four narrow Gaussians whose behaviour agreed, in many cases, with that of the z-centred Gaussian momenta to a surprisingly high degree of accuracy.

As in case of discrete systems, further insight into the workings of continuous systems was provided by visualisation of their orbits. We gained a more detailed understanding of how varying the initial states, their widths and momenta, changes the entanglement of spins.

Chapter 6

Transfer of entanglement

6.1 Is there transfer of entanglement?

In the two previous chapters we studied two particle entanglement and established that it changes non-trivially under Lorentz boosts. This raises the question of how to explain the behaviour of entanglement in relativistic systems. Do we witness a genuine change of the amount of entanglement or is it just that entanglement is shuffled around between subsystems of the total system while its total amount remains invariant? Many authors have concluded that the latter is the case. The verdict seems to originate in the very first papers published on the subject. For instance, in [15] the authors claim that "Lorentz boosts introduce a transfer of entanglement between degrees of freedom, that could be used for entanglement manipulation. While the entanglement between spin or momentum alone may change due to Lorentz boosts, the entanglement of the entire wave function (spin and momentum) is invariant." They reason that Lorentz boosts perform local unitary transformations of the form $U(\Lambda) \otimes U(\Lambda)$ and since local unitaries do not change the measure of entanglement, the total entanglement of the wave function remains invariant. The appearance of the change of entanglement comes from the fact that some degrees of freedom are traced out. For instance, if we trace out momentum degrees of freedom, then spin-spin entanglement does indeed change. Yet this constitutes merely transfer of entanglement between different degrees of freedom, while the sum total of entanglement remains intact under Lorentz boosts. In the same vein, in [44] the authors state that "Entanglement was shown to be an invariant quantity for observers in uniform relative motion in the sense that, although different inertial observers may see these correlations distributed among several degrees of freedom in different ways, the total amount of entanglement is the same

in all inertial frames", and a similar conclusion is reached in [60, 96].

However, we think there are grounds to believe that the issue needs further analysis. Recall that above we observed that in single particle systems in general the total entanglement between spin and momentum degrees of freedom does not remain invariant under Lorentz boosts. A spin-momentum product state can be be transformed into an entangled state. More importantly, we saw that Lorentz boosts can be regarded as controlled operations where momentum plays the role of a control qubit and spin is a target qubit. This implies that Lorentz boosts perform nonlocal transformations on single particle systems. This, in turn, suggests entanglement in two particle systems might be not merely shuffled around between different degrees of freedom but could be genuinely generated and destroyed under Lorentz boosts. Indeed, in [92] the authors explicitly challenge the claim of entanglement transfer in two particle systems. They observe that a decrease of spin-spin entanglement under a Lorentz boost is not accompanied by an increase of momentum entanglement, casting doubt on the claim that the amount of entanglement is invariant under Lorentz boosts.

Our aim in this chapter is to make progress in clarifying the issue by studying the behaviour of entanglement of the momentum state in different boost scenarios [92]. To ease the discussion, we will adopt the same simplifying assumptions about momenta as in chapter 4 above. The momenta will be regarded as sufficiently narrow that we can use orthogonal state vectors at different momentum values, formally satisfying the relationship $\langle \mathbf{p}_i | \mathbf{p}_j \rangle = \delta_{ij}$. This allows us to treat momenta as a discrete basis. Each momentum state will then generate a single Thomas-Wigner rotation. The model we are going to study essentially reduces to a four qubit system of two momenta and two spins, where momenta can be viewed as control qubits and spins are target qubits. Note also that by considering only finite dimensional momenta we avoid the complication of having to deal with the entanglement of continuous variables, see [97, 98] for review.

The chapter is organised as follows. We start by discussing the idea that entanglement transfer occurs between the spin and momentum degrees of freedom and consider the boost scenarios studied in the previous chapters. Thereafter we turn to looking at the hypothesis that entanglement might be changing with respect to the partitioning of the system into two particles. We summarise our findings in section 6.4.

6.2 Degrees of freedom partitions

The common opinion has it that if the total amount of entanglement remains invariant, while the entanglement in the spin degree of freedom decreases, then momenta must become more entangled. To see whether or not this inference is valid, we will calculate the entanglement of the momentum state for the boost scenarios discussed in the two previous chapters.

6.2.1 Product momenta

We start by considering product momenta, which can be written in a succinct form $\left|M^{\Sigma}\right\rangle = \sum_{i,j=1}^{2} \psi(\mathbf{p}_i, \mathbf{q}_j) \left|\mathbf{p}_i, \mathbf{q}_j\right\rangle$. The initial state of the two particle system is given by

$$|\psi\rangle = \left(\sum_{i,j=1}^{2} \psi(\mathbf{p}_i, \mathbf{q}_j) \left|\mathbf{p}_i, \mathbf{q}_j\right\rangle \right) \otimes |\Psi\rangle \ . \tag{6.1}$$

A Lorentz boost Λ transforms the state to

$$\left|\psi''\right\rangle = \sum_{i,j=1}^{2} \psi(\mathbf{p}_i, \mathbf{q}_j) \left|\Lambda\mathbf{p}_i, \Lambda\mathbf{q}_j\right\rangle \otimes R(\mathbf{p}_i, \mathbf{q}_j) \left|\Psi\right\rangle \ , \tag{6.2}$$

where we have used the abbreviation $R(\mathbf{p}_1, \mathbf{p}_2) \equiv U(\Lambda, \mathbf{p}_1) \otimes U(\Lambda, \mathbf{p}_2)$ for two particle rotations. The corresponding density matrix $\rho'' = |\psi''\rangle \langle\psi''|$ is given by

$$\rho'' = \sum_{i,j,k,m=1}^{2} \psi(\mathbf{p}_i, \mathbf{q}_j)\psi^*(\mathbf{p}_k, \mathbf{q}_m) \left|\Lambda\mathbf{p}_i, \Lambda\mathbf{q}_j\right\rangle \left\langle\Lambda\mathbf{p}_k, \Lambda\mathbf{q}_m\right| \otimes R(\mathbf{p}_i, \mathbf{q}_j) \left|\Psi\right\rangle \left\langle\Psi\right| R^{\dagger}(\mathbf{p}_k, \mathbf{q}_m) \ . \tag{6.3}$$

In order to obtain the momentum state we trace out the spin degrees of freedom, $\rho''_M = \mathsf{Tr}_{\mathrm{spin}}(\rho'')$,

$$\begin{aligned} \rho''_M = \sum_{k,m,i,j=1}^{2} & \psi(\mathbf{p}_i, \mathbf{q}_j)\psi^*(\mathbf{p}_k, \mathbf{q}_m) \left|\Lambda\mathbf{p}_i, \Lambda\mathbf{q}_j\right\rangle \left\langle\Lambda\mathbf{p}_k, \Lambda\mathbf{q}_m\right| \\ & \times \left\langle\Psi\right| R^{\dagger}(\mathbf{p}_k, \mathbf{q}_m) R(\mathbf{p}_i, \mathbf{q}_j) \left|\Psi\right\rangle \ . \end{aligned} \tag{6.4}$$

Since we have labelled the momentum of each particle separately, $i, j, k, m \in \{1, 2\}$, the correspondence with a 4×4 matrix enumeration is $11 \mapsto 1$, $12 \mapsto 2$, $21 \mapsto 3$, $22 \mapsto 4$, and the diagonal elements of ρ''_M are just $|\psi(\mathbf{p}_i, \mathbf{q}_j)|^2 \left|\Lambda\mathbf{p}_i, \Lambda\mathbf{q}_j\right\rangle \left\langle\Lambda\mathbf{p}_i, \Lambda\mathbf{q}_j\right|$,

$i, j = 1, 2$. For the six independent off-diagonal elements we need to calculate products $R^\dagger(\mathbf{p}_k, \mathbf{q}_m)R(\mathbf{p}_i, \mathbf{q}_j)$ of rotation matrices. By substituting the product momentum $\left|M^\Sigma\right\rangle$ into (6.4), we obtain the following expressions for off-diagonal elements in the 4×4 enumeration,

$$\begin{aligned}
(\rho''_M)_{12}: &\quad R^\dagger(\mathbf{p}_1, \mathbf{q}_2)R(\mathbf{p}_1, \mathbf{q}_1) = \mathbf{1} \otimes R^{-1}(\mathbf{q}_2)R(\mathbf{q}_1) \\
(\rho''_M)_{13}: &\quad R^\dagger(\mathbf{p}_2, \mathbf{q}_1)R(\mathbf{p}_1, \mathbf{q}_1) = R^{-1}(\mathbf{p}_2)R(\mathbf{p}_1) \otimes \mathbf{1} \\
(\rho''_M)_{14}: &\quad R^\dagger(\mathbf{p}_2, \mathbf{q}_2)R(\mathbf{p}_1, \mathbf{q}_1) = R^{-1}(\mathbf{p}_2)R(\mathbf{p}_1) \otimes R^{-1}(\mathbf{q}_2)R(\mathbf{q}_1) \\
(\rho''_M)_{23}: &\quad R^\dagger(\mathbf{p}_2, \mathbf{q}_1)R(\mathbf{p}_1, \mathbf{q}_2) = R^{-1}(\mathbf{p}_2)R(\mathbf{p}_1) \otimes R^{-1}(\mathbf{q}_1)R(\mathbf{q}_2) \\
(\rho''_M)_{24}: &\quad R^\dagger(\mathbf{p}_2, \mathbf{q}_2)R(\mathbf{p}_1, \mathbf{q}_2) = R^{-1}(\mathbf{p}_2)R(\mathbf{p}_1) \otimes \mathbf{1} \\
(\rho''_M)_{34}: &\quad R^\dagger(\mathbf{p}_2, \mathbf{q}_2)R(\mathbf{p}_2, \mathbf{q}_1) = \mathbf{1} \otimes R^{-1}(\mathbf{q}_2)R(\mathbf{q}_1)\ .
\end{aligned} \tag{6.5}$$

We will next consider concrete scenarios and assume throughout that the spin state $|\Psi\rangle$ is given by $|\Phi^+\rangle$.

6.2.1.1 Case $R_i \otimes \mathbf{1}$

To implement single particle rotations, we choose the momentum state to be the same as in section 4.5.2.1, $\left|M^\Sigma\right\rangle = (|\mathbf{p}_y\rangle + |-\mathbf{p}_y\rangle)\,|\mathbf{q}_1\rangle\,/\sqrt{2}$, where $|\mathbf{q}_1\rangle$ is a momentum that leaves the second particle alone. The first particle is rotated around the x-axis and we denote $R_X(\pm\omega) \equiv R_X(\pm\mathbf{p}_y)$. Substituing $\left|M^\Sigma\right\rangle$ into (6.5), we obtain only one independent non-vanishing off-diagonal element $(\rho''_M)_{13}$,

$$\begin{aligned}
(\rho''_M)_{13} &= \frac{1}{2}\left\langle\Phi^+\right|(R_X^\dagger(-\omega) \otimes \mathbf{1})(R_X(\omega) \otimes \mathbf{1})\left|\Phi^+\right\rangle = \frac{1}{2}\left\langle\Phi^+\right| R_X(2\omega) \otimes \mathbf{1}\left|\Phi^+\right\rangle \\
&= \frac{\cos\omega}{2}\ .
\end{aligned} \tag{6.6}$$

To find concurrence, we calculate the eigenvalues of the matrix $\rho\widetilde{\rho}$. They all vanish, which implies that concurrence $C(\rho''_M) = 0$.

6.2.1.2 Case $R_i \otimes R_i$

For two particle rotations around the same axis we choose the momenta to lie along the x-axis,

$$\left|M^\Sigma\right\rangle = \frac{1}{2}\,(|\mathbf{p}_x\rangle + |-\mathbf{p}_x\rangle)\,(|\mathbf{p}_x\rangle + |-\mathbf{p}_x\rangle)\ . \tag{6.7}$$

Supposing the boost is in the z-direction, the Thomas-Wigner rotation will occur around the y-axis, $R_Y(\pm\omega) \equiv R_Y(\pm\mathbf{p}_x)$. By substituting momentum into (6.5), we

calculate the products for the off-diagonal elements,

$$\begin{aligned}
(\rho''_M)_{12}: &\quad \mathbf{1}\otimes R_Y^\dagger(-\omega)R_Y(\omega)=\mathbf{1}\otimes R_Y(2\omega)\\
(\rho''_M)_{13}: &\quad R_Y^\dagger(-\omega)R_Y(\omega)\otimes\mathbf{1}=R_Y(2\omega)\otimes\mathbf{1}\\
(\rho''_M)_{14}: &\quad R_Y^\dagger(-\omega)R_Y(\omega)\otimes R_Y^\dagger(-\omega)R_Y(\omega)=R_Y(2\omega)\otimes R_Y(2\omega)\\
(\rho''_M)_{23}: &\quad R_Y^\dagger(-\omega)R_Y(\omega)\otimes R_Y^\dagger(\omega)R_Y(-\omega)=R_Y(2\omega)\otimes R_Y(-2\omega)\\
(\rho''_M)_{24}: &\quad R_Y^\dagger(-\omega)R_Y(\omega)\otimes\mathbf{1}=R_Y(2\omega)\otimes\mathbf{1}\\
(\rho''_M)_{34}: &\quad \mathbf{1}\otimes R_Y^\dagger(-\omega)R_Y(\omega)=\mathbf{1}\otimes R_Y(2\omega)\ .
\end{aligned}\tag{6.8}$$

Since we have assumed the the spin state is $|\Phi^+\rangle$, the off-diagonal elements evaluate as follows,

$$\begin{aligned}
&(\rho''_M)_{12}=(\rho''_M)_{13}=(\rho''_M)_{24}=(\rho''_M)_{34}=\frac{\cos\omega}{4}\,,\\
&(\rho''_M)_{23}=\frac{\cos 2\omega}{4}\,,\quad (\rho''_M)_{14}=\frac{1}{4}\,.
\end{aligned}\tag{6.9}$$

To find concurrence, we calculate the eigenvalues of the matrix $\rho\widetilde{\rho}$,

$$\frac{\sin^4\omega}{4}\,,\ \frac{\sin^4\omega}{4}\,,\ 0\,,\ 0\,,$$

which implies that the concurrence $C(\rho''_M)=0$.

6.2.1.3 Case $R_i\otimes R_j$

In order to implement mixed rotations, we choose the momentum to be

$$\left|M^\Sigma\right\rangle=\frac{1}{2}\left(|\mathbf{p}_y\rangle+|-\mathbf{p}_y\rangle\right)\left(|\mathbf{p}_x\rangle+|-\mathbf{p}_x\rangle\right)\ ,\tag{6.10}$$

and supposing boost is in the z-direction, the first particle undergoes $R_X(\pm\omega)$ and the second $R_Y(\pm\omega)$ rotations. We calculate for the off-diagonal elements,

$$\begin{aligned}
(\rho''_M)_{12}: &\quad \mathbf{1}\otimes R_Y^\dagger(-\omega)R_Y(\omega)=\mathbf{1}\otimes R_Y(2\omega)\\
(\rho''_M)_{13}: &\quad R_X^\dagger(-\omega)R_X(\omega)\otimes\mathbf{1}=R_X(2\omega)\otimes\mathbf{1}\\
(\rho''_M)_{14}: &\quad R_X^\dagger(-\omega)R_X(\omega)\otimes R_Y^\dagger(-\omega)R_Y(\omega)=R_X(2\omega)\otimes R_Y(2\omega)\\
(\rho''_M)_{23}: &\quad R_X^\dagger(-\omega)R_X(\omega)\otimes R_Y^\dagger(\omega)R_Y(-\omega)=R_X(2\omega)\otimes R_Y(-2\omega)\\
(\rho''_M)_{24}: &\quad R_X^\dagger(-\omega)R_X(\omega)\otimes\mathbf{1}=R_X(2\omega)\otimes\mathbf{1}\\
(\rho''_M)_{34}: &\quad \mathbf{1}\otimes R_Y^\dagger(-\omega)R_Y(\omega)=\mathbf{1}\otimes R_Y(2\omega)\ .
\end{aligned}\tag{6.11}$$

For the spin state $|\Phi^+\rangle$, the off-diagonal elements evaluate as follows,

$$(\rho''_M)_{12} = (\rho''_M)_{13} = (\rho''_M)_{24} = (\rho''_M)_{34} = \frac{\cos\omega}{4}\,,$$
$$(\rho''_M)_{14} = (\rho''_M)_{23} = \frac{\cos^2\omega}{4}\,. \tag{6.12}$$

To find concurrence, we calculate that the eigenvalues of $\rho\widetilde{\rho}$ are all $\left(\sin^4\omega\right)/16$ which implies that the concurrence $C(\rho''_M) = 0$.

6.2.2 Entangled momenta

For entangled momenta, it suffices that we study either $\left|M^{\Phi+}\right\rangle$ or $\left|M^{\Psi+}\right\rangle$, which can be written generally $|M\rangle = \sum_{i=1}^{2}\psi(\mathbf{p}_i,\mathbf{q}_i)\,|\mathbf{p}_i,\mathbf{q}_i\rangle$, so the rest frame state is

$$|\psi\rangle = \left(\sum_{i=1}^{2}\psi(\mathbf{p}_i,\mathbf{q}_i)\,|\mathbf{p}_i,\mathbf{q}_i\rangle\right)\otimes|\Psi\rangle\ . \tag{6.13}$$

We note that this is identical to the product momentum (6.1) if we set $i = j$. We then immediately obtain the boosted momentum density matrix from Equation (6.4) by setting $i = j$ and $k = m$,

$$\rho''_M = \sum_{i,k=1}^{2}\psi(\mathbf{p}_i,\mathbf{q}_i)\psi^*(\mathbf{p}_k,\mathbf{q}_k)\,|\Lambda\mathbf{p}_i,\Lambda\mathbf{q}_i\rangle\,\langle\Lambda\mathbf{p}_k,\Lambda\mathbf{q}_k| \times\langle\Psi|\,R^\dagger(\mathbf{p}_k,\mathbf{q}_k)R(\mathbf{p}_i,\mathbf{q}_i)\,|\Psi\rangle\ . \tag{6.14}$$

This implies the density matrix contains only one independent off-diagonal element,

$$|\Lambda\mathbf{p}_1,\Lambda\mathbf{q}_1\rangle\,\langle\Lambda\mathbf{p}_2,\Lambda\mathbf{q}_2|\,\langle\Psi|\,R^\dagger(\mathbf{p}_2,\mathbf{q}_2)R(\mathbf{p}_1,\mathbf{q}_1)\,|\Psi\rangle\ , \tag{6.15}$$

and we will again assume with no restriction of generality that the spin state is given by $|\Phi^+\rangle$ in all three scenarios $R_i\otimes\mathbf{1}$, $R_i\otimes R_i$, $R_i\otimes R_j$.

6.2.2.1 Case $R_i\otimes R_i$

We saw above in section 4.5.4.1 that this case splits into two, the trivial and the non-trivial one. Only the latter is interesting for present purposes, so we assume

that the momenta lie symmetrically along the x-axis, $\mathbf{p}_1 = -\mathbf{q}_1 = -\mathbf{p}_2 = \mathbf{q}_2 = \mathbf{p}_x$,

$$\left|M^{\Psi+}\right\rangle = \frac{1}{\sqrt{2}}\left(|\mathbf{p}_x, -\mathbf{p}_x\rangle + |-\mathbf{p}_x, \mathbf{p}_x\rangle\right) \ , \tag{6.16}$$

and the Lorentz boost is in the z-direction. The spins will be rotated in the $x-z$-plane by $R_Y(\pm\omega) \equiv R(\pm\mathbf{p}_x)$. For the only off-diagonal term we calculate the product of rotation operators,

$$R_Y^\dagger(-\omega,\omega)R_Y(\omega,-\omega) = R_Y(2\omega)\otimes R_Y(-2\omega) \ , \tag{6.17}$$

and for $|\Phi^+\rangle$ the off-diagonal element evaluates to

$$(\rho''_M)_{23} = \left\langle\Phi^+\right| R_Y(2\omega)\otimes R_Y(-2\omega)\left|\Phi^+\right\rangle = \frac{\cos 2\omega}{2} \ . \tag{6.18}$$

For concurrence we find the square roots of eigenvalues of $\rho\widetilde{\rho}$,

$$\frac{1}{8}\left(3+4|\cos 2\omega| + \cos 4\omega\right), \ \frac{1}{8}\left(3-4|\cos 2\omega| + \cos 4\omega\right), \ 0 \, , \ 0 \, .$$

which implies that the concurrence for ρ''_M is

$$C(\rho''_M) = |\cos 2\omega| \ . \tag{6.19}$$

This is plotted in Figure 6.1. We see that entanglement in the momentum degree of freedom behaves *exactly* in the same way as spin entanglement, see section 4.5.4.1. It decoheres under Lorentz boosts.

We note that this result was first found by [92]. They choose a boost scenario with a boost angle $\theta = \pi/2$ and obtain the same analytic formula for both the spin and momentum concurrence. Our slightly different analytic calculation confirms their result.

6.2.2.2 Case $R_i \otimes R_j$

In order to implement mixed rotations, we choose the momentum state as follows,

$$\left|M^{\Psi+}\right\rangle = \frac{1}{\sqrt{2}}\left(|\mathbf{p}_y, -\mathbf{p}_x\rangle + |-\mathbf{p}_y, \mathbf{p}_x\rangle\right) \ , \tag{6.20}$$

so the particle undergoes $R_X \otimes R_Y$ rotations. We calculate the off-diagonal term,

$$(\rho''_M)_{23} = \left\langle\Phi^+\right| R_X(2\omega)\otimes R_Y(-2\omega)\left|\Phi^+\right\rangle = \frac{\cos^2\omega}{2} \ . \tag{6.21}$$

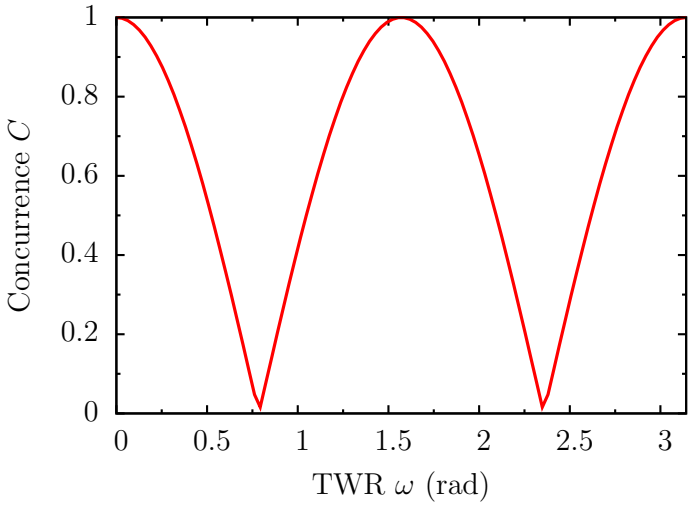

Figure 6.1. Momentum concurrence for spin rotations of type $R_i \otimes R_i$ generated by entangled momenta $|M^{\Psi+}\rangle$.

To find concurrence, we calculate the eigenvalues of $\rho\widetilde{\rho}$,

$$\frac{1}{16}\left(3+\cos 2\omega\right)^2\,,\ \frac{1}{4}\sin^4\omega,\ 0\,,\ 0\,,$$

so the expression for concurrence is

$$C(\rho''_M) = \cos^2\omega\ . \tag{6.22}$$

This is plotted in Figure 6.2. In analogy to the previous case, we observe that momentum entanglement mirrors the behaviour of spin entanglement, see section 4.5.4.2.

6.3 Particle partitions

Our investigations so far have not confirmed the hypothesis that spin entanglement is transferred to the momentum degrees of freedom. In case of the single particle we observed that entanglement between the spin and the momentum degree of freedom changed as a result of boost. Might it be that entanglement is redistributed within a single particle? To see whether or not this is true, we will calculate the concurrence of a particle in different boost scenarios.

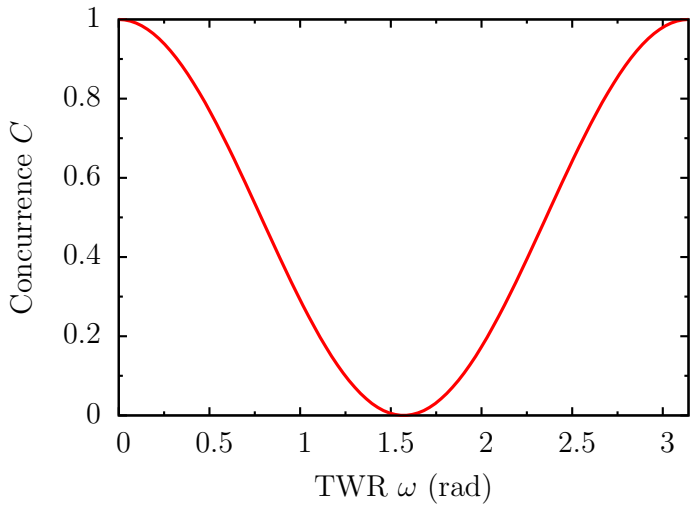

Figure 6.2. Momentum concurrence for spin rotations of type $R_i \otimes R_j$ generated by entangled momenta $\left|M^{\Psi+}\right\rangle$.

6.3.1 Product momenta

We begin by considering product momenta $\left|M^{\Sigma}\right\rangle = \frac{1}{2}\sum_{i,j=1}^{2}\left|\mathbf{p}_i, \mathbf{q}_j\right\rangle$. The initial state of the two particle system is given by

$$\left|\psi\right\rangle = \left(\frac{1}{2}\sum_{i,j=1}^{2}\left|\mathbf{p}_i, \mathbf{q}_j\right\rangle\right) \otimes \left|\Phi^{+}\right\rangle \ . \tag{6.23}$$

A Lorentz boost Λ transforms the state to

$$\left|\psi''\right\rangle = \frac{1}{2}\sum_{i,j=1}^{2}\left|\Lambda\mathbf{p}_i, \Lambda\mathbf{q}_j\right\rangle \otimes R(\mathbf{p}_i, \mathbf{q}_j)\left|\Phi^{+}\right\rangle \ , \tag{6.24}$$

and the density matrix $\rho'' = \left|\psi''\right\rangle\left\langle\psi''\right|$ is given by

$$\rho'' = \frac{1}{4}\left[\sum_{i,j,k,m=1}^{2}\left|\Lambda\mathbf{p}_i, \Lambda\mathbf{q}_j\right\rangle\left\langle\Lambda\mathbf{p}_k, \Lambda\mathbf{q}_m\right| \otimes R(\mathbf{p}_i, \mathbf{q}_j)\left|\Phi^{+}\right\rangle\left\langle\Phi^{+}\right| R^{\dagger}(\mathbf{p}_k, \mathbf{q}_m)\right] \ . \tag{6.25}$$

To obtain the state of the second particle, we trace out the first particle $\rho_2'' = \mathsf{Tr}_1\left(\rho''\right)$,

$$\rho_2'' = \frac{1}{4}\left[\sum_{i,j,k,m=1}^{2}\left\langle\Lambda\mathbf{p}_i|\Lambda\mathbf{p}_k\right\rangle\left|\Lambda\mathbf{q}_j\right\rangle\left\langle\Lambda\mathbf{q}_m\right|\right.$$

$$\otimes \left(\frac{1}{2} \sum_{s,t=0}^{1} \mathsf{Tr}\left(R(\mathbf{p}_i) \left|s\right\rangle \left\langle t\right| R^{\dagger}(\mathbf{p}_k) \right) R(\mathbf{q}_j) \left|s\right\rangle \left\langle t\right| R^{\dagger}(\mathbf{q}_m) \right) \Bigg] \ , \tag{6.26}$$

where we have used the expansion $|\Phi^+\rangle\langle\Phi^+| = \frac{1}{2}\sum_{s,t=0}^{1} |ss\rangle\langle tt|$ for the density matrix of the Bell state. We take into account that the boosted momenta satisfy the orthogonality condition, $\langle \Lambda \mathbf{p}_i | \Lambda \mathbf{p}_k \rangle = \delta_{ik}$, and that the trace of the spin state gives

$$\begin{aligned} \mathsf{Tr}\left(R(\mathbf{p}_i) \left|s\right\rangle \left\langle t\right| R^{\dagger}(\mathbf{p}_i) \right) &= \langle t| R^{\dagger}(\mathbf{p}_i) R(\mathbf{p}_i) |s\rangle = \delta_{ii} \langle s|t\rangle \\ &= \delta_{ii}\delta_{st} \ . \end{aligned} \tag{6.27}$$

Substituting this into (6.26) and taking sum over i, we get

$$\begin{aligned} \rho_2'' &= \frac{1}{4} \left[\sum_{j,m=1}^{2} |\Lambda \mathbf{q}_j\rangle \langle \Lambda \mathbf{q}_m| \otimes \left(\sum_{s=0}^{1} R(\mathbf{q}_j) |s\rangle \langle s| R^{\dagger}(\mathbf{q}_m) \right) \right] \\ &= \frac{1}{4} \sum_{j,m=1}^{2} |\Lambda \mathbf{q}_j\rangle \langle \Lambda \mathbf{q}_m| \otimes R(\mathbf{q}_j) R^{\dagger}(\mathbf{q}_m) \ , \end{aligned} \tag{6.28}$$

where in the last line we have used that the spins satisfy the resolution of identity, $\sum_{s=0}^{1} |s\rangle\langle s| = \mathbf{1}_2$. We can rewrite this in a form,

$$\rho_2'' = \frac{1}{4} \left(\mathbf{1}_2 \otimes \mathbf{1}_2 + \sum_{\substack{j,m=1 \\ j \neq m}}^{2} |\Lambda \mathbf{q}_j\rangle \langle \Lambda \mathbf{q}_m| \otimes R(\mathbf{q}_j) R^{\dagger}(\mathbf{q}_m) \right) \ , \tag{6.29}$$

where the diagonal and off-diagonal terms are clearly separated.

For all three types of rotations $R_i \otimes \mathbf{1}$, $R_i \otimes R_i$, $R_i \otimes R_j$, $i \neq j$, the off-diagonal term takes the form $|\Lambda \mathbf{q}_1\rangle \langle \Lambda \mathbf{q}_2| \otimes R(2\omega)$, implying that the concurrence $C(\rho_2'') = 0$.

6.3.2 Entangled momenta

For an entangled momentum $\left|M^{\Phi+}\right\rangle = \frac{1}{\sqrt{2}} \sum_{i=0}^{1} |\mathbf{p}_i, \mathbf{q}_i\rangle$, the boosted state can be obtained immediately from the expression (6.28) by noting that $j = m$, hence

$$\rho_2'' = \frac{1}{4} \mathbf{1}_2 \otimes \mathbf{1}_2 \ . \tag{6.30}$$

The result holds for all entangled momentum states where the $|\mathbf{p}_1\rangle$ and $|\mathbf{p}_2\rangle$ are orthogonal. Since this is true for all three types of rotations $R_i \otimes \mathbf{1}$, $R_i \otimes R_i$, $R_i \otimes R_j$,

$i \neq j$, the concurrence $C(\rho_2'') = 0$ in all three scenarios. We note that [92] find the same result for the scenario $R_i \otimes R_i$.

6.4 Summary and discussion

The conclusion that the decrease of pairwise entanglement in the spin-spin degrees of freedom is not compensated by an increase of pairwise entanglement between momenta was first established in [92] where the authors study entangled momenta of the form $\left|M^{\Psi^-}\right\rangle$. We confirm this finding by extending the analysis to a wider class of momentum states. If momentum qubits are initially in a separable state, the momentum state which is obtained by tracing out the spin degree of freedom, never becomes entangled for any value of spin rotation in any of the scenarios. Initially entangled momenta behave somewhat differently—the change of concurrence mimics that of spin entanglement for both the $R_i \otimes R_i$ and $R_i \otimes R_j$ scenarios.

Drawing on the single particle, i.e. the fact that Lorentz boosts entangle the spin and momentum of a single particle, one might argue that spin-spin entanglement is rather shuffled around in the particle-partition of the system, that is, between the spin and the momentum qubit of a single particle. While in section 6.3 we found that the concurrence of a single particle vanishes for both the product and entangled momenta, the treatment we adopted only establishes that there is no bipartite entanglement present between the degrees of freedom of a single particle. Multipartite entanglement between three or four of the spin and momentum degrees of freedom can still be present. This is because determining multiparticle entanglement requires a more elaborate approach than the one used above. To detect whether the entanglement, which initially resides in the spin-spin degree of freedom, has been shuffled into the particle-partitions, one can find out how the entanglement between the whole particle-partitions changes as a result of boosts. That is, one finds the state of the first particle by tracing out the second particle and then calculates the entropy of the first particle. Comparison of the entropy of the initial and the final states of the particle then shows whether or not the spin-spin entropy has been transferred into the particle-partition of the total system.[1]

In summary, the issue of entanglement transfer under Lorentz boosts remains open. The results obtained in this chapter do not yield a full account of how entanglement is redistributed between different subsystems of two particles when the system is viewed from different relativistic frames. A more thorough analysis

[1] See e.g. [99, 100] and references therein for multiparticle entanglement. I would like to thank Pieter Kok and Viv Kendon for drawing my attention to this, as well as for a useful discussion.

is needed where we conceive of the system in terms of four qubits, accompanied with a comprehensive analysis of multiparticle entanglement. We envisage this as part of future research.

Chapter 7

Conclusion

We will now summarise the findings of the thesis and provide some possible avenues for future research. We began our investigation in chapter 3 by focussing on the simplest nontrivial system of interest: a single massive spin-$1/2$ particle with momentum, which constitutes the qubit in the context of relativistic quantum information. We confirmed the general observation that entanglement is observer dependent. Lorentz boosts change the entanglement between the spin and momentum degrees of freedom. While previous works in the literature focussed on systems involving various idealisations, we generalised the treatment in three ways, which to the best of our knowledge had not been done before. First, we extended the discussion to realistic systems described by Gaussian wavepackets with finite width. We secondly generalised the analysis to geometries involving a large variety of boost angles and established that the behaviour of entanglement is sensitive to the boost geometry. Maximal entanglement between spin and momentum components of a single particle can be achieved with sub-luminal boosts. However, if achieving a particular level of entanglement is significant in the given context, then the boost parameters must be chosen carefully since due to rich geometric setting too large or too small boosts do not yield the desired result and may instead lead to deterioration of entanglement. We also confirm that the effect persists for wave packets. Lastly, we introduced another sense in which geometry plays a crucial role: as a form of explanation. It turns out that all the diverse qualitative features of entanglement behaviour of systems with discrete and continuous momenta can be understood in a simple geometric manner.

In chapter 4 we turned to examine entanglement in the spin degree of freedom of a two particle system. By systematically studying different kinds of product and entangled momenta in various boost scenarios, the aim was to survey and classify

the structure of maps that momenta induce on spins under Lorentz boosts. We assumed that momenta are discrete and spins are in the Werner state. The latter subsume the Bell states. The results are summarised in Tables 4.3 and 4.4. The overall conclusion is that Lorentz boosts generally cause non-trivial behaviour of entanglement in the spin degree of freedom of two particle systems. In analogy to the single particle system, the spin-spin entanglement of two particles is observer dependent. However, whether or not, and to what extent, the state and entanglement of spins changes depends substantially on the spin and momentum states involved, as well as on the geometry of the boost scenario. Whereas some states and geometries leave entanglement invariant, others give rise to rapid changes of concurrence. Examples of the former comprise Bell states with product momenta of the form $|\mathbf{p}, \mathbf{q}\rangle$, as well as the interesting special case of type $R_i \otimes R_i$ for entangled momenta where spin is an eigenstate of rotation, represented by the equivalence class $[R_Y \otimes R_Y, \rho_{\mathrm{d}}^{M\Phi+}, \rho^W]$. All other types of rotations and momenta were found to bring about entanglement change in Bell states that ranges from maximal to zero, with the class $[R_X \otimes R_X, M^{\Phi+}, \Phi^+]$ for the entangled momenta causing the fastest decay and rebirth of entanglement.

While the literature on relativistic entanglement commonly analyses pure entangled states, it is important to consider mixed states as well in order to gain full understanding. The present work makes a step in this direction by classifying the behaviour of the Werner states, whose entanglement ranges between maximal and no entanglement at all. Compared to pure states, they display less change as the maximal degree of entanglement is bounded by the parameter λ. The latter highlights an important conclusion, which applies to both pure and entangled spin states: spin entanglement cannot be increased under Lorentz boosts if there is no spin-momentum entanglement present in the first place. This result was first proved for pure states in [15], our investigation confirms that it holds true for mixed spin states as well if spin and momentum initially factorise. It should be stressed though that the result is valid only for initial states whose spin-momentum factorise [15]. If spin and momentum degrees are initially entangled, the boosted state might be more entangled than the initial one. Although proper study of this very interesting case is beyond the scope of the current thesis, as noted in section 4.2, it has been implicit to some extent in the scenarios we examined.

We also gained valuable qualitative insights. The geometric framework introduced in the chapter on single particle systems remained in place. Using this we could understand the various results reported in the literature, i.e. that spin entan-

glement did or did not change in a particular boost scenario, by explaining them in a convenient, simplified framework which involves discrete momenta and spins. As an example, we saw that the seemingly contradictory results reported in [17] and [15] could be explained away by observing that the authors used different momentum states. The continuous states involved in the example can modelled in many situations quite accurately in terms of the state $|M^{\times}\rangle$, as discussed in detail in chapter 5, where we turned to two particles with continuous momenta.

The treatment of continuous systems was parallel to those of discrete momenta in that we systematically surveyed a number of boost scenarios with momenta both in product and entangled states. Attention was confined to pure spins only, which were assumed to be in the Bell state $|\Phi^{+}\rangle$. We observed relatively good agreement between discrete systems and Gaussians of narrower widths with $\sigma/m = 1$. Wave packets of larger widths led to deviation from the idealised discrete models. In analogy to the the single particle system, the analysis was numerical throughout as the two particle system is too complex to be tackled by analytic methods. However, the lack of analytic models was to some extent compensated by the discrete model, according to which systems involving three dimensional Gaussians can be thought of as fields comprising spins at a large number of discrete momenta. Boosting means that each spin undergoes a different, momentum dependent rotation for a given value of rapidity. It was remarkable that such a complex behaviour can be reduced to simple models. We highlight two cases which further justify its use. In section 5.3.2 we were able to understand the somewhat counterintuitive behaviour of z-axis centred Gaussians in terms of a simple discrete 2D model involving two spins. And in section 5.3.3 we employed the $|M^{\times}\rangle$ and $f^{\times}$ states to obtain another simple model involving four narrow Gaussians whose behaviour agreed, in many cases, with that of the z-centred Gaussian momenta to a surprisingly high degree of accuracy. In analogy to discrete systems, further insight into the workings of continuous systems was provided by visualisation of their orbits. We gained a more detailed understanding of how varying the initial states, their widths and momenta, changes the entanglement of spins.

In chapter 6 we discussed the notion of entanglement transfer. We confirmed the conclusion that the decrease of pairwise entanglement in the spin-spin degree of freedom is not compensated by an increase of pairwise entanglement between momenta, a result that was first established for entangled momenta in [92]. We extended the analysis to a wider class of momentum states. If momentum qubits are initially in a separable state, the momentum state, which is obtained by tracing out

the spin degree of freedom, never becomes entangled for any value of spin rotation in any of the scenarios. Entangled momenta behave somewhat differently—the change of concurrence mimics that of spin entanglement for both the $R_i \otimes R_i$ and $R_i \otimes R_j$ scenarios. Interestingly, momentum entanglement decoheres in exactly the same way as spin entanglement. We also considered another hypothesis, namely, that spin-spin entanglement is shuffled around in the particle-partitions of the system, that is, between the spin and the momentum qubit of a single particle. However, although we found that the concurrence of a single particle vanishes for both the product and entangled momenta, the treatment we adopted does not establish conclusively that there was no entanglement present between the degrees of freedom of a single particle. This is because determining multiparticle entanglement requires a more elaborate approach than the one used above. We conclude that more work is needed to obtain a full account of how entanglement is redistributed between different subsystems of two particles when the system is viewed from different relativistic frames. We envisage this as part of future research.

7.1 Outlook

Relativistic quantum information lies at the intersection of quantum theory, relativity and information theory. It remains a field of active research with a number of interesting topics. In this thesis, we have attempted to make progress in understanding the key question—the behaviour of entanglement—by emphasising the role of geometry. To close off, we would like to outline a possible avenue of research which offers an interesting extension of the ideas pursued above.

The common understanding of the Thomas-Wigner rotation is in the context of group theory. Yet the geometric perspective offers a fruitful, complementary approach. This picture emphasises the fact that the relativistic velocity space is a Riemannian manifold with hyperbolic geometry [67]. Each point can be transformed into any other, meaning that it is a homogeneous space of the Lorentz group. Lorentz boosting corresponds to parallel transporting in this space. Since the manifold has a constant curvature, parallel transporting a vector around a closed loop results in a non-trivial transformation. In the context of differential geometry, this phenomenon is known as *holonomy* [101, 102]. This allows to conceptualise Thomas-Wigner rotation as a holonomy of the relativistic velocity space [103], implying that Thomas-Wigner rotation belongs to the kind of phenomena of which Berry's phase is an another example [104, 105].

In this framework, the physical situation we have been concerned with throughout the thesis now appears as a particular case, which we can call a *two-boost* scenario. In general, however, we can consider an arbitrary loop in the velocity space, leading to a wide variety of *multi-boost* scenarios. Physically, the two-boost scenario corresponds to a passive boost situation involving two observers in different frames. A multi-boost scenario can be interpreted in an active manner, with the system undergoing change of movement. The importance of this is that while the magnitude of Thomas-Wigner rotation in the two-boost situation ranges between 0 and π, in general in the multi-boost scenario any angle between 0 and 2π can be achieved. This implies we can in principle manipulate a qubit by letting it traverse a particular trajectory in the velocity space. Especially interesting examples involve schemes which generate maximally entangled states with speeds well below the speed of light. Another is a possible experimental verification of the Thomas-Wigner rotation with non-relativistic speeds. If possible, the third is perhaps most intriguing: implement an arbitrary single qubit gate by devising a suitable path in the velocity space. It would be interesting to see if these intuitive arguments can be realised in a rigorous setting.

Appendix A

Example of source code: single particle

This appendix describes the code that was used to carry through the numerical calculations for single particle systems with continuous momenta. It is written in the Java programming language and needs the package `Jampack` to run. The latter can be downloaded at NIST [106]. The variables `mass` and `sigma` specify the mass and width of the particle. The variables `px0`, `py0` and `pz0` define the centers of the Gaussian wave packets. The rapidity is defined using the variable `rapidity`. All these variables need to be set using the method `setParams` before the method `calculateIntegral` is called.

```
1  import java.io.FileInputStream;
2  import java.io.FileOutputStream;
3  import java.io.IOException;
4  import java.io.*;
5
6  import java.util.*;
7  import java.lang.Number.*;
8  import java.nio.*;
9
10 import graphutil.*;
11 import org.matrixutil.*;
12
13 public class TwoGaussVer4 implements paramsTwoGaussVer4
14 {
15   //constants
16   private double sigma = 0.08, sigma2 = 0;
17   private double mass = 0.01, mass2 = 0;
18   private double rapidity = 0;
19   private double coshRapidity = 0, sinhRapidity = 0, coshRapidityHalf = 0,
         sinhRapidityHalf = 0;
```

```
20
21    //energy and boosted energy
22    private double Energy = 0;
23
24    //integration dummies
25    private double px = 0, py = 0, pz = 0; //dummy Cart3D variables
26    private double px2 = 0, py2 = 0, pz2 = 0; //squared dummies to increase
          speed
27    private double invariantInfElement = 0;
28    private double invariantIntegrationMeasureCart = 0;
29    private double dpx = 0, dpy = 0, dpz = 0; //increment
30
31    private double[][] doubleFourMomentum = new double[4][1];
32
33    private double px0 = 0, py0 = 0, pz0 = 0; //displacement for Gaussian
34
35    //integration limits
36    private double pxmin = 0, pxmax = 0, pymin = 0, pymax = 0, pzmin = 0,
          pzmax = 0; //domain min, max
37
38    private double offSetX = 0;
39    private double offSetY = 0;
40    private double offSetZ = 0;
41
42    //Integration area limits
43    private double pxmin0 = 0;
44    private double pxmax0 = 0;
45    private double pymin0 = 0;
46    private double pymax0 = 0;
47    private double pzmin0 = 0;
48    private double pzmax0 = 0;
49    private double pxmax02 = 0; //squared dummies
50    private double pymax02 = 0;
51    private double pzmax02 = 0;
52    private double EnergyPxmax0 = 0;
53    private double EnergyPymax0 = 0;
54    private double EnergyPzmax0 = 0;
55    private double pzmax2 = 0, pzmin2 = 0, EnergyPzmax = 0, EnergyPzmin = 0;
56    private double pzMaxBoosted = 0, pzMinBoosted = 0;
57
58    //XYZ-Grid
59    private double noOfXPoints = GridXSize; //X resolution
60    private double noOfYPoints = GridYSize; //Y resolution
61    private double noOfZPoints = GridZSize; //Z resolution
62
63    //Gaussian
64    private double f1 = 0, f1a = 0, f1aInf = 0; //UNBoosted Gaussian
65    private double f1pos = 0, f1neg = 0; //UNBoosted shifted Gaussian
66
67    private double f2a = 0; //Boosted Gaussian
68    private double f2pos = 0, f2neg = 0; //Boosted shifted Gaussian
69    private double f2sum = 0; //boosted sum
70    private double f2aSquaredSum = 0;
```

```
71    private double f2aSquared = 0;
72
73    private double norm = 1; //by default norm = 1
74
75    //progress count
76    private double tenPercentCount = 0, initialPercent = 0;
77
78    //matrix size
79    int matrixSize = 2;
80
81    //timestring
82    private String currentTimeString = "";
83
84    //we store all the data computed
85    private double[][][] graphData = new double[GridXSize + 1][GridZSize +
          2][6];
86
87    //Bloch vector compos
88    private double rxBloch = 0, ryBloch = 0, rzBloch = 0;
89    private int kHalfWay = 0;
90    private double pzBoostedDistanceMax = 0, pzBoostedDistanceMin = 0;
91
92    //Z = -1
93    Jampack.Z minusONE = new Jampack.Z(-1, 0);
94
95    //spin z-up
96    static final double[][] SPIN_Z_UP = {
97    {1},
98    {0}
99    };
100   Jampack.Zmat initialSpin = new Jampack.Zmat(SPIN_Z_UP);
101   Jampack.Zmat initialSpinWithGauss = new Jampack.Zmat(2, 1);
102
103   //lorentz boost unit
104   Jampack.Zmat lorentzBoostDirection = new Jampack.Zmat(
          LORENTZ_BOOST_DIRECTION);
105
106   LorentzBoost lorentzBoost = new LorentzBoost();
107   Jampack.Zmat lorentzBoostMatrix;
108   WignerRotation wignerRotation = new WignerRotation();
109   Jampack.Zmat wignerRotationMatrix;
110
111   Jampack.Zmat rotatedSpinVector = new Jampack.Zmat(2, 1);
112   Jampack.Zmat rotatedSpinMatrix = new Jampack.Zmat(2, 2);
113   Jampack.Zmat rotatedSpinMatrixInf = new Jampack.Zmat(2, 2);
114   Jampack.Zmat spinMatrixNormed = new Jampack.Zmat(2, 2);
115   Jampack.Zmat totalRotatedSpinMatrix = new Jampack.Zmat(2, 2); //2x2
          matrix initialize to zero
116   Jampack.Zmat fourMomentum = new Jampack.Zmat(4, 1);
117   Jampack.Zmat boostedFourMomentum = new Jampack.Zmat(4, 1);
118   Jampack.Zmat boostedThreeMomentum = new Jampack.Zmat(3, 1);
119
120   //bloch vector
```

```
121   private double[][] blochVector = new double[3][1];
122
123   //matrix operations
124   private MatrixUtil matrixOp = new org.matrixutil.MatrixUtil();
125
126   //utility objects
127   Jampack.Times dummyTimes = new Jampack.Times();
128   Jampack.Plus dummyPlus = new Jampack.Plus();
129   Jampack.Print dummyPrint = new Jampack.Print();
130
131   //METHODS START
132   public static void TwoGaussVer4() {}
133
134   public void setParams(double tempSigma, double tempMass, double
          tempRapidity, double tempPx0, double tempPy0, double tempPz0) {
135     sigma = tempSigma;
136     mass = tempMass;
137     rapidity = tempRapidity;
138     px0 = tempPx0;
139     py0 = tempPy0;
140     pz0 = tempPz0;
141   }
142
143   public void setZResolution(int tempZResolution) {
144     noOfZPoints = tempZResolution;
145   }
146
147   public double getTrace()
148   {
149     //trace
150     Jampack.Z trace = new Jampack.Z(0);
151
152     for (int i = 0; i < matrixSize; i++) {
153       trace.Plus(trace, this.spinMatrixNormed.get(i + 1, i + 1));
154     }
155
156     if (trace.im != 0) {
157       System.out.format("\nACHTUNG: trace is complex! trace = ");
158       new Jampack.Print().o(trace);
159     }
160
161     return(trace.re);
162   }
163
164   //call this to set norm
165   public double calculateNorm(double tempSigma, double tempMass, double
          tempRapidity, double tempPx0, double tempPy0, double tempPz0) {
166
167     this.setParams(tempSigma, tempMass, 0, tempPx0, tempPy0, tempPz0);
168     this.setIntegrationArea();
169
170     norm = Math.sqrt(this.calculateIntegral());
171
```

```
172     System.out.format("Calculated norm = %12.8f\n\n", norm); //DEBUG
173
174     return(norm);
175   }
176
177   public void setNorm(double normValue)
178   {
179     //wavefunction norm
180     if (normValue > 0) {
181       this.norm = normValue;
182     }
183     else {
184       System.out.format("\nTwoGaussVer4.setNorm(): ERROR: norm = %8.5f is
              not positive definite.\n", normValue);
185     }
186   }
187
188   public void setSpinMatrixNormed()
189   {
190     //throws an error if norm = 0
191     Jampack.Z tempZ = new Jampack.Z((1 / Math.pow(this.norm, 2)), 0.0);
192
193     this.spinMatrixNormed = dummyTimes.o(tempZ, this.totalRotatedSpinMatrix)
          ;
194   }
195
196   public Jampack.Zmat getSpinMatrixNormed()
197   {
198     return(this.spinMatrixNormed);
199   }
200
201   public double[][][] getGaussianGraphData() {
202     return graphData;
203   }
204
205   public void setIntegrationArea() {
206
207     //calculate these constants to increase speed
208     coshRapidity = Math.cosh(rapidity);
209     sinhRapidity = Math.sinh(rapidity);
210     mass2 = Math.pow(mass, 2);
211
212     pxmin = -px0 - (3 * Math.sqrt(2) * sigma);
213     pxmax = px0 + (3 * Math.sqrt(2) * sigma);
214     pymin = py0 - (3 * Math.sqrt(2) * sigma);
215     pymax = py0 + (3 * Math.sqrt(2) * sigma);
216
217     pzmin = pz0 - (5 * Math.sqrt(2) * sigma);
218     pzmax = pz0 + (5 * Math.sqrt(2) * sigma); //just a hunch
219
220     EnergyPzmax = Math.sqrt(Math.pow(pzmax, 2) + Math.pow(pymax, 2) + Math.
          pow(pxmax, 2) + mass2);
221     EnergyPzmin = Math.sqrt(Math.pow(pzmin, 2) + mass2);
```

```
222
223     pzMaxBoosted = EnergyPzmax * sinhRapidity + pzmax * coshRapidity;
224     pzMinBoosted = EnergyPzmin * sinhRapidity + pzmin * coshRapidity;
225
226     pzmax = pzMaxBoosted;
227     pzmin = pzMinBoosted;
228
229     System.out.format("calculated unboosted pzmin = %10.5f pzmax = %10.5f\n"
            , pzmin, pzmax); //DEBUG
230   }
231
232   public double calculateIntegral() {
233
234     Jampack.Z dummyZ = new Jampack.Z();
235
236     //calculate these constants to increase speed
237     coshRapidity = Math.cosh(rapidity);
238     sinhRapidity = Math.sinh(rapidity);
239     coshRapidityHalf = Math.cosh(rapidity / 2);
240     sinhRapidityHalf = Math.sinh(rapidity / 2);
241     sigma2 = Math.pow(sigma, 2);
242     mass2 = Math.pow(mass, 2);
243
244     //L^{-1}(xi) = L(-xi)
245     lorentzBoost.setParams(-rapidity, lorentzBoostDirection);
246     lorentzBoostMatrix = lorentzBoost.getLorentzBoost();
247
248     //DEBUG
249     System.out.format("Lorentz boost matrix for all gaussians = ");
250     dummyPrint.o(lorentzBoostMatrix);
251
252     //DEBUG
253     System.out.format("Energypzmax = %10.5f sinhrap = %10.5f coshrap = %10.5
            f\n", EnergyPzmax, sinhRapidity, coshRapidity); //DEBUG
254     System.out.format("Energypzmin = %10.5f\n", EnergyPzmin);
255
256     //increment
257     dpx = Math.abs((pxmax - pxmin)) / noOfXPoints;
258     dpy = Math.abs((pymax - pymin)) / noOfYPoints;
259     dpz = Math.abs((pzmax - pzmin)) / noOfZPoints;
260
261     //initialize dummy integration variables
262     px = pxmin;
263     py = pymin;
264     pz = pzmin;
265
266     //set initial values to 0 for things we sum over before calculation
267     f2sum = 0;
268
269     //percent counter
270     tenPercentCount = noOfXPoints / 10;
271     initialPercent = tenPercentCount;
272
```

```
273     //k half way
274     kHalfWay = (int) noOfYPoints / 2;
275
276     //START
277
278     //print time
279     currentTimeString = graphUtil.getCurrentTimeHours();
280
281     //DEBUG
282     System.out.format("Initial totalRotatedSpinMatrix = ");
283     dummyPrint.o(totalRotatedSpinMatrix);
284     System.out.format("Initial spin = ");
285     dummyPrint.o(initialSpin);
286
287     //DEBUG
288     System.out.format("initial f2sum = %20.10f \n", f2sum);
289     System.out.format("kHalfWay = %d \n", kHalfWay);
290
291     System.out.println(currentTimeString + " BEGIN calculateGaussianCart3D()
            \n");
292     System.out.format("mass = %10.6f sigma = %10.6f rapidity = %4.2f\n",
            mass, sigma, rapidity);
293     System.out.format("px0 = %10.6f py0 = %10.6f pz0 = %10.6f\n", px0, py0,
            pz0);
294     System.out.format("dpx = %10.6f dpy = %10.6f dpz = %10.6f\n", dpx, dpy,
            dpz);
295     System.out.format("XGrid = [%6.2f, %6.2f, %8.0f]%n", pxmin, pxmax,
            noOfXPoints);
296     System.out.format("YGrid = [%6.2f, %6.2f, %8.0f]%n", pymin, pymax,
            noOfYPoints);
297     System.out.format("ZGrid = [%6.2f, %6.2f, %8.0f]%n%n", pzmin, pzmax,
            noOfZPoints);
298     System.out.print("Progress: 0% | ");
299
300     //integrate
301     for(int i = 0; i < noOfXPoints + 1; i++){ //x - coordinate
302
303       px = pxmin + i * dpx;
304       //store data
305       graphData[i][0][0] = px;
306
307       //percent count
308       if (i > initialPercent) {
309         //timestamp
310         currentTimeString = graphUtil.getCurrentTimeHours();
311         System.out.print(currentTimeString + " ");
312         //percent stamp
313         System.out.format("%2.0f%% px = %10.6f | ", (initialPercent /
                tenPercentCount) * 10, px);
314         initialPercent = initialPercent + tenPercentCount;
315       }
316
317       for (int k = 0; k < noOfYPoints + 1; k++) { //y - coordinate
```

```
318
319         py = pymin + k * dpy;
320
321         for (int m = 0; m < noOfZPoints + 1; m++) { //z - coordinate
322
323           try {
324             pz = pzmin + m * dpz;
325
326             px2 = Math.pow(px, 2);
327             py2 = Math.pow(py, 2);
328             pz2 = Math.pow(pz, 2);
329             Energy = Math.sqrt(px2 + py2 + pz2 + mass2);
330
331             //4-momentum vector
332             dummyZ.im = 0;
333             dummyZ.re = Energy;
334             fourMomentum.put(1, 1, dummyZ);
335             dummyZ.re = px;
336             fourMomentum.put(2, 1, dummyZ);
337             dummyZ.re = py;
338             fourMomentum.put(3, 1, dummyZ);
339             dummyZ.re = pz;
340             fourMomentum.put(4, 1, dummyZ);
341
342             boostedFourMomentum = dummyTimes.o(lorentzBoostMatrix,
                    fourMomentum);
343             boostedThreeMomentum = boostedFourMomentum.get(2, 4, 1, 1);
344
345             invariantIntegrationMeasureCart = 1 / (2 * Energy);
346             invariantInfElement = dpx * dpy * dpz *
                    invariantIntegrationMeasureCart;
347
348             //f1 is UNboosted
349             f1pos = Math.exp(-(Math.pow((px - px0), 2) + Math.pow((py - py0)
                    , 2) + Math.pow((pz - pz0), 2)) / (2 * sigma2));
350             f1neg = Math.exp(-(Math.pow((px + px0), 2) + Math.pow((py - py0)
                    , 2) + Math.pow((pz - pz0), 2)) / (2 * sigma2));
351             //covariant measure
352             f1a = f1pos + f1neg;
353             //norm
354             f1aInf = f1a * invariantInfElement;
355
356             //f2 is Boosted
357             f2pos = Math.exp(-0.5 * Math.pow((boostedThreeMomentum.get(3, 1)
                    .re - pz0), 2) / sigma2) * Math.exp((-0.5 * (Math.pow((px +
                    px0), 2) + Math.pow((py - py0), 2))) / sigma2);
358             f2neg = Math.exp(-0.5 * Math.pow((boostedThreeMomentum.get(3, 1)
                    .re - pz0), 2) / sigma2) * Math.exp((-0.5 * (Math.pow((px -
                    px0), 2) + Math.pow((py - py0), 2))) / sigma2);
359
360             //sum
361             f2a = f2pos + f2neg;
362             f2sum = f2sum + ((f2a * f2a) * invariantInfElement);
```

```
363
364             //Wigner rotation
365             wignerRotation.setParams(mass, rapidity, lorentzBoostDirection,
                    boostedThreeMomentum);
366             wignerRotationMatrix = wignerRotation.getWignerMatrix();
367
368             dummyZ.re = f2a;
369             dummyZ.im = 0;
370
371             initialSpinWithGauss = dummyTimes.o(dummyZ, initialSpin);
372
373             //spin vector
374             rotatedSpinVector = dummyTimes.o(wignerRotationMatrix,
                    initialSpinWithGauss);
375
376             //spin matrix
377             rotatedSpinMatrix = matrixOp.outerProduct(rotatedSpinVector,
                    matrixOp.vectorToCCVector(rotatedSpinVector));
378
379             //matrix * d
380             dummyZ.re = invariantInfElement;
381             rotatedSpinMatrixInf = dummyTimes.o(dummyZ, rotatedSpinMatrix);
382
383             totalRotatedSpinMatrix = dummyPlus.o(totalRotatedSpinMatrix,
                    rotatedSpinMatrixInf);
384
385             //store the Gaussian
386             if (k == kHalfWay) { //we harvest values on the y-plane
387
388               graphData[i][m + 1][0] = pz;
389               graphData[i][m + 1][1] = f2a;
390
391                           //init bloch vector
392               BlochVector blochVectorObject = new BlochVector();
393               blochVectorObject.setParams(rotatedSpinMatrix);
394               blochVector = blochVectorObject.getBlochVector();
395
396               //Bloch vector compos
397               rxBloch = blochVector[0][0];
398               ryBloch = blochVector[1][0];
399               rzBloch = blochVector[2][0];
400
401               graphData[i][m + 1][2] = rxBloch;
402               graphData[i][m + 1][3] = rzBloch;
403               //plot these using gnuplot
404               graphData[i][m + 1][4] = rxBloch * f2a;
405               graphData[i][m + 1][5] = rzBloch * f2a;
406             }
407           }
408           catch (Jampack.JampackException e) {
409             System.err.println("TwoGaussVer4(): Caught JampackException: "
410                       + e.getMessage());
411           }
```

```
412         }
413       }
414     }
415
416     //set normed matrix
417     setSpinMatrixNormed();
418
419     //print time and results
420     currentTimeString = graphUtil.getCurrentTimeHours();
421     System.out.println();
422     System.out.println(currentTimeString + " FINISH\n");
423
424     System.out.format("fUNBoostSum/Norm = %12.6f fBoostSum = %12.6f
            fBoostSum.normed = %12.6f\n", norm, f2sum, f2sum / Math.pow(norm, 2)
            );
425     System.out.format("\nfUNBoostSum/Norm = %12.6E fBoostSum = %12.6E
            fBoostSum.normed = %12.6E\n", norm, f2sum, f2sum / Math.pow(norm, 2)
            );
426
427     //print spin matrix
428     System.out.format("\nSpinMatrix =");
429     dummyPrint.o(getSpinMatrixNormed());
430
431     //print trace
432     System.out.format("Trace = %8.6f\n\n", getTrace());
433
434     //return: if rapidity = 0, then this is norm
435     return(f2sum);
436
437   } //finish calculateIntegral()
438
439 } //END
```

Appendix B

Example of source code: two particles

In this appendix we describe the code that was used to perform the numerical calculations for two particle systems with continuous momenta. It is written in the Java programming language and needs the package `Jampack` to run. `Jampack` can be downloaded at NIST [106]. The variables `mass` and `sigma` specify the mass and width of both particles. The variables `px0`, `py0` and `pz0` define the centers of the Gaussian wave packets. The rapidity is defined using the variable `rapidityZ`. All these variables need to be set using the method `setParams` before the method `calculateIntegral` is called.

```
1  import java.io.FileInputStream;
2  import java.io.FileOutputStream;
3  import java.io.IOException;
4  import java.io.*;
5
6  import java.util.*;
7  import java.lang.Number.*;
8  import java.nio.*;
9
10 import graphutil.*;
11 import org.matrixutil.*;
12
13 public class BellGaussVer4 implements paramsBellGaussVer4
14 {
15   //constants
16   private double sigma = 0.08, sigma2 = 0;
17   private double mass = 0.01, mass2 = 0;
18   private double rapidityZ = 0;
19   private double coshRapidityZ = 0, sinhRapidityZ = 0, coshRapidityZHalf =
         0, sinhRapidityZHalf = 0;
```

```
20
21    //energy and boosted energy
22    private double Energy = 0;
23
24    //integration dummies
25    private double px = 0, py = 0, pz = 0; //dummy Cart3D variables
26    private double px2 = 0, py2 = 0, pz2 = 0; //squared dummies to increase
          speed
27
28    private double px0 = 0, py0 = 0, pz0 = 0; //displacement for Gaussian
29
30    //integration dummies
31    private double invariantInfElement = 0;
32    private double invariantIntegrationMeasureCart = 0;
33    private double dpx = 0, dpy = 0, dpz = 0; //integration increment
34
35    //integration limits
36    private double pxmin = 0, pxmax = 0; //x domain min, max
37    private double pymin = 0, pymax = 0; //y
38    private double pzmin = 0, pzmax = 0; //z
39    private double EnergyPzmax = 0;
40    private double EnergyPzmin = 0;
41    private double pzMaxBoosted = 0;
42    private double pzMinBoosted = 0;
43
44    private double offSetX = 0;
45    private double offSetY = 0;
46    private double offSetZ = 0;
47
48    //XYZ-Grid
49    private int noOfXPoints = GRID_X_SIZE; //X resolution
50    private int noOfYPoints = GRID_Y_SIZE; //Y resolution
51    private int noOfZPoints = GRID_Z_SIZE; //Z resolution
52
53    //dynamical counters
54    private int graphDataIncX = 0;
55    private int graphDataincZ = 0;
56    private int graphDataXFixedPercentCount = 0;
57    private int graphDataZFixedPercentCount = 0;
58    private int graphDataXPercentCount = 0;
59    private int graphDataZPercentCount = 0;
60
61    //Gaussian
62    //unboosted gaussians
63    private double fPGaussian = 0;
64    private double fQGaussian = 0;
65
66    //unboosted gaussian sums
67    private double fPGaussianSum = 0;
68    private double fQGaussianSum = 0;
69
70    //boosted gaussians
71    private double fPGaussianBoosted = 0;
```

```
72    private double fQGaussianBoosted = 0;
73
74    //gaussian sums
75    private double fPGaussianBoostedSum = 0;
76    private double fQGaussianBoostedSum = 0;
77
78    //total boosted sum = this is norm
79    private double boostedSum = 0;
80
81    //default norm = 1
82    private double norm = 1;
83
84    //progress count
85    private double tenPercentCount = 0, initialPercent = 0;
86    //counting halfway for storage
87    private int kHalfWay = 0;
88
89    //DATA STORAGE
90    //array where we store all the computed data
91    private double[][][] graphData = new double[GRID_X_SIZE + 1][GRID_Z_SIZE
          + 2][6];
92
93    //sizes
94    private final int SPINVECTOR_SIZE = 2; //size of spin vector is 2x1
95    private final int SPIN_DENSITY_MATRIX_SIZE = 4; //size of the density
          matrix is 4x4
96
97    //timestring
98    private String currentTimeString = "";
99
100   //lorentz boost unit
101   private Jampack.Zmat lorentzBoostZDirection = new Jampack.Zmat(
          LORENTZ_BOOST_Z_DIRECTION);
102
103   private LorentzBoost lorentzBoostZ = new LorentzBoost();
104   private Jampack.Zmat lorentzBoostZMatrix;
105   private LorentzBoost lorentzBoostZInv = new LorentzBoost();
106   private Jampack.Zmat lorentzBoostZInvMatrix;
107
108   private WignerRotation wignerRotationZ = new WignerRotation();
109   private Jampack.Zmat wignerRotationZMatrix;
110
111   //momenta
112   Jampack.Zmat fourMomentum = new Jampack.Zmat(4, 1);
113   Jampack.Zmat boostedFourMomentum = new Jampack.Zmat(4, 1);
114   Jampack.Zmat boostedThreeMomentum = new Jampack.Zmat(3, 1);
115
116   //SPIN VECTORS
117   //spin z-up
118   static final double[][] SPIN_Z_UP = {
119   {1},
120   {0}
121   };
```

```
122    Jampack.Zmat initialSpin0 = new Jampack.Zmat(SPIN_Z_UP);
123
124    //spin z-down
125    static final double[][] SPIN_Z_DOWN = {
126    {0},
127    {1}
128    };
129    Jampack.Zmat initialSpin1 = new Jampack.Zmat(SPIN_Z_DOWN);
130
131    //with Gaussian
132    //P
133    private Jampack.Zmat initialSpin0WithGaussP = new Jampack.Zmat(
           SPINVECTOR_SIZE, 1);
134    private Jampack.Zmat initialSpin1WithGaussP = new Jampack.Zmat(
           SPINVECTOR_SIZE, 1);
135    //
136    private Jampack.Zmat rotatedSpin0WithGaussP = new Jampack.Zmat(
           SPINVECTOR_SIZE, 1);
137    private Jampack.Zmat rotatedSpin1WithGaussP = new Jampack.Zmat(
           SPINVECTOR_SIZE, 1);
138
139    //Q
140    private Jampack.Zmat initialSpin0WithGaussQ = new Jampack.Zmat(
           SPINVECTOR_SIZE, 1);
141    private Jampack.Zmat initialSpin1WithGaussQ = new Jampack.Zmat(
           SPINVECTOR_SIZE, 1);
142    //
143    private Jampack.Zmat rotatedSpin0WithGaussQ = new Jampack.Zmat(
           SPINVECTOR_SIZE, 1);
144    private Jampack.Zmat rotatedSpin1WithGaussQ = new Jampack.Zmat(
           SPINVECTOR_SIZE, 1);
145
146    //SPIN MATRICES
147    //|0><0|
148    private Jampack.Zmat rotatedSpin00MatrixWithGaussP = new Jampack.Zmat(
           SPINVECTOR_SIZE, SPINVECTOR_SIZE);
149    private Jampack.Zmat rotatedSpin00MatrixWithGaussQ = new Jampack.Zmat(
           SPINVECTOR_SIZE, SPINVECTOR_SIZE);
150
151    //|0><1|
152    private Jampack.Zmat rotatedSpin01MatrixWithGaussP = new Jampack.Zmat(
           SPINVECTOR_SIZE, SPINVECTOR_SIZE);
153    private Jampack.Zmat rotatedSpin01MatrixWithGaussQ = new Jampack.Zmat(
           SPINVECTOR_SIZE, SPINVECTOR_SIZE);
154
155    //|1><0|
156    private Jampack.Zmat rotatedSpin10MatrixWithGaussP = new Jampack.Zmat(
           SPINVECTOR_SIZE, SPINVECTOR_SIZE);
157    private Jampack.Zmat rotatedSpin10MatrixWithGaussQ = new Jampack.Zmat(
           SPINVECTOR_SIZE, SPINVECTOR_SIZE);
158
159    //|1><1|
```

```
160    private Jampack.Zmat rotatedSpin11MatrixWithGaussP = new Jampack.Zmat(
           SPINVECTOR_SIZE, SPINVECTOR_SIZE);
161    private Jampack.Zmat rotatedSpin11MatrixWithGaussQ = new Jampack.Zmat(
           SPINVECTOR_SIZE, SPINVECTOR_SIZE);
162
163    //spin matrices summed
164    //[0, 0]
165    private Jampack.Zmat rotatedSpin00MatrixPSum = new Jampack.Zmat(
           SPINVECTOR_SIZE, SPINVECTOR_SIZE);
166    private Jampack.Zmat rotatedSpin00MatrixQSum = new Jampack.Zmat(
           SPINVECTOR_SIZE, SPINVECTOR_SIZE);
167
168    //[0, 1]
169    private Jampack.Zmat rotatedSpin01MatrixPSum = new Jampack.Zmat(
           SPINVECTOR_SIZE, SPINVECTOR_SIZE);
170    private Jampack.Zmat rotatedSpin01MatrixQSum = new Jampack.Zmat(
           SPINVECTOR_SIZE, SPINVECTOR_SIZE);
171
172    //[1, 0]
173    private Jampack.Zmat rotatedSpin10MatrixPSum = new Jampack.Zmat(
           SPINVECTOR_SIZE, SPINVECTOR_SIZE);
174    private Jampack.Zmat rotatedSpin10MatrixQSum = new Jampack.Zmat(
           SPINVECTOR_SIZE, SPINVECTOR_SIZE);
175
176    //[1, 1]
177    private Jampack.Zmat rotatedSpin11MatrixPSum = new Jampack.Zmat(
           SPINVECTOR_SIZE, SPINVECTOR_SIZE);
178    private Jampack.Zmat rotatedSpin11MatrixQSum = new Jampack.Zmat(
           SPINVECTOR_SIZE, SPINVECTOR_SIZE);
179
180    //final 4x4 spin matrices
181    //[0, 0]
182    private Jampack.Zmat totalSpinMatrix00 = new Jampack.Zmat(
           SPIN_DENSITY_MATRIX_SIZE, SPIN_DENSITY_MATRIX_SIZE);
183    //[0, 1]
184    private Jampack.Zmat totalSpinMatrix01 = new Jampack.Zmat(
           SPIN_DENSITY_MATRIX_SIZE, SPIN_DENSITY_MATRIX_SIZE);
185    //[1, 0]
186    private Jampack.Zmat totalSpinMatrix10 = new Jampack.Zmat(
           SPIN_DENSITY_MATRIX_SIZE, SPIN_DENSITY_MATRIX_SIZE);
187    //[1, 1]
188    private Jampack.Zmat totalSpinMatrix11 = new Jampack.Zmat(
           SPIN_DENSITY_MATRIX_SIZE, SPIN_DENSITY_MATRIX_SIZE);
189    //total
190    private Jampack.Zmat totalSpinMatrix = new Jampack.Zmat(
           SPIN_DENSITY_MATRIX_SIZE, SPIN_DENSITY_MATRIX_SIZE);
191    //total spin matrix Normed
192    private Jampack.Zmat totalSpinMatrixNormed = new Jampack.Zmat(
           SPIN_DENSITY_MATRIX_SIZE, SPIN_DENSITY_MATRIX_SIZE);
193
194    //Bloch vector
195    private BlochVector blochVectorObjectP;
196    private double[][] blochVectorP = new double[3][1];
```

```
197   private double rxBlochP = 0, ryBlochP = 0, rzBlochP = 0;
198
199   //utility objects
200   private Jampack.Times dummyTimes = new Jampack.Times();
201   private Jampack.Plus dummyPlus = new Jampack.Plus();
202   private Jampack.Print dummyPrint = new Jampack.Print();
203   private MatrixUtil dummyMatrixOp = new org.matrixutil.MatrixUtil();
204
205   //START methods
206   public static void BellGaussVer4() {}
207
208   public void setParams(double tempSigma, double tempMass, double
          tempRapidityZ, double tempPx0, double tempPy0, double tempPz0) {
209     sigma = tempSigma;
210     mass = tempMass;
211     rapidityZ = tempRapidityZ;
212     px0 = tempPx0;
213     py0 = tempPy0;
214     pz0 = tempPz0;
215   }
216
217   public void setZResolution(int tempZResolution)
218   {
219     noOfZPoints = tempZResolution;
220   }
221
222   public double getTrace()
223   {
224     //trace
225     Jampack.Z trace = new Jampack.Z(0);
226
227     for (int i = 0; i < SPIN_DENSITY_MATRIX_SIZE; i++) {
228       trace.Plus(trace, this.totalSpinMatrixNormed.get(i + 1, i + 1));
229     }
230
231     //we want trace to be real and warn if this is not true
232     if (trace.im != 0) {
233       System.out.format("\nBellGaussVer4.getTrace(): ACHTUNG: TRACE IS
              COMPLEX! trace = ");
234       new Jampack.Print().o(trace);
235     }
236
237     //return ONLY the real part
238     return(trace.re);
239   }
240
241   //set norm
242   public double calculateNorm(double tempSigma, double tempMass, double
          tempRapidityZ, double tempPx0, double tempPy0, double tempPz0)
243   {
244     this.setParams(tempSigma, tempMass, 0, tempPx0, tempPy0, tempPz0);
245     this.setIntegrationArea();
246
```

```
247     norm = this.calculateIntegral();
248
249     //DEBUG
250     System.out.format("Calculated norm = %12.8f\n\n", norm);
251
252     return(norm);
253   }
254
255   public void setNorm(double normValue)
256   {
257     //wavefunction norm
258     if (normValue > 0) {
259       this.norm = normValue;
260     }
261     else {
262       System.out.format("\nBellGaussVer4.setNorm(): ERROR: norm = %8.5f is
              not positive definite.\n", normValue);
263     }
264   }
265
266   public void setSpinMatrixNormed()
267   {
268     //throws an error if norm = 0
269     Jampack.Z tempZ = new Jampack.Z((1 / Math.pow(this.norm, 2)), 0.0);
270
271     this.totalSpinMatrixNormed = dummyTimes.o(tempZ, this.totalSpinMatrix);
272   }
273
274   public Jampack.Zmat getSpinMatrixNormed()
275   {
276     return(this.totalSpinMatrixNormed);
277   }
278
279   public double[][][] getGaussianGraphData() {
280     return graphData;
281   }
282
283   public void setIntegrationArea() {
284
285     //calculate these constants to increase speed
286     coshRapidityZ = Math.cosh(rapidityZ);
287     sinhRapidityZ = Math.sinh(rapidityZ);
288     mass2 = Math.pow(mass, 2);
289
290     pxmin = -px0 - (3 * Math.sqrt(2) * sigma);
291     pxmax = px0 + (3 * Math.sqrt(2) * sigma);
292     pymin = py0 - (3 * Math.sqrt(2) * sigma);
293     pymax = py0 + (3 * Math.sqrt(2) * sigma);
294
295     pzmin = pz0 - (5 * Math.sqrt(2) * sigma);
296     pzmax = pz0 + (5 * Math.sqrt(2) * sigma);
297
```

```
298     EnergyPzmax = Math.sqrt(Math.pow(pzmax, 2) + Math.pow(pymax, 2) + Math.
            pow(pxmax, 2) + mass2);
299     EnergyPzmin = Math.sqrt(Math.pow(pzmin, 2) + mass2);
300
301     pzMaxBoosted = EnergyPzmax * sinhRapidityZ + pzmax * coshRapidityZ;
302     pzMinBoosted = EnergyPzmin * sinhRapidityZ + pzmin * coshRapidityZ;
303
304     pzmax = pzMaxBoosted;
305     pzmin = pzMinBoosted;
306
307     //DEBUG
308     System.out.format("setIntegrationArea(): calculated pzmin = %10.5f pzmax
            = %10.5f\n", pzmin, pzmax);
309   }
310
311   public double calculateIntegral() {
312
313     Jampack.Z dummyZ = new Jampack.Z();
314     Jampack.Z dummyZP = new Jampack.Z();
315     Jampack.Z dummyZQ = new Jampack.Z();
316     Jampack.Z dummyZInf = new Jampack.Z();
317
318     //initialize total gaussian sum
319     fPGaussianBoostedSum = 0;
320     fQGaussianBoostedSum = 0;
321
322     //rapidityZ
323     coshRapidityZ = Math.cosh(rapidityZ);
324     sinhRapidityZ = Math.sinh(rapidityZ);
325     coshRapidityZHalf = Math.cosh(rapidityZ / 2);
326     sinhRapidityZHalf = Math.sinh(rapidityZ / 2);
327     sigma2 = Math.pow(sigma, 2);
328     mass2 = Math.pow(mass, 2);
329
330     //Lorentz boost matrices
331     lorentzBoostZ.setParams(rapidityZ, lorentzBoostZDirection);
332     lorentzBoostZMatrix = lorentzBoostZ.getLorentzBoost();
333
334     lorentzBoostZInv.setParams(-rapidityZ, lorentzBoostZDirection);
335     lorentzBoostZInvMatrix = lorentzBoostZInv.getLorentzBoost();
336
337     //DEBUG
338     System.out.format("Lorentz boost L_z, L_z^{-1} matrix = ");
339     dummyPrint.o(lorentzBoostZMatrix);
340     dummyPrint.o(lorentzBoostZInvMatrix);
341
342     //increment
343     dpx = Math.abs((pxmax - pxmin)) / noOfXPoints;
344     dpy = Math.abs((pymax - pymin)) / noOfYPoints;
345     dpz = Math.abs((pzmax - pzmin)) / noOfZPoints;
346
347     //ensure that dpx does not become greater than DPX_THRESHOLD
348     if (dpx > DPX_THRESHOLD) {
```

```
349
350       dpx = DPX_THRESHOLD;
351       noOfXPoints = (int) Math.abs((pxmax - pxmin) / DPX_THRESHOLD);
352
353       //DEBUG
354       System.out.format("DEBUG: calculateIntegral(): increase noOfXPoints to
              %d\n", noOfXPoints);
355
356     }
357
358     //ensure that dpx does not become greater than DPZ_THRESHOLD
359     if (dpz > DPZ_THRESHOLD) {
360
361       dpz = DPZ_THRESHOLD;
362       noOfZPoints = (int) Math.abs((pzmax - pzmin) / DPZ_THRESHOLD);
363
364       //DEBUG
365       System.out.format("DEBUG: calculateIntegral(): increase noOfZPoints to
              %d\n", noOfZPoints);
366
367     }
368
369     //dpy
370     if (dpy > DPY_THRESHOLD) {
371
372       dpy = DPY_THRESHOLD;
373       noOfYPoints = (int) Math.abs((pymax - pymin) / DPY_THRESHOLD);
374
375       //DEBUG
376       System.out.format("DEBUG: calculateIntegral(): increase noOfYPoints to
              %d\n", noOfYPoints);
377
378     }
379
380     //determine graphData size
381     graphData = new double[noOfXPoints + 1][noOfZPoints + 2][6];
382
383     //graphdata size
384     graphDataIncX = (int) (noOfXPoints - 1) / GRAPHDATA_SIZE_X;
385     graphDataincZ = (int) (noOfZPoints - 1) / GRAPHDATA_SIZE_Z;
386     graphDataXFixedPercentCount = (int) (GRAPHDATA_SIZE_X - 1) / 10; //10
          means 10%
387     graphDataZFixedPercentCount = (int) (GRAPHDATA_SIZE_Z - 1) / 10; //10
          means 10%
388     graphDataXPercentCount = 0; //graphDataXTenPercentCount;
389     graphDataZPercentCount = 0; //graphDataZTenPercentCount;
390
391     //DEBUG
392     System.out.format("\nDEBUG: calculateIntegral(): graphData size = [%d][%
          d][%d]\n", graphData.length, graphData[0].length, graphData[0][0].
          length);
393
394     //initialize dummy integration variables
```

```
395     px = pxmin;
396     py = pymin;
397     pz = pzmin;
398
399     //percent counter
400     tenPercentCount = noOfXPoints / 10;
401     initialPercent = tenPercentCount;
402
403     //k half way
404     kHalfWay = (int) noOfYPoints / 2;
405
406     //print time
407     currentTimeString = graphUtil.getCurrentTimeHours();
408
409     //DEBUG
410     System.out.format("Initial totalSpinMatrix = ");
411     dummyPrint.o(totalSpinMatrix);
412     System.out.format("Initial fPGaussianBoostedSum = %20.10f \n",
            fPGaussianBoostedSum); //DEBUG
413     System.out.format("kHalfWay = %d \n", kHalfWay); //DEBUG
414
415     System.out.println(currentTimeString + " BEGIN: BellGaussVer4()\n");
416     System.out.format("mass = %10.6f | sigma = %10.6f | rapidityZ = %4.2f\n"
            , mass, sigma, rapidityZ);
417     System.out.format("dpx = %10.6f dpy = %10.6f dpz = %10.6f\n", dpx, dpy,
            dpz);
418     System.out.format("XGrid = [%6.2f, %6.2f, %d]\n", pxmin, pxmax,
            noOfXPoints);
419     System.out.format("YGrid = [%6.2f, %6.2f, %d]\n", pymin, pymax,
            noOfYPoints);
420     System.out.format("ZGrid = [%6.2f, %6.2f, %d]\n\n", pzmin, pzmax,
            noOfZPoints);
421     currentTimeString = graphUtil.getCurrentTimeHours();
422     System.out.print("Progress: " + currentTimeString + " 0% ");
423     System.out.format("px = %10.6f | ", pxmin);
424
425     //start integration
426     for(int i = 0; i < noOfXPoints + 1; i++){ //x - coordinate
427
428       px = pxmin + i * dpx;
429       graphData[i][0][0] = px;
430
431       //percent count if needed
432       if (i > initialPercent) {
433         //timestamp
434         currentTimeString = graphUtil.getCurrentTimeHours();
435         System.out.print(currentTimeString + " ");
436         //percent stamp
437         System.out.format("%2.0f%% px = %10.6f | ", (initialPercent /
                tenPercentCount) * 10, px);
438         initialPercent = initialPercent + tenPercentCount;
439       }
440
```

```
441       for (int k = 0; k < noOfYPoints + 1; k++) { //y - coordinate
442
443         py = pymin + k * dpy;
444
445         for (int m = 0; m < noOfZPoints + 1; m++) { //z - coordinate
446
447           try {
448             pz = pzmin + m * dpz;
449
450             //squared dummies
451             px2 = Math.pow(px, 2);
452             py2 = Math.pow(py, 2);
453             pz2 = Math.pow(pz, 2);
454             Energy = Math.sqrt(px2 + py2 + pz2 + mass2);
455
456             //4-momentum vector
457             dummyZ.im = 0;
458             dummyZ.re = Energy;
459             fourMomentum.put(1, 1, dummyZ);
460             dummyZ.re = px;
461             fourMomentum.put(2, 1, dummyZ);
462             dummyZ.re = py;
463             fourMomentum.put(3, 1, dummyZ);
464             dummyZ.re = pz;
465             fourMomentum.put(4, 1, dummyZ);
466
467             //boosted 4-momentum
468             boostedFourMomentum = dummyTimes.o(lorentzBoostZInvMatrix,
                    fourMomentum);
469             boostedThreeMomentum = boostedFourMomentum.get(2, 4, 1, 1);
470
471             //measure
472             invariantIntegrationMeasureCart = 1 / (2 * Energy);
473             invariantInfElement = dpx * dpy * dpz *
                    invariantIntegrationMeasureCart;
474             dummyZInf.im = 0;
475             dummyZInf.re = invariantInfElement;
476
477             //unboosted gaussians
478             fPGaussian = Math.sqrt(Math.exp(
479               -(1 / (2 * sigma2)) *
480               (Math.pow((px - px0), 2) +
481               Math.pow((py - py0), 2) +
482               Math.pow((pz - pz0), 2))
483               ));
484             fQGaussian = Math.sqrt(Math.exp(
485               -(1 / (2 * sigma2)) *
486               (Math.pow((px + px0), 2) +
487               Math.pow((py - py0), 2) +
488               Math.pow((pz - pz0), 2))
489               ));
490             //unboosted gaussian sums
```

```
491             fPGaussianSum = fPGaussianSum + ((fPGaussian * fPGaussian) *
                    invariantInfElement);
492             fQGaussianSum = fQGaussianSum + ((fQGaussian * fQGaussian) *
                    invariantInfElement);
493
494             //p-gaussian:
495             fPGaussianBoosted = Math.sqrt(
496               Math.exp(
497               -(1 / (2 * sigma2)) *
498               (
499               Math.pow((boostedThreeMomentum.get(1, 1).re - px0), 2) +
500               Math.pow((boostedThreeMomentum.get(2, 1).re - py0), 2) +
501               Math.pow((boostedThreeMomentum.get(3, 1).re - pz0), 2)
502               )
503               )
504               +
505               Math.exp(
506               -(1 / (2 * sigma2)) *
507               (
508               Math.pow((boostedThreeMomentum.get(1, 1).re + px0), 2) +
509               Math.pow((boostedThreeMomentum.get(2, 1).re - py0), 2) +
510               Math.pow((boostedThreeMomentum.get(3, 1).re - pz0), 2)
511               )
512               )
513               );
514             //q-gaussian
515             fQGaussianBoosted = Math.sqrt(
516               Math.exp(
517               -(1 / (2 * sigma2)) *
518               (
519               Math.pow((boostedThreeMomentum.get(1, 1).re + px0), 2) +
520               Math.pow((boostedThreeMomentum.get(2, 1).re - py0), 2) +
521               Math.pow((boostedThreeMomentum.get(3, 1).re - pz0), 2)
522               )
523               )
524               +
525               Math.exp(
526               -(1 / (2 * sigma2)) *
527               (
528               Math.pow((boostedThreeMomentum.get(1, 1).re - px0), 2) +
529               Math.pow((boostedThreeMomentum.get(2, 1).re - py0), 2) +
530               Math.pow((boostedThreeMomentum.get(3, 1).re - pz0), 2)
531               )
532               )
533               );
534
535             //sum for checking purposes
536             fPGaussianBoostedSum = fPGaussianBoostedSum + (fPGaussianBoosted
                    * fPGaussianBoosted * invariantInfElement);
537             fQGaussianBoostedSum = fQGaussianBoostedSum + (fQGaussianBoosted
                    * fQGaussianBoosted * invariantInfElement);
538
539             //START if
```

```
540             if ((fPGaussianBoosted > FN_THRESHOLD) || (fQGaussianBoosted >
                    FN_THRESHOLD)) {
541               //Wigner rotation matrices
542               wignerRotationZ.setParams(mass, rapidityZ,
                      lorentzBoostZDirection, boostedThreeMomentum);
543               wignerRotationZMatrix = wignerRotationZ.getWignerMatrix();
544
545               //complex gaussian p-space
546               dummyZP.re = fPGaussianBoosted;
547               dummyZP.im = 0;
548
549               //complex gaussian q-space
550               dummyZQ.re = fQGaussianBoosted;
551               dummyZQ.im = 0;
552
553               //spin with p-gaussian
554               initialSpin0WithGaussP = dummyTimes.o(dummyZP, initialSpin0);
555               rotatedSpin0WithGaussP = dummyTimes.o(wignerRotationZMatrix,
                      initialSpin0WithGaussP);
556
557               initialSpin1WithGaussP = dummyTimes.o(dummyZP, initialSpin1);
558               rotatedSpin1WithGaussP = dummyTimes.o(wignerRotationZMatrix,
                      initialSpin1WithGaussP);
559
560               //spin with q-gaussian
561               initialSpin0WithGaussQ = dummyTimes.o(dummyZQ, initialSpin0);
562               rotatedSpin0WithGaussQ = dummyTimes.o(wignerRotationZMatrix,
                      initialSpin0WithGaussQ);
563
564               initialSpin1WithGaussQ = dummyTimes.o(dummyZQ, initialSpin1);
565               rotatedSpin1WithGaussQ = dummyTimes.o(wignerRotationZMatrix,
                      initialSpin1WithGaussQ);
566
567               //spin matrices
568               //[0, 0]
569               rotatedSpin00MatrixWithGaussP = dummyMatrixOp.outerProduct(
                      rotatedSpin0WithGaussP, dummyMatrixOp.vectorToCCVector(
                      rotatedSpin0WithGaussP));
570               rotatedSpin00MatrixWithGaussQ = dummyMatrixOp.outerProduct(
                      rotatedSpin0WithGaussQ, dummyMatrixOp.vectorToCCVector(
                      rotatedSpin0WithGaussQ));
571
572               //[0, 1]
573               rotatedSpin01MatrixWithGaussP = dummyMatrixOp.outerProduct(
                      rotatedSpin0WithGaussP, dummyMatrixOp.vectorToCCVector(
                      rotatedSpin1WithGaussP));
574               rotatedSpin01MatrixWithGaussQ = dummyMatrixOp.outerProduct(
                      rotatedSpin0WithGaussQ, dummyMatrixOp.vectorToCCVector(
                      rotatedSpin1WithGaussQ));
575
576               //[1, 0]
577               rotatedSpin10MatrixWithGaussP = dummyMatrixOp.outerProduct(
                      rotatedSpin1WithGaussP, dummyMatrixOp.vectorToCCVector(
```

```
                rotatedSpin0WithGaussP));
578             rotatedSpin10MatrixWithGaussQ = dummyMatrixOp.outerProduct(
                    rotatedSpin1WithGaussQ, dummyMatrixOp.vectorToCCVector(
                    rotatedSpin0WithGaussQ));
579
580             //[1, 1]
581             rotatedSpin11MatrixWithGaussP = dummyMatrixOp.outerProduct(
                    rotatedSpin1WithGaussP, dummyMatrixOp.vectorToCCVector(
                    rotatedSpin1WithGaussP));
582             rotatedSpin11MatrixWithGaussQ = dummyMatrixOp.outerProduct(
                    rotatedSpin1WithGaussQ, dummyMatrixOp.vectorToCCVector(
                    rotatedSpin1WithGaussQ));
583
584             //spin matrices summed
585
586             //[0, 0]
587             rotatedSpin00MatrixPSum = dummyPlus.o(rotatedSpin00MatrixPSum,
                    dummyTimes.o(dummyZInf, rotatedSpin00MatrixWithGaussP));
588             rotatedSpin00MatrixQSum = dummyPlus.o(rotatedSpin00MatrixQSum,
                    dummyTimes.o(dummyZInf, rotatedSpin00MatrixWithGaussQ));
589
590             //[0, 1]
591             rotatedSpin01MatrixPSum = dummyPlus.o(rotatedSpin01MatrixPSum,
                    dummyTimes.o(dummyZInf, rotatedSpin01MatrixWithGaussP));
592             rotatedSpin01MatrixQSum = dummyPlus.o(rotatedSpin01MatrixQSum,
                    dummyTimes.o(dummyZInf, rotatedSpin01MatrixWithGaussQ));
593
594             //[1, 0]
595             rotatedSpin10MatrixPSum = dummyPlus.o(rotatedSpin10MatrixPSum,
                    dummyTimes.o(dummyZInf, rotatedSpin10MatrixWithGaussP));
596             rotatedSpin10MatrixQSum = dummyPlus.o(rotatedSpin10MatrixQSum,
                    dummyTimes.o(dummyZInf, rotatedSpin10MatrixWithGaussQ));
597
598             //[1, 1]
599             rotatedSpin11MatrixPSum = dummyPlus.o(rotatedSpin11MatrixPSum,
                    dummyTimes.o(dummyZInf, rotatedSpin11MatrixWithGaussP));
600             rotatedSpin11MatrixQSum = dummyPlus.o(rotatedSpin11MatrixQSum,
                    dummyTimes.o(dummyZInf, rotatedSpin11MatrixWithGaussQ));
601
602             //store the Gaussian
603             if (k == kHalfWay) {
604
605               //increase counters
606               graphDataXPercentCount = graphDataXPercentCount +
                      graphDataXFixedPercentCount;
607               graphDataZPercentCount = graphDataZPercentCount +
                      graphDataZFixedPercentCount;
608
609               graphData[i][m + 1][0] = pz;
610               graphData[i][m + 1][1] = fPGaussianBoosted;
611
612               //get bloch vector
613               BlochVector blochVectorObjectP = new BlochVector();
```

```
614                 blochVectorObjectP.setParams(rotatedSpin00MatrixWithGaussP);
615                 blochVectorP = blochVectorObjectP.getBlochVector();
616
617                 rxBlochP = blochVectorP[0][0];
618                 ryBlochP = blochVectorP[1][0];
619                 rzBlochP = blochVectorP[2][0];
620
621                 //store in graphdata
622                 graphData[i][m + 1][2] = rxBlochP;
623                 graphData[i][m + 1][3] = rzBlochP;
624                 graphData[i][m + 1][4] = rxBlochP;
625                 graphData[i][m + 1][5] = rzBlochP;
626
627               }
628             //END if threshold
629             } else if (k == kHalfWay) {
630
631               //increase counters
632               graphDataXPercentCount = graphDataXPercentCount +
                      graphDataXFixedPercentCount;
633               graphDataZPercentCount = graphDataZPercentCount +
                      graphDataZFixedPercentCount;
634
635               graphData[i][m + 1][0] = pz;
636               graphData[i][m + 1][1] = fPGaussianBoosted;
637
638               //get bloch vector
639               BlochVector blochVectorObjectP = new BlochVector();
640               blochVectorObjectP.setParams(rotatedSpin00MatrixWithGaussP);
641               blochVectorP = blochVectorObjectP.getBlochVector();
642
643               rxBlochP = blochVectorP[0][0];
644               ryBlochP = blochVectorP[1][0];
645               rzBlochP = blochVectorP[2][0];
646
647               //store in graphdata
648               graphData[i][m + 1][2] = rxBlochP;
649               graphData[i][m + 1][3] = rzBlochP;
650               graphData[i][m + 1][4] = rxBlochP; // * f2a;
651               graphData[i][m + 1][5] = rzBlochP; // * f2a;
652
653                        //END else if
654             }
655                    //END try
656           } catch (Jampack.JampackException e) {
657             System.err.println("BellGaussVer4(): Caught JampackException: "
                      + e.getMessage());
658           }
659         } //END of m
660       } //END of k
661     } //END of i
662
663     //kronecker product
```

```
664     //[0, 0]
665     totalSpinMatrix00 = dummyMatrixOp.kroneckerProduct(
            rotatedSpin00MatrixPSum, rotatedSpin00MatrixQSum);
666     //[0, 1]
667     totalSpinMatrix01 = dummyMatrixOp.kroneckerProduct(
            rotatedSpin01MatrixPSum, rotatedSpin01MatrixQSum);
668     //[1, 0]
669     totalSpinMatrix10 = dummyMatrixOp.kroneckerProduct(
            rotatedSpin10MatrixPSum, rotatedSpin10MatrixQSum);
670     //[1, 1]
671     totalSpinMatrix11 = dummyMatrixOp.kroneckerProduct(
            rotatedSpin11MatrixPSum, rotatedSpin11MatrixQSum);
672     //sum up
673     try {
674
675       totalSpinMatrix = dummyPlus.o(totalSpinMatrix00, totalSpinMatrix01);
676       totalSpinMatrix = dummyPlus.o(totalSpinMatrix, totalSpinMatrix10);
677       totalSpinMatrix = dummyPlus.o(totalSpinMatrix, totalSpinMatrix11);
678     } catch (Jampack.JampackException e) {
679       System.err.println("BellGaussVer4(): Caught JampackException: " + e.
              getMessage());
680     }
681
682     //norm the matrix
683     setSpinMatrixNormed();
684
685     //correct vector norm
686     boostedSum = Math.sqrt(2 * fPGaussianBoostedSum * fQGaussianBoostedSum);
687
688     //DEBUG
689     System.out.format("\n\ntotalSpinMatrix = ");
690     dummyPrint.o(totalSpinMatrix);
691     System.out.println();
692     System.out.format("totalSpinMatrixNormed = ");
693     dummyPrint.o(totalSpinMatrixNormed);
694
695     System.out.format("norm = %12.6f | fPGaussianBoostedSum = %12.6f |
            fQGaussianBoostedSum = %12.6f | \nboostedSum = %12.6f | norm /
            boostedSum = %12.6f\n",
696       norm,
697       fPGaussianBoostedSum,
698       fQGaussianBoostedSum,
699       boostedSum,
700       norm / boostedSum);
701
702     //trace
703     System.out.format("\nTrace = %2.6f\n\n", getTrace());
704
705     //print time
706     currentTimeString = graphUtil.getCurrentTimeHours();
707     System.out.format("\n" + currentTimeString + " FINISH\n");
708
709     //return boosted gaussian sums
```

```
710      return(boostedSum);
711
712    } //END of integration
713  }
```

Bibliography

1. Schrödinger, E. Discussion of Probability Relations Between Separated Systems. *Proceedings of the Cambridge Philosophical Society* **31,** 555–563 (1935).
2. Bell, J. On the Einstein-Podolsky-Rosen paradox. *Physics* **1,** 195–200 (1964).
3. Maudlin, T. *Quantum Non-Locality and Relativity: Metaphysical Intimations of Modern Physics* 2nd ed (Blackwell Publishers, Malden, Mass, 2002).
4. Dickson, W. M. *Quantum Chance and Non-Locality: Probability and Non-Locality in the Interpretations of Quantum Mechanics* (Cambridge University Press, Cambridge, 1998).
5. Dickson, M. Quantum Logic Is Alive $\wedge$ (It Is True $\vee$ It Is False). *Philosophy of Science* **68,** S274–S287 (2001).
6. Bacciagaluppi, G. in *Handbook of Quantum Logic* Editors: D. Gabbay, D. Lehmann and K. Engesser, 49–78 (Elsevier, Amsterdam, 2009).
7. Palge, V. & Dunningham, J. Generation of maximally entangled states with subluminal Lorentz boosts. *Physical Review A* **85,** 042322 (2012).
8. Dunningham, J., Palge, V. & Vedral, V. Entanglement and nonlocality of a single relativistic particle. *Physical Review A* **80,** 044302 (2009).
9. Palge, V., Vedral, V. & Dunningham, J. A. Behavior of entanglement and Cooper pairs under relativistic boosts. *Physical Review A* **84,** 044303 (2011).
10. Dunningham, J., Rico Gutiérrez, L. & Palge, V. Observing superpositions of different number states. *Optics and Spectroscopy* **111,** 528–534 (2011).
11. Gutiérrez, L. M. R., Palge, V. & Dunningham, J. Observing the Superposition of a Single Particle with the Vacuum. *Mathematical Structures in Computer Science* **20,** 1051–1065 (2010).

12. Schrödinger, E. Discussion of Probability Relations Between Separated Systems. *Proceedings of the Cambridge Philosophical Society* **32,** 446–451 (1936).

13. Hughes, R. I. G. *The Structure and Interpretation of Quantum Mechanics* (Harvard University Press, Cambridge, Mass, 1989).

14. Czachor, M. Einstein-Podolsky-Rosen-Bohm experiment with relativistic massive particles. *Physical Review A* **55,** 72–77 (1997).

15. Gingrich, R. M. & Adami, C. Quantum Entanglement of Moving Bodies. *Physical Review Letters* **89,** 270402 (2002).

16. Terashima, H. & Ueda, M. Relativistic Einstein-Podolsky-Rosen Correlation And Bell's Inequality. *International Journal of Quantum Information* **01,** 93–114 (2003).

17. Alsing, P. M. & Milburn, G. J. Lorentz invariance of entanglement. *Quantum Information and Computation* **2,** 487–512 (2002).

18. Peres, A., Scudo, P. F. & Terno, D. R. Quantum Entropy and Special Relativity. *Physical Review Letters* **88,** 230402 (2002).

19. Gingrich, R., Bergou, A. & Adami, C. Entangled light in moving frames. *Physical Review A* **68,** 042102 (2003).

20. Caban, P. & Rembieliński, J. Photon polarization and Wigner's little group. *Physical Review A* **68,** 042107 (2003).

21. Caban, P. & Rembieliński, J. Lorentz-covariant quantum mechanics and preferred frame. *Physical Review A* **59,** 4187–4196 (1999).

22. Lamata, L., Martin-Delgado, M. A. & Solano, E. Relativity and Lorentz Invariance of Entanglement Distillability. *Physical Review Letters* **97,** 250502 (2006).

23. Czachor, M. & Wilczewski, M. Relativistic Bennett-Brassard cryptographic scheme, relativistic errors, and how to correct them. *Physical Review A* **68,** 010302 (2003).

24. Caban, P. & Rembieliński, J. Lorentz-covariant reduced spin density matrix and Einstein-Podolsky-Rosen-Bohm correlations. *Physical Review A* **72,** 012103 (2005).

25. Li, H. & Du, J. Relativistic invariant quantum entanglement between the spins of moving bodies. *Physical Review A* **68,** 022108 (2003).

26. Ahn, D., Lee, H.-j., Moon, Y. H. & Hwang, S. W. Relativistic entanglement and Bell's inequality. *Physical Review A* **67,** 012103 (2003).

27. Lee, D. & Chang-Young, E. Quantum entanglement under Lorentz boost. *New Journal of Physics* **6,** 67–67 (2004).

28. Caban, P., Rembieliński, J. & Włodarczyk, M. Strange behavior of the relativistic Einstein-Podolsky-Rosen correlations. *Physical Review A* **79,** 014102 (2009).

29. Jordan, T., Shaji, A. & Sudarshan, E. Maps for Lorentz transformations of spin. *Physical Review A* **73,** 032104 (2006).

30. Pachos, J. & Solano, E. Generation and degree of entanglement in a relativistic formulation. *Quantum Information and Computation* **3,** 115–120 (2003).

31. Wang, J. & Jing, J. Quantum decoherence in noninertial frames. *Physical Review A* **82,** 032324 (2010).

32. Montero, M., León, J. & Martín-Martínez, E. Fermionic entanglement extinction in noninertial frames. *Physical Review A* **84,** 042320 (2011).

33. Yu, T. & Eberly, J. H. Sudden Death of Entanglement. en. *Science* **323,** 598–601 (2009).

34. Moradi, S. Relativistic quantum nonlocality for the three-qubit Greenberger-Horne-Zeilinger state. *Physical Review A* **77,** 024101 (2008).

35. Nasr Esfahani, B. & Aghaee, M. Relativistic Entanglement for Spins and Momenta of a Massive Three-Particle System. *International Journal of Quantum Information* **09,** 1255–1265 (2011).

36. Nasr-Esfahani, B. & Aghaee, M. Tripartite entanglements seen from a relativistically moving frame. *Quantum Information Processing* **11,** 529–540 (2012).

37. Lindner, N. H., Peres, A. & Terno, D. R. Wigner's little group and Berry's phase for massless particles. en. *Journal of Physics A: Mathematical and General* **36,** L449 (2003).

38. Caban, P. Einstein-Podolsky-Rosen correlations of photons: Quantum-field-theory approach. *Physical Review A* **76,** 052102 (2007).

39. Landulfo, A., Matsas, G. E. A. & Torres, A. C. Influence of detector motion in entanglement measurements with photons. *Physical Review A* **81,** 044103 (2010).

40. Caban, P., Rembieliński, J., Witas, P. & Włodarczyk, M. Einstein-Podolsky-Rosen correlations in a hybrid system. *Physical Review A* **83,** 032115 (2011).

41. Bradler, K. Relativistically invariant photonic wave packets. *Journal of the Optical Society of America B* **28,** 727–736 (2011).

42. Rideout, D., Jennewein, T., Amelino-Camelia, G., Demarie, T. F., Higgins, B. L., Kempf, A., Kent, A., Laflamme, R., Ma, X., Mann, R. B., Martín-Martínez, E., Menicucci, N. C., Moffat, J., Simon, C., Sorkin, R., Smolin, L. & Terno, D. R. Fundamental quantum optics experiments conceivable with satellites—reaching relativistic distances and velocities. *Classical and Quantum Gravity* **29,** 224011 (2012).

43. Zhou, T., Cui, J. & Cao, Y. Influence of detector motion on discrimination between photon polarizations. *Quantum Information Processing* **12,** 747–759 (2013).

44. Alsing, P. M., Fuentes-Schuller, I., Mann, R. B. & Tessier, T. E. Entanglement of Dirac fields in noninertial frames. *Physical Review A* **74,** 032326 (2006).

45. Fuentes-Schuller, I. & Mann, R. Alice Falls into a Black Hole: Entanglement in Noninertial Frames. *Physical Review Letters* **95,** 120404 (2005).

46. Terashima, H. & Ueda, M. Spin decoherence by spacetime curvature. *Journal of Physics A: Mathematical and General* **38,** 2029 (2005).

47. Adesso, G., Fuentes-Schuller, I. & Ericsson, M. Continuous-variable entanglement sharing in noninertial frames. *Physical Review A* **76,** 062112 (2007).

48. Alsing, P. & Milburn, G. J. Teleportation with a Uniformly Accelerated Partner. *Physical Review Letters* **91,** 180404 (2003).

49. Ge, X.-H. & Shen, Y.-G. Teleportation in the background of Schwarzschild space-time. *Physics Letters B* **606,** 184–188 (2005).

50. Hosler, D., van de Bruck, C. & Kok, P. Information gap for classical and quantum communication in a Schwarzschild spacetime. *Physical Review A* **85,** 042312 (2012).

51. Downes, T. G., Ralph, T. C. & Walk, N. Quantum Communication with an Accelerated Partner. *arXiv:1203.2716* (2012).

52. Kok, P. & Braunstein, S. L. Relativistic quantum information processing with bosonic and fermionic interferometers. *International Journal of Quantum Information* **04,** 119–130 (2006).

53. Friis, N. & Fuentes, I. Entanglement generation in relativistic quantum fields. *Journal of Modern Optics* **60,** 22–27 (2013).

54. Friis, N., Bruschi, D. E., Louko, J. & Fuentes, I. Motion generates entanglement. *Physical Review D* **85,** 081701 (2012).

55. Dragan, A., Doukas, J. & Martín-Martínez, E. Localized detection of quantum entanglement through the event horizon. *arXiv:1207.4275* (2012).

56. Bruschi, D. E., Dragan, A., Lee, A. R., Fuentes, I. & Louko, J. Motion-generated quantum gates and entanglement resonance. *arXiv:1201.0663* (2012).

57. Friis, N., Huber, M., Fuentes, I. & Bruschi, D. E. Quantum gates and multipartite entanglement resonances realized by non-uniform cavity motion. *Physical Review D* **86,** 105003 (2012).

58. Hwang, M.-R., Park, D. & Jung, E. Tripartite entanglement in a noninertial frame. *Physical Review A* **83,** 012111 (2011).

59. Smith, A. & Mann, R. B. Persistence of tripartite nonlocality for noninertial observers. *Physical Review A* **86,** 012306 (2012).

60. Alsing, P. M. & Fuentes, I. Observer-dependent entanglement. *Classical and Quantum Gravity* **29,** 224001 (2012).

61. Martín-Martínez, E., Aasen, D. & Kempf, A. Processing quantum information with relativistic motion of atoms. *arXiv:1209.4948* (2012).

62. Czachor, M. & Wilczewski, M. Relativistic Bennett-Brassard cryptographic scheme, relativistic errors, and how to correct them. *Physical Review A* **68** (2003).

63. Geroch, R. *Mathematical Physics* (University of Chicago Press, Chicago, 1985).

64. Streater, R. F. & Wightman, A. S. *PCT, Spin and Statistics, and All That* (Princeton University Press, 2000).

65. Ferraro, R. & Thibeault, M. Generic composition of boosts: an elementary derivation of the Wigner rotation. *European Journal of Physics* **20,** 143–151 (1999).

66. Ryder, L. H. *Quantum Field Theory* 2nd ed (Cambridge University Press, Cambridge, 1996).

67. Sexl, R. U. & Urbantke, H. K. *Relativity, groups, particles: special relativity and relativistic symmetry in field and particle physics* Rev. ed (Springer, New York, 2001).

68. Thomas, L. H. The Motion of the Spinning Electron. *Nature* **117,** 514–514 (1926).

69. Thomas, L. H. The kinematics of an electron with an axis. *Philosophical Magazine. 7* **3,** 1–22 (1927).

70. Rhodes, J. A. & Semon, M. D. Relativistic velocity space, Wigner rotation, and Thomas precession. *American Journal of Physics* **72,** 943–960 (2004).

71. Fisher, G. P. The Thomas precession. *American Journal of Physics* **40,** 1772–1781 (1972).

72. Uhlenbeck, G. E. Fifty Years of Spin: Personal Reminiscences. *Physics Today* **29,** 43–48 (1976).

73. Ungar, A. A. *Beyond the Einstein Addition Law and Its Gyroscopic Thomas Precession: The Theory of Gyrogroups and Gyrovector Spaces* (Kluwer, 2001).

74. Wigner, E. On Unitary Representations of the Inhomogeneous Lorentz Group. *The Annals of Mathematics. Second Series* **40,** 149–204 (1939).

75. Halpern, F. R. *Special Relativity and Quantum Mechanics* (Prentice-Hall, 1968).

76. Tung, W.-K. *Group Theory in Physics* (World Scientific, Philadelphia, 1985).

77. Weinberg, S. *The Quantum Theory of Fields* (Cambridge University Press, Cambridge, 1995).

78. Lo, H.-K., Spiller, T. & Popescu, S. *Introduction to quantum computation and information* en (World Scientific, 1998).

79. Horodecki, R., Horodecki, P., Horodecki, M. & Horodecki, K. Quantum entanglement. *Reviews of Modern Physics* **81,** 865–942 (2009).

80. Werner, R. Quantum states with Einstein-Podolsky-Rosen correlations admitting a hidden-variable model. *Physical Review A* **40,** 4277–4281 (1989).

81. Bennett, C., Bernstein, H. J., Popescu, S. & Schumacher, B. Concentrating partial entanglement by local operations. *Physical Review A* **53,** 2046–2052 (1996).

82. Hill, S. & Wootters, W. K. Entanglement of a Pair of Quantum Bits. *Physical Review Letters* **78,** 5022–5025 (1997).

83. Wootters, W. Entanglement of Formation of an Arbitrary State of Two Qubits. *Physical Review Letters* **80,** 2245–2248 (1998).

84. Peres, A. & Terno, D. Quantum information and relativity theory. *Reviews of Modern Physics* **76,** 93–123 (2004).

85. Nielsen, M. A. & Chuang, I. L. *Quantum Computation and Quantum Information* (Cambridge University Press, Cambridge, 2000).

86. Caban, P. & Rembieliński, J. Einstein-Podolsky-Rosen correlations of Dirac particles: Quantum field theory approach. *Physical Review A* **74,** 042103 (2006).

87. Bengtsson, I. & Życzkowski, K. *Geometry of Quantum States: An Introduction to Quantum Entanglement* (Cambridge University Press, 2006).

88. Gheorghiu, V. & Griffiths, R. B. Entanglement transformations using separable operations. *Physical Review A* **76,** 032310 (2007).

89. Gheorghiu, V. & Gour, G. Multipartite entanglement evolution under separable operations. *Physical Review A* **86,** 050302 (2012).

90. Einstein, A., Podolsky, B. & Rosen, N. Can Quantum-Mechanical Description of Physical Reality Be Considered Complete? *Physical Review* **47,** 777–780 (1935).

91. Bohm, D. & Aharonov, Y. Discussion of Experimental Proof for the Paradox of Einstein, Rosen, and Podolsky. *Physical Review* **108,** 1070–1076 (1957).

92. Jordan, T., Shaji, A. & Sudarshan, E. Lorentz transformations that entangle spins and entangle momenta. *Physical Review A* **75,** 022101 (2007).

93. Friis, N., Bertlmann, R. A. & Huber, M. Relativistic entanglement of two massive particles. *Physical Review A* **81,** 042114 (2010).

94. Bertlmann, R. A., Narnhofer, H. & Thirring, W. Geometric picture of entanglement and Bell inequalities. *Physical Review A* **66,** 032319 (2002).

95. Horodecki, M., Horodecki, P. & Horodecki, R. Separability of mixed states: necessary and sufficient conditions. *Physics Letters A* **223,** 1–8 (1996).

96. Terno, D. in *Quantum Information Processing* (eds Angelakis, D. G., Christandl, M., Ekert, A., Kay, A. & Kulik, S.) *NATO Science Series* III (IOS Press, 2006).

97. Parker, S., Bose, S. & Plenio, M. Entanglement quantification and purification in continuous-variable systems. *Physical Review A* **61,** 032305 (2000).

98. Braunstein, S. & Loock, P. v. Quantum information with continuous variables. *Reviews of Modern Physics* **77,** 513–577 (2005).

99. Kendon, V. M., Życzkowski, K. & Munro, W. J. Bounds on entanglement in qudit subsystems. *Physical Review A* **66,** 062310 (2002).

100. Hayden, P., Leung, D. W. & Winter, A. Aspects of Generic Entanglement. English. *Communications in Mathematical Physics* **265,** 95–117 (2006).

101. Eguchi, T., Gilkey, P. B. & Hanson, A. J. Gravitation, gauge theories and differential geometry. *Physics Reports* **66,** 213–393 (1980).

102. Schutz, B. F. *Geometrical Methods of Mathematical Physics* (Cambridge University Press, Cambridge; New York, 1980).

103. Urbantke, H. Physical holonomy, Thomas precession, and Clifford algebra. *American Journal of Physics* **58,** 747 (1990).

104. Berry, M. V. Quantal Phase Factors Accompanying Adiabatic Changes. en. *Proceedings of the Royal Society of London. A. Mathematical and Physical Sciences* **392,** 45–57 (1984).

105. Simon, B. Holonomy, the Quantum Adiabatic Theorem, and Berry's Phase. *Physical Review Letters* **51,** 2167–2170 (1983).

106. Stewart, G. W. *Jampack. A Java Package For Matrix Computations.* NIST and the University of Maryland.
`ftp://math.nist.gov/pub/Jampack/Jampack/AboutJampack.html`.
Accessed 2013-07-22.